An investigation of the efficiency of the receiver of a solar thermal cooker with thermal energy storage

Heiko Martin Heilgendorff

August 25, 2013

Submitted in fulfillment of the academic
requirements for the degree of
Master of Science in the
School of Chemistry and Physics,
University of KwaZulu-Natal,
Durban

The financial assistance of the National Research Foundation (NRF) towards this research is hereby acknowledged. Opinions expressed and conclusions arrived at, are those of the author and are not necessarily to be attributed to the NRF.

As the candidate's supervisor I have approved this dissertation for submission

Signed: ..... Name: ..... Date:.....

Abstract

A small scale solar concentrator cooker with a thermal energy storage system was designed, constructed and tested on the roof of the Physics building at UKZN, Westville campus (GPS co-ordinates: -29.817897, 30.942771) in Durban, South Africa. The system consisted of a 2.4 m diameter half-parabolic concentrating dish, a receiver, an automated solar tracking system, an oil heat transfer system and a pebble bed thermal storage. The efficiencies of a flat coil receiver and a cavity receiver were tested and compared, and the efficiency of the thermal energy storage was investigated. The tests were conducted under similar conditions of solar insolation, wind speed and ambient temperature during the months of December 2012 and January 2013. The cavity receiver was found to have an efficiency of 47 $\pm$ 12 %, which was more efficient than the flat coil receiver which had an efficiency of 40 $\pm$ 11 %. The thermal energy storage was found to have an efficiency of 87 $\pm$ 3 %.

Declaration

I, Heiko Martin Heilgendorff declare that

1. The research reported in this thesis, except where otherwise indicated, is my original research.
2. This thesis has not been submitted for any degree or examination at any other university.
3. This thesis does not contain other persons data, pictures, graphs or other information, unless specifically acknowledged as being sourced from other persons.
4. This thesis does not contain other persons' writing, unless specifically acknowledged as being sourced from other researchers. Where other written sources have been quoted, then:

   (a) Their words have been re-written but the general information attributed to them has been referenced.

   (b) Where their exact words have been used, then their writing has been placed in italics and inside quotation marks, and referenced.
5. This thesis does not contain text, graphics or tables copied and pasted from the Internet, unless specifically acknowledged, and the source being detailed in the thesis and in the References sections.

Signed: .....

Dedication

This research is dedicated to the memory of Professor Sadha Pillay, as well as to my family, my darling wife and to God.

Contents

List of Tables

List of Figures

Acknowledgements

I would like to thank Mr Padayachee and his team at the Central Academic Workshop for all their hard work in constructing the various parts of this experiment. I would also like to thank Mr Enock Chekure and Mr Evans Zhandire for all of their help and guidance and the many hours they put into this project. I would like to thank my co-supervisor, Prof. Jørgen Løvseth, and Mr Robert Van den Heetkamp for their guidance throughout this project and Ms Paulene Govender for her friendship and assistance. Finally I would like to thank the late Prof. Sadha Pillay for getting me involved in this project and Dr Alan Matthews for taking over as supervisor and giving huge amounts of his time and effort, even while on sabbatical.

Chapter 1

Introduction

1.1 Research Overview

A small scale concentrating solar thermal cooker was designed, constructed and mounted onto an existing platform on the roof of the Physics building at the University of KwaZulu-Natal, Westville campus. The system consisted of a 2.4 m diameter parabolic half-dish solar radiation concentrator, a two-axis solar tracking system, a heat transfer system, a thermal energy storage, a measurement system and a receiver.

The surface of the concentrator was covered with trapezoidal mirror tiles, which reflected the incident solar radiation to the focal area of the dish. The concentrator was mounted onto the tracking system, which ensured that the concentrator always faced the sun directly. The receiver was mounted at the focal area of the concentrator and was connected to the storage by flexible steel hoses. The concentrator reflected direct solar radiation onto the receiver, which transferred the solar thermal energy into the heat resistant oil, which was pumped between the receiver and the storage to transfer the thermal energy. The thermal storage unit was a large drum which was filled with pebbles. The temperature stratification in the storage was measured using thermocouples which had been placed at different heights in the storage container.

A flat stainless steel plate, painted black with high temperature resistant paint, was placed at the focal area of the collector and its temperature was measured using a thermal imaging camera to determine an accurate thermal map of the focal area. Then the plate was replaced with a coiled pipe receiver, which was 25 cm in diameter. The temperature of the heat transfer fluid flowing through the receiver was measured at the entrance and exit of the receiver using thermocouples, and these measurements, along with the velocity of the heat transfer fluid, were used to determine how much energy had been transferred by the receiver. The incident solar radiation was also measured, along with the ambient air temperature and wind speed so that the amount of energy incident upon the receiver was known and the amount of energy lost to the surroundings could be estimated. This allowed the receiver's efficiency to be determined. This experiment was conducted for two different receivers, one a flat coil and the other a cavity receiver, and their efficiencies were compared. The temperatures at different levels within the storage container were measured overnight so that heat losses of the storage could be estimated, allowing the overall efficiency of the thermal energy collection process of the system to be determined.

1.1.1 Aims and Objectives

1. To refurbish the small scale solar cooker on the roof of the Physics building at UKZN Westville campus.
2. To automate the solar tracking system.
3. To design and construct a new receiver.
4. To test the old receiver and the new receiver under similar conditions and compare their efficiency.
5. To determine the efficiency of the thermal energy storage.

1.2 Thesis Overview

This thesis consists of six chapters. Chapter one is the introduction, which discusses the need for this research, the history of solar cooking and a description of this project. Chapter two is a detailed discussion of the solar resource. Chapter three is an overview of different solar energy systems and an investigation of previous research, specifically focused on small scale solar concentrating cookers. Chapter four is a description of the design and construction of the system, as well as a description of how the experiment and analyses were performed. Chapter five presents the experimental results followed by a detailed discussion of those results and Chapter six is the conclusion.

1.3 Motivation for Research

Solar cooking offers the opportunity to cook a meal without using electricity to provide heat. Research into solar cooking will allow the development of cheaper, more powerful and more efficient systems and methods, making solar cooking a viable alternative to electrical or gas cooking. Research into thermal energy storage systems will improve the amount of thermal energy that can be stored, as well as the length of time for which it can be stored. This is very important as an efficient thermal energy storage system will allow food to be cooked using solar power at any time, even when the local solar insolation is zero.

The implementation of solar cookers in schools, hospitals and other community centres, as well as in private homes would have many benefits. Food could be cooked at a fraction of the price, when compared to the cost of electrical cooking, and it could be cooked at any time, even when no electricity is available. Large scale implementation of solar cooking would assist in reducing carbon emissions and would reduce the impact of cooking on climate change.

1.3.1 Climate Change

The phenomenon of climate change has been a topic of fierce debate for many years. Some argue that increased global temperatures caused by the burning of fossil fuels and the consequent emission of greenhouse gases could have a devastating effect on global weather patterns while others believe that climate change does not exist. Still others argue that climate change is natural and is not influenced by human activities at all. In recent years, scientific evidence has begun to show that global temperatures are indeed changing. For example, analyses performed on the temperature-depth profile of boreholes show a Surface Air Temperature (SAT) increase of 1.4 °C in the period 1880 to 2008 [1]. Evidence is also beginning to show a link

between increased global temperatures and climate change. Naidu et al [2] evaluated the frequencies of rainy days having different rainfall limits in northeast monsoon season over South Peninsular India for the period 1951 to 2008. They split the data into two time periods: 1951 to 1969 (pre-global warming period) and 1970 to 2008. They found that there was an increase in rainfall in the global warming period which they associated with an intensification of the easterly wind belt in the lower troposphere over the major part of the area that they were investigating. They also found that there was a decrease in the frequency of days with zero rainfall. In 2003, Nordell [3] stated that while the phenomenon of global warming had been accepted by the international scientific community, there was no agreement on its cause. Suggested causes range from changes in the amount of energy provided by the sun [4], [5], the greenhouse effect and thermal pollution. Nordell found that by 2001 the global mean temperature had increased by 0.7 °C since the 1880 figure of 13.6 °C and, in 2012, Kharseh and Altorkmany stated that if the current climate change trends were to continue, average global temperatures could increase by 4-6 °C [6]. Nordell suggested that this was due to the amount of heat or thermal pollution generated by the consumption of nonrenewable energy.

The greenhouse effect as it occurs in nature is essential to life on Earth. Greenhouse gases such as carbon dioxide, methane and water vapour absorb incident solar radiation, as well as radiation reflected or emitted from the Earth's surface and act as a greenhouse, keeping the Earth warm. Without this system in place, the global mean ambient temperature would be about -18 °C [7]. However, since the Industrial Revolution in the 18th and 19th centuries, [8] emissions of greenhouse gases have increased to the point where they have now begun to affect the global climate. The main contributers to these emissions are the burning of fossil fuels in the production of electricity and the emmissions from automobiles.

1.3.2 South Africa's Contribution to Climate Change

South Africa's electricity consumption has risen steadily from 5.0768×10^4 GWh in 1971 to a peak of 2.414×10^5 GWh in 2009 before dropping to 2.151×10^5 GWh in 2010. This means that South Africa is currently ranked as the 16th highest electricity consumer in the world [9]. South Africa is also the 13th highest CO_2 emitter with an annual emission of about 435 878 thousand metric tonnes, which contributes to 1.45% of the total global percentage, with China topping the list at 23.33% [10]. Eskom, South africa's main electricity producer, is responsible for the production of about 95% of the country's electricity. It also produces about 45% of the electricity consumed in Africa. A large portion of this electricity is used by the industrial sector, which uses 26.2% of the electricity produced by Eskom and the mining sector, which uses 14.5%. Eskom has several means of generating electricity including coal-fired, hydro-electric, pumped storage, gas turbine, nuclear and wind turbine power stations. According to their figures in 2011, 2.20219×10^5 GWh of electricity was produced by coal-fired power stations. This was followed by 1.2099×10^4 GWh produced from nuclear power stations, 2.953×10^4 GWh produced from pumped storage, 1.960×10^3 GWh from hydro-electric power stations, 197 GWh from Gas turbines and 2 GWh produced from wind turbines. Other renewable energy resources such as solar power are negligible [11].

South Africa is the sixth largest producer of coal in the world [9]. Most of this coal is mined from open cast mines, which destroy the immediate environment of the mine. The burning of coal to make electricity releases harmful greenhouse gases as well as considerable thermal pollution. Thus ninety percent of South Africa's electricity is contributing to the destruction of our environment, making it absolutely crucial to find other sources of power. Thankfully, the South African government is aware of this and is taking positive steps towards increasing

the use of renewable energy in electricity production and in the fullfillment of other energy requirements.

1.3.3 Electricity in Remote Areas

South Africa contains vast amounts of rural land. Much of this land is far from power stations and it is thus expensive and difficult to provide it with power from the main grid. Cable lines that have to stretch over hundreds of kilometers have a high risk of damage and theft, which makes them impractical and inefficient. It seems that one way to solve these problems is to set up smaller renewable energy stations in rural areas, which can then provide them with cheap, sustainable energy without depending on the national grid. Solar energy radiated from the sun is one of the most readily available sources of renewable energy but there is still plenty of research required to find cheap, simple and efficient methods of harnessing this energy and making it accessible to the general public.

1.3.4 Renewable Energy

Conventional sources of energy such as fossil fuels and natural gas are in finite supply, and while there are still considerable resources available on the planet, harvesting these resources is becoming more difficult, more expensive, and more damaging to the environment. By contrast, renewable energy is not limited to finite stores located deep beneath the Earth's surface. Instead, renewable energy is constantly being replenished and, for the most part, easily accessible, although it does require the use of technology to convert it from its natural form to a form of energy that can be used, for example, in cooking. There are several types of renewable energy that are found in sunlight, wind, rivers, oceans, biomass and in geothermal heat and all of these can be used to produce useful energy such as electricity and heat. South Africa is abundant in all of these forms of renewable energy and the adoption of these energy sources in place of coal and other conventional energy sources would have a positive impact on our environment.

1.3.5 Why Solar Cookers?

Solar cooking is viewed as a possible solution for cooking in poor and remote places that may not be able to afford or may not have access to conventional forms of cooking such as electric or gas [12]. After all, solar cooking requires no wood to burn, no electricity to heat an element and no gas to provide a flame. The only source of energy it needs is the most abundant and freely available natural resource on Earth - sunlight. Thus a large amount of research is being conducted across the world to develop not only the most effective devices and methods of solar cooking, but also to determine how solar cooking would affect the lives of ordinary people and how willingly ordinary people would embrace the concept of solar cooking. There are various socioeconomic factors that are being studied and considered. Pohekar, Kumar and Ramachandran [13] investigated the different cooking energy options in India, in 2005, with the intention of understanding the socioeconomic factors that affected the use of these various cooking options. They found that India had great potential for solar cooking, but that it was under-utilized because of intermittent sunshine and the time it takes to cook with solar energy, amongst other reasons. They also discussed what policy interventions were required to increase the adoption of renewable energy cookers. Wentzel and Pouris [14], while reviewing research based in South Africa on the impact of solar cooking, found that the use of solar cookers resulted in an appreciable reduction in cooking time and an increase in fuel savings. Biermann, Grupp and Palmer [15] investigated the acceptance of solar cookers in South Africa in 1999. They tested seven different types of solar cookers, including a parabolic

dish concentrator, by giving them to 66 families and 14 institutions for the period of one year. Each family had one type of cooker for two months before switching it with another type of cooker. Thirty families had no solar cookers and were used as a control. They found that the high use rate of solar cookers indicated acceptance and the considerable fuel savings result in an acceptable pay-back period to recover the initial costs of the solar cooking device. No clear favourite type of cooker was identified, but the parabolic solar cooker was one of the most popular and was selected for a pilot dissemination project.

1.4 A Brief History of Solar Cooking and an Introduction to Previous Research

Mankind has always been fascinated with the idea of harnessing the power of the sun. The ancient world used curved mirrors to concentrate the sun's power and cause objects to spontaneously ignite. They realised that this was indeed a mighty power and used it in their religious ceremonies to light altar fires. They also believed this technology could be used in war. Historical records from ancient Greece and Rome indicate that in 212 BC at the Battle of Syracuse, the famous Greek mathematician Archimedes built a solar concentrator that was able to set the Roman ships on fire [16]. Though this is more likely a myth than truth, the idea has so captured the human imagination that physicists and engineers are still trying to get the fabled "Archimedes' Death Ray" to work today [17]. Unfortunately, there is little evidence to suggest that the ancient world ever tried to apply their knowledge of solar concentrating to harness the sun's energy for more practical applications such as cooking and heating water, although it is believed that Archimedes managed to boil water using a concave mirror[7]. As a result, the first instances of solar cooking involved leaving food to cook on stones that had been heated by the sun. The Essenes, a Jewish sect, used this method to cook wafers [18].

It took over a thousand years before the great Leonardo da Vinci thought of using concave mirrors to heat water at the Vatican in the 1500's [19]. In 1615, Salmon de Caux published the first application of solar energy since the fall of the Roman Empire. He built a device that created a small water fountain when glass mirrors concentrated sunlight onto the base of an airtight metal container which was filled with water and air [20]. Also in the 1600's, a German physicist named E.W von Tschirnhousen used large concentrating lenses to boil water in a clay pot [21] and it took another hundred years before the French - Swiss physicist Horace-Benedict de Saussure, now considered the grandfather of solar cooking, began his experiments with glass box heat traps in 1767 [22]. He began his experiments by constructing five glass boxes that were placed one inside another. This assembly was placed upon a black wooden table, which could be rotated to follow the sun so that the glass surface was always perpendicular to the incoming direct solar radiation. The temperature in the outer box was the lowest, and each subsequent box registered an increase in temperature until the smallest box, which had a bottom surface temperature of 87 °C. De Saussure was able to cook fruit by placing it in the smallest box. Until this time, solar cooking was nothing more than leaving food in the sun to dry out, or heating bits of bread by placing them on hot stones which had been left out in the sun. De Saussure continued to make improvements to his intitial design, reaching temperatures of 110 °C, by adding wooden sides and other insulation to stop the heat from escaping. In 1830, Sir John Herschell built a similar hot box out of mahogony while on expedition in South Africa. He recorded temperatures of 115.6 °C, easily hot enough to boil water, and used the box to boil eggs for himself and his family.

In 1747, George Buffon used 168 small planar mirrors, individually focused, to ignite a pile

of wood at a distance of about 195 ft [20]. This was an early example of the heliostat. In 1772, Antoine Lavoisier tested a solar furnace using 'the great burning-lens of Tschirnhousen'. The focal area of this device was too narrow so he used a glass lens that was filled with liquid alcohol. He used the device to prove that diamond contains only carbon atoms. The glass used in the 'liquor lens' was donated by a company called Saint-Gobain, which still supplies glass mirrors to the solar thermal industry today [23]. In 1860, Augustin Mouchot began French government funded experimentation with solar concetrating reflectors. His experiments resulted in the design and testing of the first truncated cone reflector, now known as an axicon [24]. He continued his research throughout the 1860's and 70's, resulting in the creation of the first solar oven by adding concentrating mirrors to the box heat trap developed by de Saussure. He used this idea to build a solar pump, a solar still and the first solar steam engine [25]. In 1876, W. Adams developed an octagonal oven with 8 mirrors for soldiers in India[25], and in the same year Dr Charles G Abbot built the first solar cooker with storage. The collector was outside the house and the cooking surface was inside. It used a heat transfer fluid and the storage allowed evening cooking [26].

In 1887, John Ericson, who designed solar engines, declared publicly that the world would eventually run out of fossil fuels and that it would then need to use solar power. He said that European industry would have to move to Northern Egypt [27]. Clarence Kemp was the first to patent a solar thermal water heating system [28]. He patented his system in 1891 and by 1897 his system had been installed in almost a third of the homes in Pasadena, California. Unfortunately, the advent of World War One meant that materials such as copper were difficult to come by, resulting in a decline in the solar industry. In 1909, William Bailey patented a solar water heater that separated the heat storage from the collector, allowing the hot water to be stored inside the house [28]. During the years of the First and Second World Wars, very little research was done in the field of solar cookers, as the race to build more powerful and more sophisticated weapons demanded the attention of the world's scientists. It was only after the Second World War, when resources had been consumed at a rate that had never been imagined before, that science once again turned its attention to solar cooking. In 1948, Dr Maria Telkes designed a solar heating system that stored heat chemically through the crystallization of a sodium sulphate solution [29]. In the course of her research, from the 1940's to the 1970's, she developed several solar ovens, a faster method for drying food and a portable water evaporator which was able to use solar energy to get drinkable water from sea water. She moved to the New York University College of Engineering in 1953 and set up a solar energy research lab.

In the 1960's, Lof, in describing the principles of cooking, found that the different phases of the cooking process have different energy requirements. The heat required for the actual physical and chemical changes that take place during cooking is less than the energy required during the sensible heating process when the energy requirement is at maximum. During the cooking process, bringing food to boiling temperature uses up 20 % of the heat supplied. Water vaporization uses up another 35 % and the remaining 45 % is lost through convection from cooking utensils. It was also found that a considerable reduction in heat loss can be achieved by insulating the sides of the cooking vessel and covering the vessel with a lid. In other words, provided there is enough heat supplied to overcome heat losses, the cooking rate is practically independent of the heat rate and differences in cooking time for equal quantities and types of food are mainly due to differences in the sensible heating period, or how long it took to heat the food to cooking temperature [30].

There are many possible combinations of sub-systems that can be used to constitute a solar cooker. As such, there has not been much research on a system exactly like the one used in

this experiment. However, the sub-systems such as the concentrator and the receiver have been thoroughly tested and thus the existing research has been investigated in terms of these sub-systems. For example, Kaushik and Gupta tested a solar cooker that used a parabolic dish concentrator, like the one used in this experiment, but their cooker had a different type of receiver and no thermal energy storage. Hernández et al tested a cavity solar cooker that used a cavity receiver, but the heat tranfer fluid that they used was water and the one used in this experiment was oil. A thorough review of previous research, in terms of sub-systems, is presented in Chapter 3.

1.5 Overview of the Small Scale Solar Cooker System

The cooker that was constructed and tested in this project consisted of a concentrator, a receiver, a thermal energy storage, a tracking system and a heat transfer system as shown in Figure 1.1. The concentrator and receiver were mounted on a platform, which was supported

Figure 1.1: Photograph of the solar concentrating system.

by a purpose-built wooden hut. The platform was rotated by two motors, one to control the hour angle and the other to control the declination. The platform was balanced by a counterweight. The concentrator concentrated solar energy onto the receiver, which converted the solar radiation into thermal energy. This thermal energy was transferred to the heat transfer fluid, which was pumped through the receiver and transported to the storage. Thermocouples were used to measure receiver inlet and outlet oil temperatures, as well as storage inlet and outlet oil temperatures and oil temperatures at two other heights within the storage container.

Chapter 2

The Solar Resource

The sun radiates energy through the vacuum of space in the form of electromagnetic waves at a rate of 3.9 x 10^{26} W. Radiation from the sun measured at the top of the Earth's atmosphere has an average intensity of 1353 $\mathrm{Wm}^{-2} \pm 1.5$ % [31] passing through the plane perpendicular to the direction of progagation of the radiation. This value changes constantly over time and the average is known as the solar constant [32]. The value of the solar constant has been the subject of much research and has been revised several times. The sun is about 4.6 billion years old, is situated a mean distance of 1.495 x 10^{11} m from the Earth and has an effective blackbody temperature of 5777 K [31]. Even though the sun emits radiation in all directions, the combination of the distance between the sun and the Earth and their relative diameters means that the sun subtends an angle of only 32 minutes at the Earth's surface, resulting in solar radiation reaching the Earth's surface being almost parallel beam radiation [33]. The sun holds about 98 % of the mass in the solar system. It is composed of 92.1 % hydrogen and 7.8 % helium atoms with trace amounts of heavier elements. Because it contains so many small elements, there are a lot of fusion reactions occurring in its core, with temperatures reaching many millions of degrees as the atoms collide with one another to form heavier atoms. These fusion reactions give off energy in the form of X-ray and γ-ray radiation. This radiation leaves the core and moves through the various layers of the sun, undergoing a succession of emission, absorption and reradiation interactions resulting in an increase in the radiation's wavelength as the temperature drops at larger radial distances, giving rise to the solar radiation spectrum [31].

2.1 The Solar Radiation Spectrum (SRS)

The sun emits energy through the entire range of the electromagnetic spectrum, from long wavelength radio waves to short wavelength gamma rays. However, most of the short wavelength, high frequency waves cannot penetrate the Earth's atmosphere and most of the long wavelength, low frequency waves lack sufficient energy to be used. Thus solar cookers are only concerned with a small band of the electromagnetic spectrum with a wavelength ranging from $\simeq$300 nm to $\simeq$3000 nm. This part of the electromagnetic spectrum is called the solar radiation spectrum, or SRS. The SRS can be divided into three main regions: the ultraviolet (UV) region, the visible (VIS) region and the infrared (IR) region.

2.1.1 The Ultraviolet (UV) Region

The ultraviolet region of the SRS corresponds to wavelengths of less than $\sim$ 380 nm. This wavelength is smaller than the visible range, and thus cannot be detected by the human eye. Most of the UV radiation that enters the Earth's atmosphere is absorbed by the ozone layer,

a protective layer of O_3 that surrounds the Earth. Thus, UV radiation comprises the smallest amount of solar radiation to reach the Earth's surface.

2.1.2 The Visible Region

The visible region of the SRS covers a range of wavelengths from $\sim$ 380 to $\sim$ 780 nm and can be detected by the human eye. This range of wavelengths passes through the atmosphere with very little difficulty and therefore comprises most of the solar radiation to reach the Earth's surface.

2.1.3 The Infrared (IR) Region

The infrared region of the SRS corresponds to wavelengths larger than $\sim$ 780 nm. This wavelength is greater than the visible range , and thus cannot be detected by the human eye. Twenty percent of the solar IR radiation is absorbed by water vapour and carbon dioxide in the atmosphere. Consequently only eighty percent of this radiation reaches the Earth's surface.

2.2 Components of radiation

The sun emits solar radiation into space in all directions. The radiation that reaches the top of the Earth's atmosphere directly from the sun is called the solar extraterrestrial beam radiation. Once this radiation enters the Earth's atmosphere, it is separated into two components: direct beam radiation, which is observable directly from the sun's disk, and diffuse or diffuse horizontal radiation, which has been reflected or scattered to the observer from clouds, dust particles etc. Direct normal radiation is another term used for beam radiation where the term 'normal' refers to the direction of the radiation relative to the detector. Global horizontal radiation is defined as the combined sum of beam radiation, multiplied by the cosine of the sun's zenith angle, and diffuse radiation. The term 'horizontal' is used in reference to radiation incident on a flat plate that is horizontal to the Earth's surface and is often omitted. It is important to note that only direct solar radiation can be focused, which means that solar concentrating systems require a large proportion of direct solar radiation in order to operate effectively. It is also interesting to note that even on a clear, cloudless day, at least 10% of the incident solar radiation is reflected or scattered by molecules in the atmosphere and is therefore diffuse radiation. Thus the ratio between beam and total irradiance varies from about 0.9 on a clear day to zero on a completely overcast day [34].

2.3 Atmospheric Attenuation

The activity of the sun fluctuates in an 11 year cycle, known as the solar cycle [35]. At the beginning of the cycle, during a period known as solar minimum, there is little activity on the surface of the sun and the radiation is fairly constant. However, as the cycle continues, sunspots begin to appear on the surface of the sun with increased frequency as the sun approaches its period of solar maximum, when the activity on its surface is at its peak. During this period there is an increase in the number of solar flares, which are abrupt periods of increased radiation emitted from the sun over a short time interval.

The amount of solar radiation is not only affected by the sun itself, but by seasonal and diurnal variations. Thus it is necessary to determine an average for the amount of solar radiation reaching the Earth's atmosphere, the solar constant, before one then takes atmospheric effects

into account. On a clear day, as much as 30 % of the solar energy that enters the Earth's atmosphere is absorbed, scattered or reflected by the atmosphere before it reaches the Earth's surface. On a cloudy day, this reduction in the incident solar radiation can rise to 90 % [38]. When a beam of light strikes a single particle, if only scattering occurs, then all the energy that the original beam had will be present in the radiation field surrounding the particle. However, this energy will be dispersed as radiation scattered in all directions. Thus the particle effectively becomes a new source of light. If the sum of the scattered and transmitted energy, integrated over all angles, does not equal the incident energy, then absorption has occurred and the beam has lost some of its initial energy to the particle. This energy could have been converted into heat or it may have been used by the particle to alter its chemical composition or any of a number of its other properties [36]. The more particles that a beam of light must interact with, the higher the chance that scattering and absorption will occur. Thus, scattering and absorption of the incident radiation are both functions of the number of particles and therefore the mass of the air that it must pass through. They also strongly depend on the size of those particles and the wavelength of the incident radiation, as shown by Lord Rayleigh in the early 1870's [37].

The length of the path of solar radiation through the Earth's atmosphere changes with time, being longest when the sun is near the horizon, when viewed from the Earth's surface, and shortest when the sun is at its peak. In other words, radiation from the sun has to travel further through the Earth's atmosphere at sunrise and sunset than it does at noon and thus has to travel through a larger mass of air at these times. Because of this increased path length, the higher frequencies in the SRS are scattered, resulting in a dominance in the presence of lower frequency light, making the sky appear red and reducing the intensity of the radiation. Figure 2.1 illustrates the intensity of the incident solar radiation at the top of the atmosphere and compares the intensity curve as a function of wavelength to that of a blackbody radiating at 6050 K. The curve labelled $\%I_{sc}$ indicates the percentage of the solar constant. Figure 2.2 illustrates the intesity of the incident solar radiation as a function of wavelength for different air masses at ground level. It shows that the intensity of the incident radiation reduces with increased air mass. It also shows the effects of the water vapour and carbon dioxide absorption bands in the infrared region as well as the reduction in blue, violet and ultraviolet light due to Rayleigh scattering and absorption by the ozone layer.

As can be seen in Figure 2.1, most of the UV radiation that enters the atmosphere is absorbed by the ozone layer. Conversely, only 20% of the incident IR radiation is absorbed by carbon dioxide and water vapour molecules in the atmosphere. The remaining 80% proceeds to the Earth's surface where some of it is absorbed and some is reflected back into the atmosphere. Solar radiation heats the Earth's surface from about -250 °C to about +5 °C, which causes it to radiate energy in the infrared region. Of the radiation leaving the Earth's surface, some passes through the atmosphere and escapes into space and some is absorbed by the atmosphere and reradiated back towards the Earth's surface, thus further increasing the Earth's equilibrium temperature. This phenomenon is known as the greenhouse effect. A significant contributer to the attenuation of direct solar radiation intensity is cloud cover. Clouds mainly consist of water vapour and can cover huge areas of the Earth's surface, reflecting and absorbing the incident solar radiation.

The result of all this atmospheric attenuation is that only about half of the incident solar radiation at the top of the Earth's atmosphere actually reaches the Earth's surface. The amount changes from day to day and place to place due to various atmospheric and geographical conditions. This is why it is necessary to take ground-based measurements, rather than simply

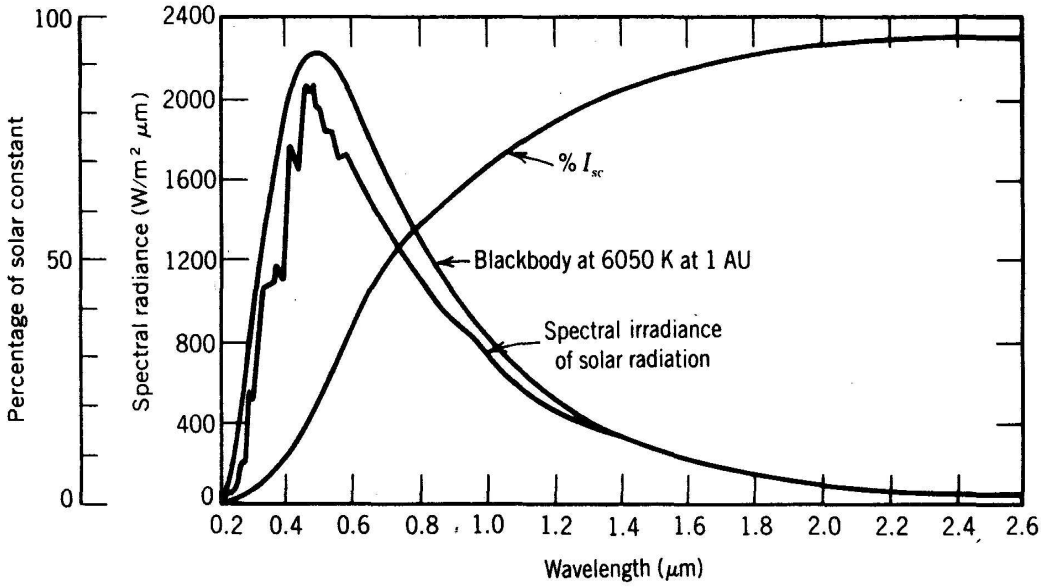

Figure 2.1: SRS spectral irradiance as a function of wavelength, adopted from the book, Power From the Sun [Stine WB, Harrigan RW, 1986] [38].

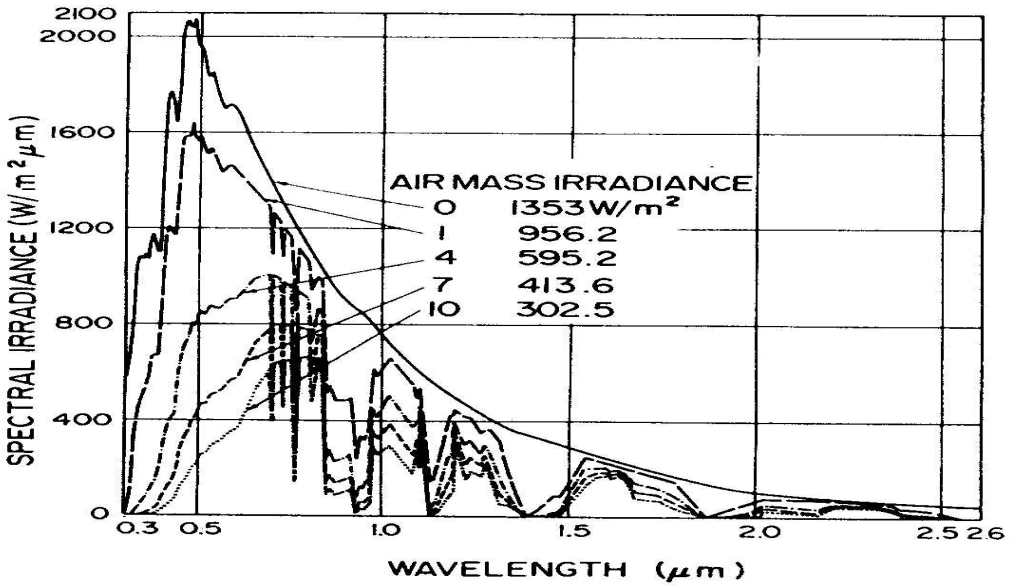

Figure 2.2: SRS spectral irradiance as a function of wavelength for different air mass values, adopted from the book, Power From the Sun [Stine WB, Harrigan RW, 1986] [38].

relying on measurements taken by satellites before the Earth's atmosphere has influenced the results.

2.4 Geographical Distribution of Solar Radiation on the Earth's Surface

There are many factors that influence the amount and intensity of solar radiation reaching a particular geographical location on the Earth's surface. These factors range from the latitude and longitude of the position, to the topography of the area, to the time of the year, to the time of the day, to the weather, etc. Thus, the spatial distribution of solar radiation is not even over the entire surface of the Earth. Figures 2.3 and 2.4 are solar radiation maps of the world, created with a combination of satellite and groundbased measurements by ©METEOTEST; based on www.meteonorm.com. Figure 2.3 is a map of the average direct normal radiation across the world for the period 1986 to 2005 and Figure 2.4 is a map of the average global horizontal radiation across the world for the same period. These figures show that the world can be divided up into regions according to how much solar radiation the region receives.

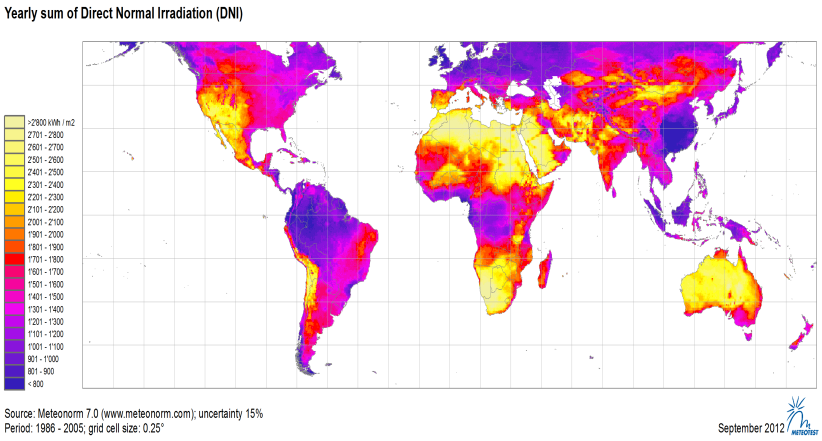

Figure 2.3: Yearly sum of Direct Normal Radiation [39].

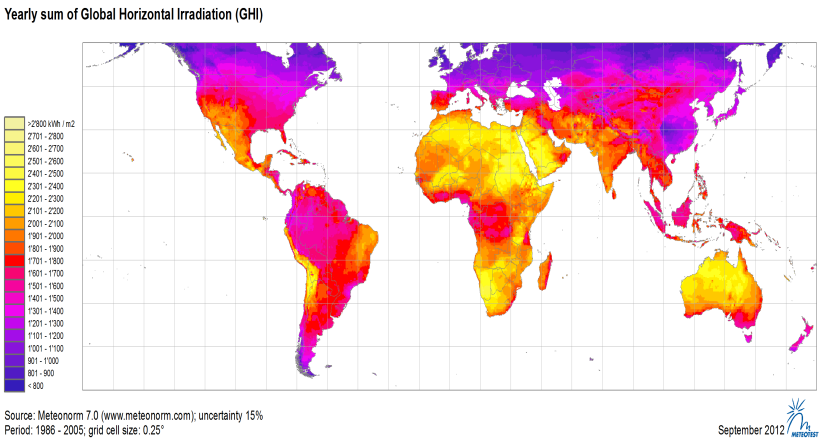

Figure 2.4: Yearly sum of Global Horizontal Radiation [39].

2.4.1 Belt with most favourable conditions

The belt with most favourable conditions lies between 15° and 35° both north and south of the equator and receives well over 2000 kWh/m^2 of solar radiation per year. It coincides with regions that are semi-arid, receiving less than 250 mm of rainfall annually and over 3000 hours of sunshine per year. There is so little rain because there is so little cloud cover, meaning that 90% of the sunlight received in these areas is direct solar radiation, which is the type of radiation required by solar concentrator systems. Of course, latitude is not the only factor involved in determining how much sunshine an area will receive. For Example, Durban is 29 ° South, which places it perfectly within the belt with the most favourable conditions, however due to other geological factors such as sea temperature and its proximity to the ocean, Durban experiences a large amount of cloud cover and thus only receives a yearly amount of 1700 - 2000 kWh/m^2, according to the scale in Figure 2.3, which makes it one of the poorest candidates for concentrated solar technology in South Africa.

2.4.2 Belt with moderately favourable conditions

This belt lies between 15° north and south of the equator and receives about 1500 kWh/m^2 of solar radiation per year. Humidity in this region is high, resulting in a large amount of cloud cover and an increased proportion of scattered solar radiation. This region receives about 2500 hours of sunshine per year. The intensity of the solar radiation in this region is fairly consistent because it is close to the equator and therefore does not experience much seasonal variation.

2.4.3 Belt with less favourable conditions

This belt lies between 35° and 45° both north and south of the equator and receives about 1000 kWh/m^2 of solar radiation per year. These regions are subject to large seasonal changes in solar radiation intensity and daylight hours because of the tilt in the Earth's axis and the elliptical orbit. As a result, the solar radiation received in winter is far less than that received in summer. However, on average, the amount of solar radiation received in these regions is similar to the amount received in the moderately favourable belt. This is because there is less cloud cover in this belt than in the moderately favourable one.

2.4.4 Belt with least favourable conditions

This belt lies between 45° and the Poles, both north and south of the equator and receives less than 1000 kWh/m^2 of solar radiation per year. About half of the solar radiation reaching these regions is diffuse because the incident rays from the sun are scattered by the large mass of air that lies between the sun and surface of the earth. The proportion of diffuse radiation is higher in winter than in summer because of frequent and extensive cloud cover.

2.4.5 Satellite vs Ground-based Measurements

Solar radiation maps use colour to indicate the intensity of the incident solar radiation on the surface of the Earth. Maps like these are useful in determining which areas of the planet are likely to experience a large amount of intense, consistent solar radiation, but they are not very accurate and they are not very specific. For example, should a company wish to build a solar power station in South Africa, Figure 2.5 would indicate that the best place to build it would be somewhere west of Kimberly. However, local ground-based measurements would be required before the final decision could be made on where exactly to build the station. One would need data on incident solar radiation intensity, average number of sunshine hours,

average cloud cover, terrain and so on before a decision could be made. Thus it is essential to be able to take large amounts of accurate ground-based measurements at the lowest possible expense.

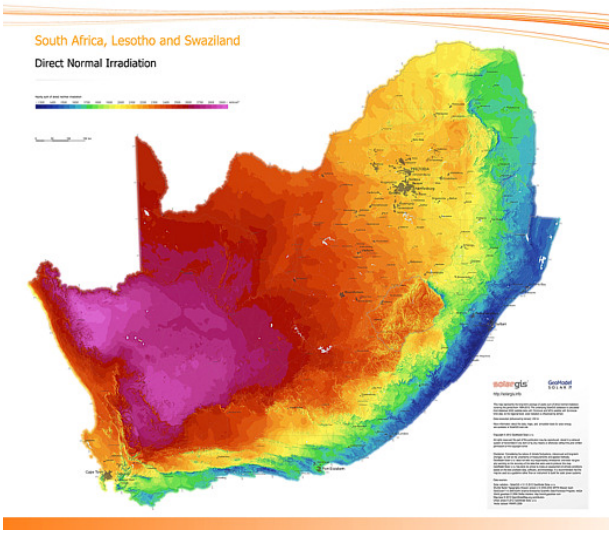

Figure 2.5: Solar radiation map of South Africa [40].

2.5 Sun-Earth Geometry

To an observer on the surface of the Earth, the sun appears to move in a circular arc across the sky, first appearing on the eastern horizon in the morning and finally disappearing under the western horizon in the evening. The geometry of the Sun-Earth system can be used to determine the exact position of the sun in the sky for a given latitude, longitude, year, day and time. Figure 2.6 is a schematic representation of the sun's path across the sky as well as the path of an incident ray from the sun towards the centre of the Earth.

Figure 2.6 shows that the strength of the incident ray depends on the zenith angle, θ, which is the angle between a beam of radiation from the sun and the vertical plane. The larger this angle is, the longer the path length and thus the weaker the incident ray and vice versa. The solar altitude, β, is the angle in the vertical plane between the beam of radiation from the sun and the projection of the sun's rays on the horizontal plane. The azimuth angle, ψ, is the angular displacement of the projection of beam radiation from the sun on the horizontal surface, measured from the north.

The angular position of the sun at noon relative to the equatorial plane is given by the declination (δ) [36], which varies 23.45° either side of 0° throughout the year because of the tilt in the Earth's axis [34]. It is this tilt that gives rise to the different seasons in the two hemispheres of the Earth. Figure 2.7 shows how the declination varies with the Earth's plane of rotation for particular days of the year. The declination and the solar altitude angle are related at solar noon by the following equation:

$$\beta = 90 + latitude - \delta \tag{2.1}$$

in the Southern Hemisphere, with the signs reversed in the Northern Hemisphere.

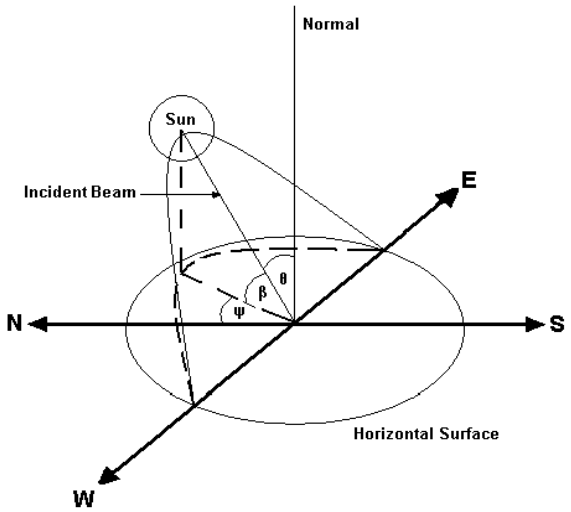

Figure 2.6: Schematic diagram of the sun's path through the sky as seen by an observer on the Earth's surface in the Southern Hemisphere for any given day.

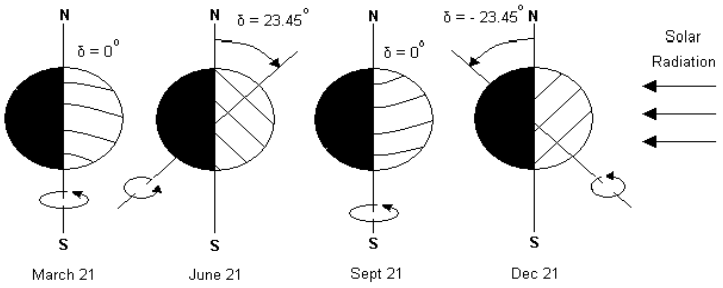

Figure 2.7: Illustration of the variation in declination for particular days of the year.

The distance between the sun and the Earth changes by about 1.7 % [31] throughout the year because of the Earth's elliptical orbit around the sun [41]. This, combined with the tilt in the Earth's axis results in a significant difference in the amount of solar radiation reaching the Earth's surface, depending on the time of year. The annual variation in the amount of solar radiation received by the Earth is about 6 % [41]. Figure 2.8 is diagram (not to scale) of the Earth's elliptical orbit.

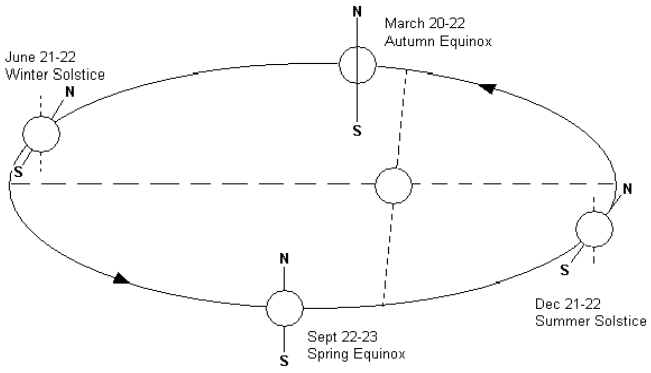

Figure 2.8: Earth's elliptical orbit (with ellipticity exaggerated) around the sun, showing the solstices and equinoxes as they occur in the Southern Hemisphere.

2.6 Solar Time and Clock Time

Solar time is defined by the sun's position in the sky and solar noon is defined as the time that the sun crosses the meridian of the observer [31]. A solar day is the amount of time it takes for the sun to return to the same meridian in the sky. This takes ~ 24.25 hours, which is slightly different to a clock day of exactly 24 hours. This difference in solar and clock time is due to the eccentricity of the Earth's orbit, which results in perturbations in the Earth's rate of rotation. Another reason for the difference between solar time and clock time arises from the difference in longitude between the observer and the longitude on which the clock time is based. These differences must both be accounted for when trying to determine the solar time relative to the clock time on a specific meridian. The equation used to correct the eccentricity of the Earth's orbit and the Earth's axial tilt is given by [31]

$$EoT = 229.2(0.000075 + 0.001868\cos B - 0.032077\sin B - 0.014615\cos 2B - 0.04089\sin 2B) \tag{2.2}$$

where EoT is the equation of time given in minutes and

$$B = (d-1)\frac{360}{365}, \tag{2.3}$$

in degrees where d is the number of days since the start of the year.

The net Time Correction Factor (in minutes) accounts for the variation in Local Solar Time within a given time zone due to the longitude variations.

$$TC = 4(LSTM - Longitude) + EoT. \tag{2.4}$$

LSTM is the Local Standard Time Meridian and the factor 4 comes from the fact that the Earth rotates 1° every 4 minutes. It is important to note that, by convention, longitudes West

are positive and longitudes East are negative. The Local Solar Time (LST) can be found using the previous 2 corrections to adjust the local time (LT)

$$LST = LT + \frac{TC}{60}. \tag{2.5}$$

The number of degrees that the sun moves across the sky is given by the hour angle ω. By noting that ω varies by 15° per hour, that $\omega = 0$ at solar noon and that the sign convention is that ω is negative before solar noon, the hour angle is given by

$$\omega = 15(LST - 12), \tag{2.6}$$

where 12 is the number of hours between solar midnight and noon.

Durban has a local meridian of 30.94 ° East and a standard meriadian of 30 ° East. Thus, at a clock time of 13:01:00 on 11 February, the solar time is 12:51:34.

2.7 Measurement of Solar Irradiation

Instruments used to measure solar radiation are called radiometers. Different radiometers make use of different detection principles to measure the incident solar radiation. The most common principles used are the thermomechanical, thermochemical, calorimetric and quantum or photodetection principles. The physics department at the University of KwaZulu-Natal has a suite of three Kipp & Zonen radiometers currently in operation: a pyrheliometer and two pyranometers, one with a shading ball to ensure that it only measures diffuse solar radiation. The pyrheliometer has an uncertainty of ±1.1% and the pyranometers have an uncertainty of ±1.4%, according to their calibration documents. These radiometers are mounted on an automatic Solys 2 Sun Tracker on the roof of the physics building, which is high enough that no ground-based structure can interfere with detectors' readings. Figure 2.9 (a) is a photograph of the radiometers mounted on the tracker.

Figure 2.9: (a) Photograph of the radiometers mounted on the tracker. (b) Photograph of the pyrheliometer. (c) Photograph of the pyranometer.

2.7.1 Pyrheliometer

A pyrheliometer is a device that measures direct solar radiation. It does not measure reflected or diffuse radiation. This is because it has a collimating tube that ensures that the only light

reaching the detector has travelled in a straight line from the entrance of the tube to the detector and is therefore direct solar radiation. Figure 2.9 (b) is a photograph of the Kipp & Zonen CH1 Pyrheliometer used to gather the direct solar radiation data during testing. A pyrheliometer is made up of a viewing window, through which the solar radiation enters the device, a collimating tube, which ensures that only direct solar radiation is detected, and a detector, which sends a signal to a data logger. The pyrheliometer in Figure 2.9 (b) is mounted on an automatic solar tracker, which moves the device in order to keep it pointing straight at the sun. The tracker is programmed to use GPS co-ordinates to determine the exact position of the sun in the sky and has to be calibrated in order to ensure that it tracks the sun accurately.

2.7.2 Pyranometer

A pyranometer measures global solar radiation. That is, it detects both direct and diffuse radiation. It is able to do this because it does not have a collimating tube. Instead, this device has a flat, horizontally orientated detector that can detect all incident solar radiation from one horizon to the other. This detector does not need to move with the sun, but this means that the detector will only detect the maximum available solar radiation intensity at solar noon because that is the only time that the zenith angle of the direct solar radiation is zero. At all other times it will be detecting maximum diffuse solar radiation and the value of the direct solar radioation multiplied by the cosine of its angle of incidence. Figure 2.9 (c) is a photograph of the Kipp & Zonen CMP11 Pyranometer at UKZN.

Chapter 3

An Overview of Solar Energy Systems

The sun emits energy in the form of radiation, and solar energy systems absorb this radiation and convert it to energy that can either be stored or used to perform work. Due to its interaction with the Earth's atmosphere, solar radiation incident upon the Earth's surface can be described as direct, diffuse or global. Solar energy systems can be split into two classes, based on which type of solar radiation they utilise. Both classes can also be further divided into large scale and small scale systems, depending on their size and function. Concentrated Solar Power or CSP systems use only direct solar radiation while Flat Plate systems use global solar radiation. The different types of solar radiation are discussed in detail in Chapter 2. When implemented on a small scale, such as domestic use, solar energy systems can be used to heat water, cook food and generate electricity. When implemented on a large scale, solar energy systems can harness enough solar energy to operate as electrical power plants, act as solar stills and desalinate water [42]. Concentrated solar power plants generate electricity by heating a fluid to turn a turbine or by powering a Sterling engine [43]. Due to the fact that solar energy is not available at all times, these large solar systems are often hybridized with conventional systems [44].

The system used in this experiment is a small scale concentrated solar power cooker with thermal energy storage. The following is an investigation of the different types of solar energy systems, followed by a review of the previous research that has been conducted on the various sub-systems that make up a solar cooker.

3.1 Flat Plate Collectors

In general, flat plate collectors do not concentrate the incident solar radiation and consequently they tend to employ a large surface area to absorb as much solar radiation as possible. The advantage of not concentrating the solar radiation is that these systems do not rely on direct solar radiation and therefore do not need to track the sun. This means that flat plate collectors still operate effectively in overcast conditions, when CSP systems are completely ineffective. The disadvantage is that flat plate systems cannot reach the temperatures that CSP systems can, but flat plate systems are generally not required to reach very high temperatures and as such this disadvantage is moot.

Although flat plate systems do not need to track the sun, their positioning is very important. They must be placed in an unshaded area, facing the equator and elevated to the degree of

latitude from the equator in order to experience maximum solar insolation. For example, if the system is 23° S, it must be elevated to 23° from the horizontal plane. There are many types of flat plate systems, with many functions. Three main types of systems are shown in Figure 3.1. These systems perform three major functions of a flat plate solar energy system: heating water, cooking, and generating electricity.

Figure 3.1: (a) Photograph of an array of photovoltaic cells [45]. (b) Diagram of a solar water heater [46]. (c) Photograph of a solar box cooker [47].

In general, flat plate systems consist of three components: a transparent cover, a housing for the collector, and an absorber [7]. The transparent cover allows solar radiation to enter the collector housing and insulates the absorber against heat loss due to convection. Unfortunately, the transparent cover does not transmit all of the incident solar radiation and some of the radiation is reflected or absorbed by the cover. The sum of the reflectance ρ, absorptance α, and transmittance τ must always equal 1 [7]. The transparent cover is usually made of glass, but the type of glass can affect how much solar radiation is absorbed, reflected or transmitted and the properties ρ, α and τ can be different for different wavelengths of solar radiation. For example, glass with a low iron content has a high transmittance, with $\tau \to 1$. The collector housing, combined with the transparent cover, insulates the absorber and protects it from the elements. The collector housing can be made of plastic, wood or metal and is insulated on the back and sides to minimize heat loss. Further heat loss minimization can be achieved by removing the air from the collector housing, leaving a vacuum which effectively stops convection between the cover and the absorber. The collector housing can reach stagnation temperatures of around 200 °C. Stagnation temperature is the temperature an object reaches when it is heated up without being able to transfer that heat to anything else. Since the absorber must be able to withstand such temperatures, it is usually made of metal, such as aluminium, copper or steel. There are many absorber designs and they are very specific to the function that the system is required to perform, so it is not possible to give a generalised description without including function of the system.

3.1.1 Flat Plate Water Heaters

Flat plate solar water heater systems range in complexity from a container filled with water and left in the sun to sophisticated and expensive systems controlled by microcontrollers, pumps and valves. A typical example of a flat plate solar water heater consists of a collector housing and transparent cover as described above, along with an absorber, a heat transfer system and a thermal energy storage. Once again there are many different absorber designs but in general they involve a flat plate of metal to increase the absorber's surface area, in contact with a metal pipe which transfers the fluid (usually water) that transfers the thermal

energy from the absorber to the storage. Figure 3.1 (b) shows a thermal water heater that uses evacuated tubes. These are tubes of glass that contain an absorber surface and a heat pipe within a high vacuum [48]. The heat pipe contains a temperature sensitive fluid such as methanol that vaporizes when the sun heats the tube. The vapour then moves up the pipe to the heat exchanger where it condenses and tranfers the energy to another fluid, which then tranfers the thermal energy to the storage. The heat transfer fluid may either be pushed about the system by a pump [49], or it could circulate itself by the thermosyphon effect [50]. Solar water heaters are often employed in conjunction with other water heaters such as gas or electrical water heaters [51]. In this configuration, the solar water heat provides warm water to the conventional heater, thus reducing the amount of energy required to heat the water to the desired temperature.

3.1.2 Box Cookers

Box cookers are generally very simple devices. They usually consist of a box with insulated back and sides, a transparent cover, which is often double-glazed to reduce heat loss [52, 53] and a cooking pot. The cooking pot is usually painted black to increase the amount of solar radiation that it absorbs and sometimes the box is painted black as well. Some boxes have reflective sides called booster mirrors to direct the solar radiation onto the cooking pot [54], while others employ concentrators to concentrate solar radiation onto the absorber surface [55]. As they do not require direct solar insolation, they do not need to track the sun [55]. They also do not store solar energy and so can only be used during the day. Mohamad et al [12] tested a simple wooden box with one reflector under field conditions in Egypt. Their tests achieved maximum temperatures of 160 °C inside the box and successfully cooked various food types. Their cooking time ranged from 1 to 2.5 hours.

Box cookers are limited by low capacity and long cooking times as well as low efficiency [56]. Concentrator type cookers are not as affected by such limitations. In 2003, Negi and Purohit [55] investigated the effect of a non-tracking concentrator on a box type solar cooker and compared their results to those of the same experiment conducted on a conventional box type cooker with a booster mirror. Both cookers were made of the same materials, had the same dimensions and were tested simultaneously under similar conditions. They found that the concentrator solar cooker reached stagnation temperatures 15-22°C higher than those of the conventional box type cooker and that the boiling point of water was reached 50 - 55 minutes faster with the concentrator cooker than the conventional box type cooker.

3.1.3 Photovoltaic (PV) Cells

Solar water heaters and solar box cookers use solar energy to generate thermal energy. Photovoltaic cells use solar energy to produce electrical energy via the photoelectric effect [7]. PV cells are made up of silicon semiconductors. In very simple terms, when an incident photon is absorbed by an atom in the semiconductor valence band, the energy from the photon is transferred to the atom's outermost electron. If the energy is sufficient to overcome the bandgap of the semiconductor, then that electron is transferred from the valence band to the conduction band and forms part of the electric current produced by the PV cell. These cells are connected together in large arrays that increase the absorption area and therefore increase the amount of electricity generated by the system[7]. There is a large amount of research into what materials are best for cheap and efficient photovoltaic cells as there are many different polymer combinations that can be tested [57, 58]. Research is even being conducted into the development of organic photovoltaic cells (OPV). OPVs have several advantages over their

inorganic counterparts such as lower cost, a simpler fabrication process and compatibility with flexible substrates [59].

3.2 Concentrated Solar Power (CSP) Systems

CSP systems absorb energy from the sun by concentrating direct solar energy onto a receiver. The ratio of the size of the concentrator aperture perpendicular to the incident solar radiation to the size of the receiver aperture gives a concentration factor. A large concentration factor results in high receiver temperatures. CSP systems generally consist of a concentrator, a receiver, a tracking mechanism, a heat transfer system, and (if required) a thermal energy storage system [60]. There are many varieties of these components and many factors that determine which type of component should be employed in a particular system. These components are not universally compatible with one another, so care must be taken when a designer chooses a specific component, as this choice will limit the number of other components that are compatible with the one chosen.

There are various configurations of concentrators and receivers and the receiver design is completely dependent on the concentrator. This is because it must have the same size and shape as the concentrator's focal area, so as not to incur losses. For example, if the receiver were too small, energy would be lost because some of the concentrated solar radiation would miss the receiver and would therefore not be absorbed. If the receiver were too big, thermal losses would occur as the receiver would then have to be heated by conduction at the parts where it was not illuminated by the concentrated solar energy. There are three major types of concentrators: parabolic, Fresnel, and heliostat, all of which can concentrate the incident solar radiation in two or three dimensions.

3.3 The Small Scale Solar Concentrating Cooker

A typical small scale solar concentrating cooker system is made up of a collector (which consists of a concentrator and a receiver), a method of transporting thermal energy from the receiver, a tracking system and sometimes a storage system. As stated previously, CSP systems can employ a variety of concentrator-receiver combinations and the same is true for concentrating solar cookers. The following is an investigation into the different solar cooker technologies that are available and the research that has been carried out to test and compare them.

3.3.1 The Concentrator

The concentrator defines the entire system. The size and shape of the concentrator affects the size and shape of the receiver and it also affects the type of solar tracking used. An effective concentrator is one that concentrates all of the solar radiation incident upon it onto as small a focal area as possible. The maximum theoretical concentration for a three dimensional concentrator, such as a parabolic dish is given by:

$$C = \frac{1}{sin^2\theta} \tag{3.1}$$

where θ is the half acceptance angle, and by:

$$C = \frac{1}{sin\theta} \tag{3.2}$$

for a two dimensional concentrator, such as a parabolic trough.

Parabolic Dish

In the ideal case, a parabolic dish focuses incident radiation to a point. That is, it focuses in three dimensions [60]. In practice, it is extremely difficult to fabricate a perfectly parabolic dish. As a result, most parabolic dish concentrators have a focal region, rather than a focal point. This is not a problem because the receiver needs to be the same size as the concentrator's focal area and a focal point would likely burn a hole in the receiver. Parabolic dishes can have two dimensional receivers such as a flat coiled pipe or they can have three dimensional receivers such as cavity receivers and convex receivers. Figure 3.2 (b) is a photograph of a parabolic dish.

Kaushik and Gupta [56] took experimental results for a comunity-size solar cooker and a domestic-size solar cooker, both with parabolic dish concentrators, and compared the instantaneous and daily energy and exergy efficiencies. The energy efficiency was defined as the ratio of the output energy to the input energy of the system and the exergy efficiency was similarly defined. The community-size cooker had a primary and secondary reflector configuration. In this configuration, the primary concentrator, with a reflective area of 7.3 m^2, focused incident solar radiation onto a secondary reflector, with a reflective area of 0.36 m^2, which directed the reflected radiation onto the cooking surface. This configuration allows the cooking surface to be somewhere other than the focal area of the primary reflector, for example, the primary reflector can be outdoors and the cooking surface can be indoors, provided there is no obstruction for the reflected radiation. The primary reflector used 3 mm thick acrylic sheets with a reflectivity of 73 % and the secondary reflector used alumimium sheets with a reflectivty of 65 %. The domestic-size cooker used a single reflector, with alumimium sheets, with a reflective area of 1.47 m^2. The community-size cooker had an average energy efficiency of 9.55 % while the domestic-size cooker had an efficiency of 25.28 %. They concluded that these low efficiencies were due to optical and thermal losses from the concentrator and receiver. They made some changes to the respective receivers, for example adding insulation, and found that the community-size system's average energy efficiency improved to 26.75 % and the domestic-size system's improved to 27.87 %.

Parabolic Trough

A parabolic trough is only parabolic in one plane, or two dimensions, and as such it focuses radiation onto a line [60]. Since the receiver must be the same size and shape as the concentrator's focal area, the ideal receiver is a straight pipe the length of the trough and the width of the focal area, placed at the focal point. Heat transfer fluid is pumped through the receiver where it absorbs the thermal energy from the receiver and transfers it to the rest of the system. The parabolic trough is a thoroughly researched and mature technology and systems that use a parabolic trough concentrator can reach temperatures of up to 400 °C [61]. Figure 3.2 (c) is a photograph of a parabolic trough.

In 2002, Hasan Hüseyin Öztürk [62] conducted experiments to evaluate the energy and exergy efficiencies (as defined above) of a parabolic solar cooker. The system consisted of a parabolic trough with a Cr-Ni alloy reflective surface and a cooking pot filled with water, placed in the centre of the concentrating reflector. The experiment ran between 10:00 and 14:00 solar time for seven days, and measurements were taken of the following quantities: ambient air temperature, water temperature profile from three thermocouples in the cooking pot, total solar radiation energy and the horizontal wind speed. These measurements were used to determine the instantaneous energy and exergy efficiency of the parabolic solar cooker. The energy efficiency of the system was found to be in the range $2.8 - 15.7$ % and the exergy efficiency was

$0.4 - 1.25$ %. The low value of exergy efficiency was expected as this is common in devices that use solar radiation. Öztürk concluded that exergy loss could be reduced by increasing the reflectivity of the reflective surface and increasing the absorptivity of the cooking pot.

Fresnel Concentrators

Fresnel concentrators use several strips of reflective material to approximate a lens [63]. They can use linear strips to approximate a parabolic trough or concentric rings to approximate a parabolic dish [60]. The same types of receivers can be used for the Fresnel concentrators as are used for their parabolic counterparts. This is because the receiver depends only on the size and shape of the focal area.

Sonune and Philip [64] tested a Fresnel concentric rings cooker in 2002. The cooker had an aperture area of 1.5 m^2 and a focal length of 0.75 m and the reflective rings were made of buffed stainless steel. They found that the cooker was capable of cooking food for up to five people. Franco et al [65] used a Fresnel type dish concentrator to pasteurize goat's milk by placing a vaporiser, which is a cylindrical coil of steel pipe, in the focal region of the dish. Water was converted to steam in the vaporiser and passed through a container of goat milk.

Heliostat

The final type of concentrator to be discussed is a heliostat. A heliostat is an array of flat mirrors, focused on a central receiver [60]. Each element of the array is able to track the sun independently of the other reflectors. As this is expensive and takes up a large amount of space, this system is usually employed by solar power towers to generate electricity on a large scale. Figure 3.2 (a) is a photograph of a solar power tower array. In 2009 Chern Sing Lim and Li Li [66] simulated the flux distribution of an 8×8 m non-image focusing heliostat with 289 mirrors which focused onto a 0.7 m aperture spherical concentrator with a 27 cm focal length and found a theoretical concentration of 25 000 suns.

(a) (b) (c)

Figure 3.2: (a) Photograph of a solar power tower [67]. (b) Photograph of a parabolic dish [68]. (c) Photograph of a parabolic trough [69].

3.3.2 The Receiver

Receivers are very specific to the system in which they are used. Their size and shape depends on the focal area of the concentrator, their position depends on the focal length of the concentrator and their operation depends on the heat transfer fluid used. There is a big difference between systems that employ a thermal storage and systems that do not. Systems without thermal storage have no need to transport the thermal energy away from the receiver. In this case, the receiver is the cooking surface, and for many systems, this is just a cooking pot, painted black and placed at the focus of the concentrator. This is obviously the most basic type of receiver. Other types of receivers include coiled pipe receivers, volumetric fibrous receivers, and cavity receivers.

Coiled Pipe Receiver

A coiled pipe receiver consists of a length of metal pipe bent into a coil and placed in the focal area of a concentrator. The heat transfer fluid moves from one end of the coil to the other, absorbing heat from the surface of the pipe and transporting it away from the receiver to the rest of the system.

In a previous version of the current experiment, Artur [70] investigated the thermal efficiency of a small scale solar cooker system which used a coiled pipe receiver. Her system consisted of a parabolic half-dish concentrator, an oil heat transfer system and an oil-pebble bed thermal storage. A pump circulated oil through the receiver to transport the thermal energy from the receiver to the storage. Her tests resulted in a system efficiency of 35 %, which was determined from the ratio of heat absorbed by the receiver to heat available to the receiver, expressed as a percentage.

Volumetric Fibrous Receiver

A typical volumetric fibrous receiver consists of metal fibres placed in the focal region of a concentrator. These fibres are often placed inside a glass dome, which stops wind from removing the thermal energy from the fibres. The heat transfer fluid (usually air) passes through the fibres and absorbs the themal energy from them and transports it to the rest of the system. The volumetric fibrous receiver can be placed within a cavity, thus making it a cavity receiver.

Cavity Receiver

A cavity receiver has an element of depth to it, allowing it to absorb solar energy on more than one surface and in more than one plane. Cavity receivers can be either convex or concave. The advantage of a concave receiver is that it can be embedded in insulation, which reduces heat loss. Further heat loss can be reduced by covering the cavity opening with a transparent material such as glass or quartz [71].

In 1994, Habeebullah et al [72] investigated the efficiency of a parabolic concentrating type cooker with an oven-type receiver as compared to the same cooker with a bare receiver. In this case, both receivers were cavity receivers. The oven-type receiver consisted of an insulated pot with a glazed insolation window. They developed numerical models for the bare receiver, which was an insulated pot without the glass window, and for the oven-type receiver to show theoretically the greater efficiency of the oven-type receiver.

In 2011, Hernández et al [73] designed and optimized a conical cavity receiver, which was able to receive solar insolation on both its outer and inner walls. The receiver was placed in the focal region of the concentrator, oriented like an upside down 'V' and was able to absorb radiation on both its inner and outer surfaces. They used detailed ray tracing simulations to compare cylindrical, conical and spherical receiver geometries and implemented the conical receiver on a 90° rim angle paraboloidal concentrator. Note, the rim angle is the angle between the central axis of the dish and a line that goes from the focal point (on the central axis) to the rim of the dish. Water was used as the heat transfer fluid and the thermal efficiency of the receiver was evaluated for different configurations of flow rate and inlet temperature. They also compared the measured fluid temperatures to those predicted by their thermal model.

Franco et al [74] improved work done previously by Saravia et al. in which they split the solar cooker into two separate parts: a 2 m^2 area concentrating Fresnel dish and an insulated box containing a pot. Franco et al. took that system, and improved its working capacity by using three different absorbers, optimized to fulfill different functions. The system was able to satisfy the needs of a communal dining centre.

Shuai et al [71] developed an energy transfer and conversion model for high temperature solar cavity receivers. They proposed a cavity receiver with a plano-convexo quartz window and a parametric study showed that the quartz window provided a more uniform solar radiation flux distribution, which resulted in a higher efficiency and lower heat loss than a windowless receiver. The window reduced convection losses and the uniform flux distribution reduced radiation losses caused by 'hotspots', which are caused by nonuniform flux distribution.

Reddy and Sendhil Kumar [75] conducted a two-dimensional numerical analysis of combined laminar natural convection and surface radiation in a modified cavity receiver. They found that the convective heat loss of the receiver was strongly influenced by its angle of inclination and the radiative heat loss was governed by the surface properties of the receiver.

Selective Absorber

Solar energy systems can improve the effectiveness of their receivers by covering them with a selective absorber coating. It is well known that black materials are excellent solar radiation absorbers. Consequently, many receivers are coated in temperature-resistant black paint to increase the temperature that they can achieve. The problem with black paint is that while it is an excellent absorber, it is bound by Kirchoff's law of emission of radiation, which states that for a given wavelength, absorptance $\alpha(\lambda)$ is equivalent to the emittance $\varepsilon(\lambda)$, which means that it is also an excellent emitter. As a consequence, the more energy it absorbs, the hotter it gets and the more energy it emits back into the surrounding environment. Glossy black paint has an emissivity of 0.92 [76]. Most of the radiation emitted by the sun has a wavelength smaller than 2 μm. A good absorber must have a very high absorptance in this range. By contrast, an absorber that has reached its stagnation temperature emits radiation in the infrared range, that is, greater than 2 μm. Thus a good absorber should have the smallest possibe absorptance in this range, because that would mean it would have poor emittance as well. A selective absorber is one that has high absorptance for radiation with wavelength less than 2 μm and low absorptance for radiation with wavelength greater than 2 μm. As a result, selective absorber coatings absorb solar radiation almost as well as black paint, but they re-emit far less infrared radiation, resulting in more thermal energy being tranferred to the heat transfer fluid. Materials used in selective absorber coatings include black chrome,

black nickel and TiNOX [7]. Even though selective absorber coatings are more expensive and more complicated to apply than black paint, their use has become common in solar thermal applications.

3.3.3 Receiver Losses

Receivers lose energy through thermal and optical losses, as well as through optical design errors. Optical design errors result in an incorrect relationship between the concentrator and the receiver, which means that some of the energy from the concentrator does not reach the receiver. Optical losses occur as a result of reflectance and transmittance losses, as well as scattering losses. Thermal losses can occur in three different ways: radiation, convection and conduction. There has been much research in determining receiver energy losses and in devising ways to limit these losses.

Prakash et al [77] investigated heat losses in a solar cavity receiver with a parabolic dish concentrator. They found that convective heat losses increased with increased mean receiver temperature and they decreased with increased receiver inclination angle (tested angles ranged from 0° with the cavity opening facing sideways to 90° with the cavity opening facing downwards). They also tested convection losses due to wind by comparing tests with no wind to those with wind speeds of 1 m/s and 3 m/s, from head-on and side-on directions. They found that wind travelling at 1 m/s induced losses of between 22 % and 75 % and a 3 m/s wind induced losses of between 30 % and 140 % for all receiver inclination angles, except for side-on wind at 0° receiver inclination angle. Note that the percentage in excess of 100 % meant that the receiver was losing more heat than it was receiving from the concentrator, in other words the receiver was actually cooling down because of the wind-induced convection losses. They concluded that a head on wind caused higher convection losses than a side-on wind.

3.3.4 Solar Tracking

Due to the Earth's rotation, the sun appears to move across the sky. CSP systems use direct solar radiation, which means that they must be properly aligned wth the sun in order to focus the solar radiation onto the receiver. Since the sun is moving, the CSP system must be able to move as well in order to keep the concentrated solar radiation focused on the receiver. This process is called solar tracking. There are several methods of approach in solar tracking: either the concentrator remains still and the receiver moves to remain in focus, or the receiver remains still and the concentrator moves to keep the receiver in focus, or the entire system moves with the receiver in a fixed position relative to the concentrator. Another method of solar tracking is the heliostat system, where many flat mirrors track the sun to focus on a central receiver [78]. Two of the most common configurations used in two-axis solar tracking systems are polar tracking and azimuth-elevation tracking [79]. For the polar tracking system, one axis is aligned along the north-south polar axis and is elevated from the hoizon to give it an angle equal to the local latitude angle. Rotation about this axis allows the collector to follow the sun's hour angle as it moves from the horizon in the east to the horizon in the west [80]. The other angle of rotation is perpendicular to this axis [81], [82] and rotation about this axis accounts for the change in the sun's path through the sky. This is referred to as the declination. For the azimuth-elevation tracking system, the collector is rotated about the zenith axis to follow the solar azimuth angle and it is rotated about the axis parallel to the Earth's surface to follow the solar elevation angle [79].

Systems that only concentrate solar radiation in two dimensions, such as parabolic troughs and linear Fresnel lenses only require one-axis tracking. They must be aligned along the local

meridian and then, as the sun passes from east to west, the concentrator simply rotates its hour angle to follow the sun.

Automation

The solar tracking system used can be fully automatic, semi-automatic or manual. Fully automatic solar tracking systems generally employ a large spectrum of electronic equipment including electric motors to move the system, sensors to detect position and some form of computer to control the operation. Fully automatic systems require no human input while they are in operation. Semi-automatic solar tracking systems can be electronic or mechanical. These systems generally operate with some sort of timer to control their operation and usually lack the ability to evaluate their position relative to that of the sun. This means that human supervision is required to ensure that the system continues to track the sun accurately. Manual solar tracking systems are unable to move themselves and require human input to direct them towards the sun. They have to be monitored and adjusted constantly to keep them tracking the sun.

Kaushik and Gupta [56] used a semi-automatic system, based on the mechanism of a clock with a counterweight pulling on a gear for their community-size solar cooker system, but chose to track the sun manually with the domestic-size cooker.

3.3.5 Heat Transfer Fluid (HTF)

The HTF transfers heat from one place to another within the system, as efficiently as possible. There are many types of HTF that could be used such as air, different types of gas, water, different refrigerants, phase change fluids and different types of oil. There are many characteristics that must be evaluated in choosing an HTF, such as boiling point, heat capacity, vapour pressure, toxicity, cost, availability and operating temperature. These characteristics must be evaluated with respect to the overall system characteristics. For example, if the system will operate at high temperatures but cannot tolerate high pressures, then water would be a poor choice of HTF because it vaporises at 100 °C and then begins to build high vapour pressures. The type of receiver also affects the type of HTF. For example, a fibrous receiver uses air as its HTF. A good HTF is essential for an efficient system.

Tirumula Tirupathi Devasthanam in India has the world's largest commercially successful solar steam cooker, which uses parabolic reflectors to concentrate direct solar radiation onto a receiver. It is an indirect cooker as it uses steam to transfer heat from the reveiver to the cooking pot. The reflector is made up of an array of 106 parabolic concentrators, mounted on the roof of a building and it produces enough steam to cook 30 000 meals per day [30].

3.3.6 Thermal Energy Storage

The Earth is diurnal, that is it has day and night. That means that the sun does not shine on one patch of ground 24 hours a day. The Earth also has weather, such as cloud cover and rain, which reflects the direct solar radiation, not allowing it to reach the Earth's surface. Thus, if one wishes to have solar energy at night or on a rainy day, an efficient method of storing this energy is required. Energy harvested from the sun can be converted into two forms, electrical energy and heat energy. There are many methods used to store energy, depending on whether the energy is electrical or thermal. Electrical energy can be stored by converting it to potential energy, which can be converted back to electrical energy when required. Chemical potential energy is stored in batteries, gravitational energy is stored by using excess energy to pump

water up to a raised storage tank and then allowing it to flow back down, using the pump as a turbine to generate electricity. Heat has to be stored as thermal energy. This means that insulation is critical as a poorly insulated thermal energy storage would lose energy rapidly and could even start a fire.

Mawire and McPherson [83] developed, simulated and tested a feed forward internal model control (IMC) structure for controlling the outlet charging temperature of an oil-pebble bed thermal storage (TES) and cooking system. Their overall system was made up of three-sub systems: energy capture, energy storage and energy utilisation. As their investigation was only concerned with the storage, the energy capture was simulated using an electrical hotplate in contact with a copper spiral coil and the utilisation was simulated using a heat exchanger. Positive displacement pumps were used to move the heat transfer oil between the three systems. They found that the feedforward IMC structure performed better than the combined feedforward and PID feedback structure in terms of stability in tracking the set temperature. They concluded that the feedforward IMC structure could be implemented successfully to control the outlet charging temperature of TES systems under variable electrical heating power.

Schwarzer and Vieira da Silva [84] designed and tested a solar cooking system which could operate with or without storage. The system consisted of three basic components: the collector, the cooking unit and the storage. The storage is of particular interest to this report as it was an oil pebble-bed storage system which consisted of a tank filled with pebbles and a vegetable oil heat transfer fluid which circulated through the system in natural thermosyphon flow. They tested the system by measuring cooking power and efficiency. They found that the system worked well, but it was expensive and costs would have to be reduced through mass production in the country where they would be used and financial aid if large scale use of solar cookers was to be realised.

3.3.7 Comparison of Different Types of Solar Cookers

There are many different types of solar cookers that utilise solar energy in different ways to achieve the goal of cooking food. As such, it is difficult to compare one type of cooker with another, as they use very different methods to achieve the same goal. Schwarzer and Vieira da Silva [85] compared the thermal performance of different types of solar cookers in 2008. To do this, they first classified solar cookers into different types, based on the type of concentrator and whether or not the cooking process was direct or indirect. Then they defined the basic characteristics and the experimental procedures required to test the cookers. Finally they used the variables that they had measured to calculate the parameters required for the comparison. They also presented a simplified analytical model for the design of simple cooking systems.

Pohekar and Ramachandran [86] compared the parabolic solar cooker with eight other domestic cooker devices in India. They evaluated thirty different criteria using the Multi Attribute Utility Theory model and found, on the basis of expert opinion and user preference that parabolic solar cookers ranked fourth out of the nine devices. They then identified possible areas of improvement for the increased use of parabolic solar cookers. They concluded that more people would use parabolic solar cookers if an effort was made to increase awareness, confidence and technical improvement. They carried out similar investigations in 2005 [87].

Hosny and Abou-Ziyan [88] compared the performance of two full tracking solar cookers. They designed, constructed and tested a paraboloid dish solar cooker (PDSC) and a booster mirror

solar box cooker (BMSBC). The tests were carried out under the same operating conditions during a winter season in Cairo. They found that the PDSC had a higher rate of cooking than the BMSBC and it was also able to handle various types of cooking, even under intermittent sunny and cloudy conditions. They also made comparisons between receivers that had been painted black as opposed to unpainted receivers and investigated the effect that wind speed had on heat loss for the PDSC receiver. After performing various indoor tests with varying windspeeds up to 8m/s they developed a wind shield, which reduced heat loss by up to 35% .

In 1998, Patel and Philip [89] conducted tests on three types of domestic solar concentrating cookers to evaluate their thermal performance and cooking abilities. They measured the stagnation temperature of all three devices, as well as their ability to cook food and to heat water. Two of the devices were Fresnel ring concetrators and the other was a paraboloidal concentrator. The reflective surface on all three devices was aluminium film. Even though the paraboloidal cooker outperformed its rivals in all three tests, Patel and Philip concluded that the Fresnel rings concentrator was better because it gave an even concentration distribution, whereas the paraboloidal concentrator's point focus could result in uneven heat distribution in the cooking vessel, which could in turn result in burnt food.

Chapter 4

System Construction and Design

The solar concentrator cooker system used in this project was based on the system that was used by Celia Artur during her Masters research in 2009-2010 [70]. The original system, designed and constructed by Robert Van den Heetkamp and used by Artur, had fallen into complete disrepair and had to be largely reconstructed and partly redesigned. Figure 4.1 is a diagram of the system, as used in this experiment. The original system consisted of a concentrator, a receiver (designed and constructed by Artur), a tracking system, a heat transfer system, a thermal energy storage and a measurement system. The design and construction of the new system is discussed in the following sections.

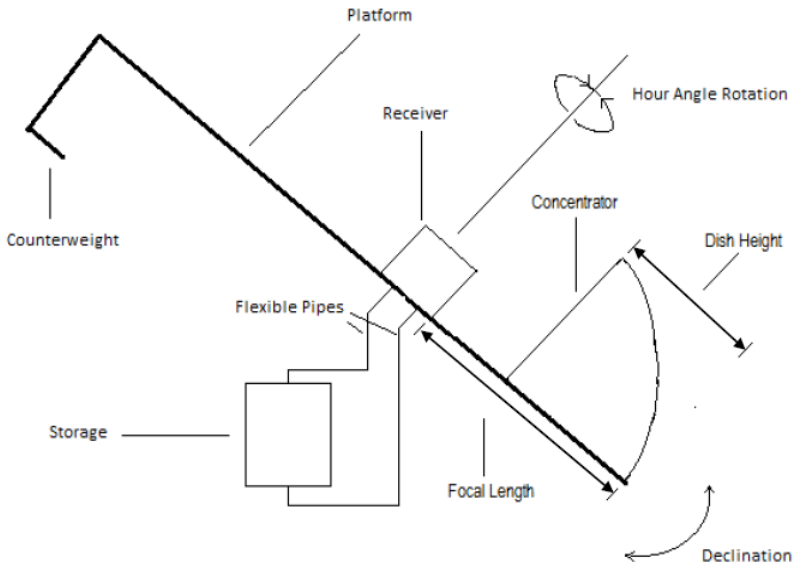

Figure 4.1: Simple diagram of the solar cooker system (not to scale).

4.1 Concentrator

The solar radiation concentrator was half of a parabolic satellite dish. The full dish consisted of six equal petals, so the half dish used was made up of three petals. These petals were covered with trapezoidal mirror tiles and focused using a manual raytracing technique, which

will be discussed later. The three petals were then mounted together onto a flat steel plate and mounted onto the tracking structure. According to the dish specifications, the concentrator had a diameter of 2.4 m, a focal length of 0.915 m and a height of 0.039 m (see Figure 4.1). The collector surface area of 2.49 m^2 was calculated using equation 4.7 and then applying equation 4.8, since the concentrator was only half of a parabolic dish. The concentrator aperture area of 2.26 m^2 was calculated using equation 4.1 and applying equation 4.2. Figure 4.2 is a photograph of the concentrator. The following sections describe how the concentrator

Figure 4.2: Photograph of the concentrator dish mounted on the steel plate.

was designed, constructed and installed.

4.1.1 A Mathematical Description of the Parabolic Dish

The following is a mathematical description of a paraboloid. The satellite dish used in this experiment was not a perfect paraboloid, and the mirror tiles placed upon the surface of the dish do not amount to a perfect paraboliod, but they approximate a perfect paraboloid, and so the mathermatics will be assumed to be the same. Before a mathematical treatment can begin, a few terms must be defined (see Figure 4.3). The *focus* of the parabolic reflector is the point where all the reflected rays converge. The *vertex* is the point at the centre of the parabolic reflector. The *focal length* is the distance from the vertex of the parabolic reflector to its focus. The *aperture* is the opening of the parabolic reflector and is described by [90]

$$A = \frac{\pi D^2}{4} \tag{4.1}$$

where D is the diameter of the parabolic reflector. For a half dish, as used in this experiment, the *aperture* is given by

$$A_{half} = \frac{A}{2}. \tag{4.2}$$

The area concentration ratio as defined by Duffie and Beckman [31] is given by

$$C = \frac{A_a}{A_r} \tag{4.3}$$

where A_a is the area of the concentrator aperture and A_r is the area of the receiver surface. The focal length of a parabolic dish is given by [90]

$$f = \frac{D^2}{16d} \tag{4.4}$$

where D is the diameter of the dish and d is its depth. The general equation for a parabola in terms of its focal length f is given by [90]

$$y = ax^2 \tag{4.5}$$

where

$$a = \frac{1}{4f}. \tag{4.6}$$

The surface area of a parabolic dish is given by [90]

$$S = \pi \frac{(a^2D^2 + 1)^{3/2} - 1}{6a^2}. \tag{4.7}$$

Since the dish used in this experiment was half a parabola, its surface area was determined by

$$S_{half} = \frac{S}{2}. \tag{4.8}$$

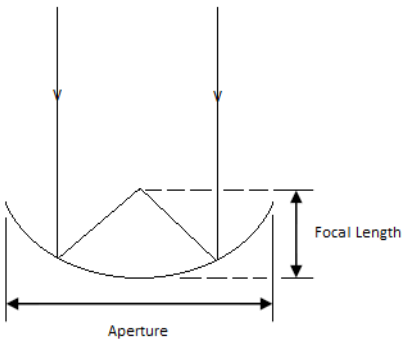

Figure 4.3: Diagram of a paraboloid.

4.1.2 Design

The original decision to use a half dish concentrator as opposed to a full dish concentrator was made by Robert van den Heertkamp in the design of the old system, and since the concentrator was integral to the overall design, it was not possible to change the concentrator without changing the entire system. As a result, a similar parabolic half dish concentrator was designed and constructed for the new system.

In order for the concentrator to reflect the solar radiation onto the receiver, the surface of the concentrator had to be covered with a reflective material. Several reflective materials were considered, such as reflective paint, reflective film, and glass or perspex mirror. Reflective paint was not reflective enough and it depended too much on the dish having a good focus. It was also not very resilient against scratches, which is not good for a device that permanently operates outdoors. Reflective film had similar problems in terms of reliance on dish accuracy and resilience and although it was highly reflective, it was rather expensive and had to be imported from the USA. Reflective materials that were not considered include Aluminium and Silver.

Glass vs Perspex Mirrors

The old concentrator used perspex mirrors, but many of those tiles had been damaged, either cracked or desilvered. The advantage of perspex is that it is lighter and less fragile than glass, but it is also expensive and since this experiment is meant to be low cost, it was decided to use glass mirrors. Considerable time was spent trying to source glass mirror with low iron content. Iron in glass absorbs solar radiation, so glass with low iron content would be even more reflective. Unfortunately, low iron content glass mirror could not be sourced, so ordinary glass mirror was selected. A glass thickness of 1 - 2 mm would have been ideal, as thicker glass is heavier and absorbs more radiation, but unfortunately the thinnest glass mirror that could be found was 3 mm thick.

Mirror Tile Design Program

The sheets of glass mirror were cut into trapezoidal tiles in order to fit onto the surface of the parabolic dish. The tile dimensions were determined using a Matlab program designed by Professor Jørgen Løvseth from the Norwegian University of Science and Technology (NTNU). Trapezoidal tiles cover more of the parabolic dish surface area than rectangular tiles because the top side of the tile is wider than the bottom side. To understand this, consider a three dimensional parabola as shown in Figure 4.4. If a horizontal strip is removed from the parabola and then measured, one would find that the top side of the strip is longer than the bottom side because as the parabola increases in height, it spreads outward, away from the central axis. The program used the dish dimensions as inputs and calculated the dimensions and number

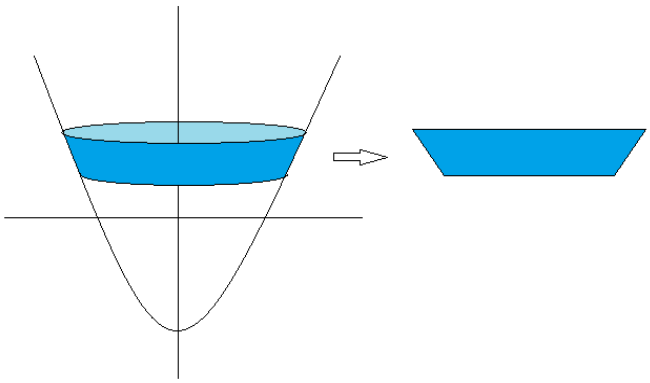

Figure 4.4: Diagram of a paraboloid, with a horizontal strip.

of trapezoidal tiles required to effectively cover the surface of the dish. Once the program was run, paper tiles were cut to the dimensions given by the program. These tiles were then placed onto the petals and attached with a temporary adhesive called “Presstick”which could easily be removed. Unfortunately, the dimensions given by the company who sold the dish were inaccurate and the dish was not very well made (different petals are clearly slightly different in size). Since the program required precise inputs, it did not manage to produce tiles with dimensions that fit perfectly to the petals. As a result, the program had to be run and tested several times until a fairly good match was found, and then the paper tile dimensions were still adjusted slightly to get a better fit. Once a satisfactory set of paper tiles was made, they were sent to Build It Hardware Store for the mirror tiles to be cut by hand. Obviously, hand cut tiles cannot be as accurate as laser or laserjet cut tiles, but accuracy of the tiles was not

critical and it was decided that it would be quicker and cheaper to have them handcut. See Table A.1 in the appendix for more information regarding tile dimensions.

4.1.3 Construction

Once the tiles had been received, they were placed onto the petals with Presstick so that the focal region of the dish could be found. This was done using a raytracing technique similar to that described by Van den Heetkamp et al [91] when they proved that a laser diode could be used to determine the focal length of a concentrator and the spatial extent of the focal point. The raytracing was performed manually using a laser, a target and a mounting for the dish petals. The laser was mounted on an extendible arm, which in turn was mounted on wheels. This meant that the laser was easy to manoeuvre over the petal to point at the centre of any single mirror tile. The laser was also mounted on a swivel joint and weighted so that it always pointed vertically downwards. The petal was placed on the floor and the rim was rested on a metal structure, constructed to give the petal a height of exactly 39 cm, which was the given height of the dish. The target was then placed in front of the petal and set to a specific height. The target was a perspex sheet with holes in all four corners, which allowed it to be moved up and down. A sheet of paper was then placed on the perspex and attached with Presstick. The laser was pointed to the centre of a tile, and the position of the reflected point was marked on the sheet of paper. This process was repeated for every tile on the petal and then the height of the target was changed and the experiment was repeated. This allowed a rough focal length to be determined. Figure 4.5 is a diagram illustrating the experimental setup used during raytracing.

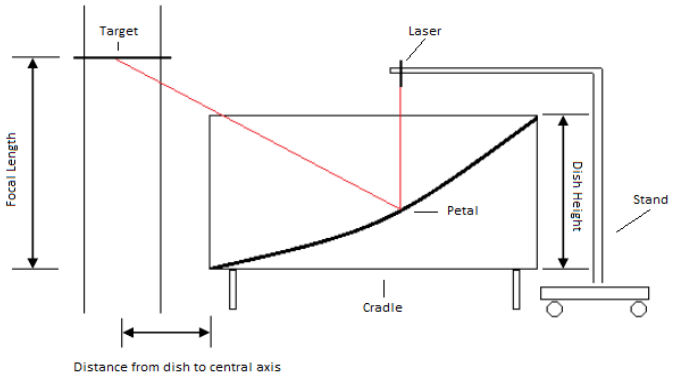

Figure 4.5: Diagram illustrating the raytracing experimental setup.

One problem with this setup was that the petal was not properly secured and could easily be bumped out of position, so a cradle, shown in Figure 4.5, was constructed to hold the petal in place. Figure 4.6 is a photograph of a petal mounted in the cradle. It was decided to construct the cradle by measuring the dimensions of the backing plate to which the collector would be mounted. The backing plate was measured to give the dish a height of 40 cm, not the 39 cm required. This slight difference would have resulted in a significant difference in the position of the focal point of the petal and would have ruined the experiment had the dish been focused using a height of 39 cm and then mounted to the backing plate with a height of 40 cm.

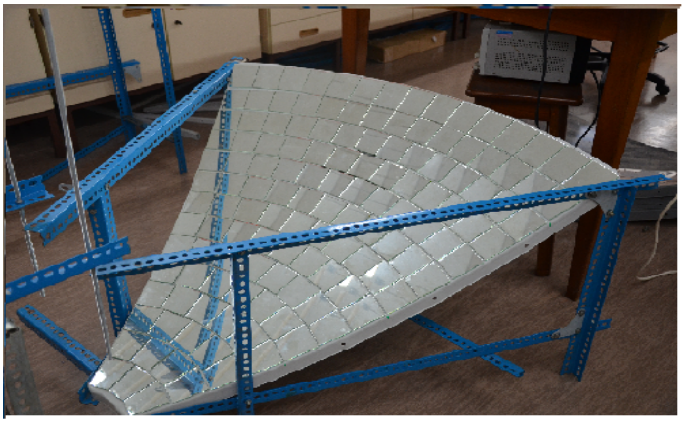

Figure 4.6: Photograph of a petal mounted in the cradle.

Finding the Central Axis

It was initially assumed that the central axis would be the point where the two sides of the petal would meet if extended, which indicated that the central axis of the parabolic dish was 12.5 cm from the tip of the petal. This was found to be incorrect when the different petals' focal regions did not overlap at this distance. So a measuring tape was used to measure 1.2 m (the radius) from a perpendicular line dropped from the rim of the petal. This method found that the central axis of the parabolic dish was actually 16 cm from the tip of the petal. This measurement was confirmed when the petals were bolted together to form a half-dish and the semicircle between them was measured.

Finding the Focal Region

Since each petal is supposed to be identical, and is supposed to focus radiation to the same point as all the other petals, once the focal region was found for one petal, it was assumed to be the same for all the others. As mentioned above, the tiles were first stuck to the petals with Presstick. Raytracing, as described above was then performed at different focal heights. The given focal length of the dish was 0.915 m, so tests were performed over a range from 1 to 0.75 m, in steps of 0.05 m. It was found that a focal length of 0.90 m yielded the smallest grouping of points. A second series of scans from 0.92 to 0.88 m in steps of 0.005 m showed that the manufacturer's length of 0.915 m had the smallest grouping of points. However, while the grouping was small, it centered on a point about 0.08 m from the central axis. This meant that when all three petals were combined, each petal focused on a different point, 0.08 m from the central axis, as shown in Figure 4.7 where the different colours represent points from the different petals (similarly in Figures 4.8 and 4.9. It was decided that it would be easier to reduce the size of the focal area (by better focusing of the mirror tiles) than to change the point at which the petal focused.

As can be seen from Figures 4.7 and 4.8, using different focal lengths, when combining the petals changed not only the size of each respective petal's focal area but also the combined focal area of all three petals. Thus a compromise precision and accuracy had to be reached which would allow the smallest focal area per petal (precision) as well as the smallest combined focal area (accuracy). A focal length of 0.840 m was selected as this was the focal length at which the focus was centred on the central axis, as shown in Figure 4.8. The focus of the three petals was combined by running the ray trace test on all three petals, one after the other,

using the same piece of target paper, but rotating the target with respect to the petal so that it would have the same orientation as it would have when the petals were mounted.

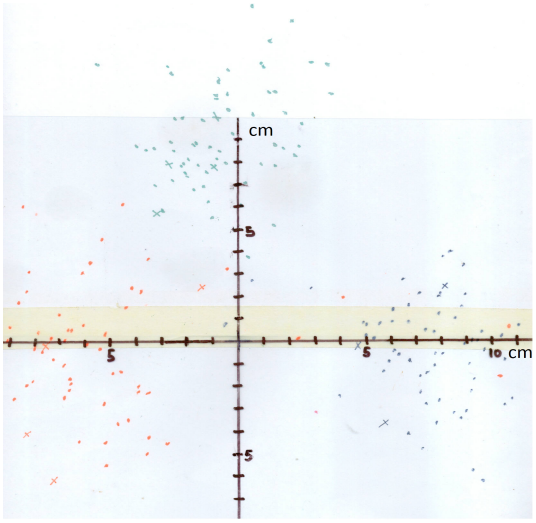

Figure 4.7: Combined focal area of all three petals for focal length of 0.915 m. The three colours represent the three petals.

Once a focal length was chosen, the mirrors all had to be removed from the petals, cleaned

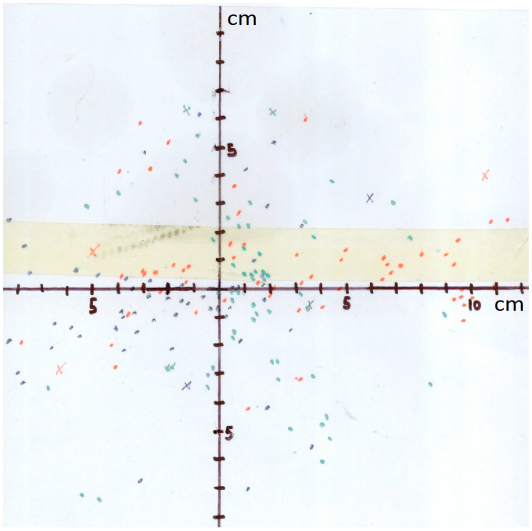

Figure 4.8: Combined focal area of all three petals for focal length of 0.840 m. The three colours represent the three petals.

up and then placed back onto the petal with silicone placed on the back of the mirror. Ray tracing was then repeated and the mirror was adjusted, by pressing down on the required corner, so that the laser would be reflected to as close to the centre of the target as possible. Once all the mirrors had been placed and allowed to set, a final combined raytracing was performed using each petal and the same target to determine the final focus of the dish. This is shown in Figure 4.9. Figure 4.8 shows points spread across a target radius of well over 10

cm whereas Figure 4.9 shows points confined within a target radius of under 5 cm, showing a significant improvement in the focus of the dish.

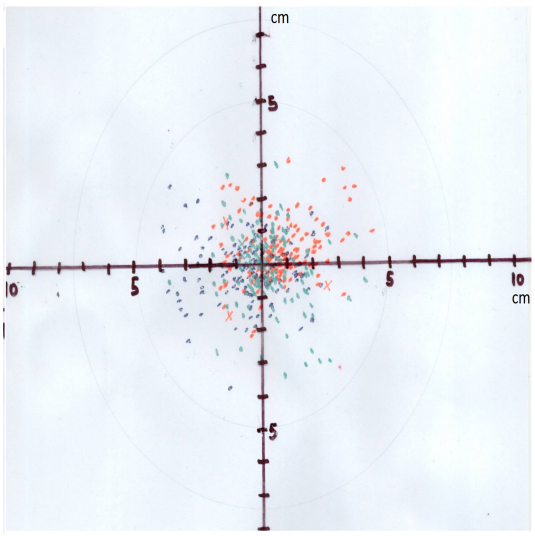

Figure 4.9: Combined focal area of all three petals for focal length of 0.840 m, after focusing. The three colours represent the three petals.

4.2 Receiver

Two different receivers and a test plate were used in this experiment. Figure 4.10 is a photograph of the receivers and the test plate.The test plate was a flat plate of stainless steel, the first receiver was a flat coiled pipe receiver designed and constructed by Artur [70] and the second was a coiled pipe cavity receiver. All three were painted black on the side facing the concentrator so that they would be able to absorb the maximum amount of thermal energy and so that their absorbtivity was uniform. The test plate was used to determine where the focal area of the concentrator was. In other words, it was used to determine where the receiver should be placed in relation to the concentrator. It was also used to measure the stagnation temperature of the system as it had no heat transfer fluid to remove the thermal energy that it had absorbed. The plate was circular with a diameter of 300 mm and a 1 mm thickness. The flat coil receiver was used as a benchmark against which the cavity receiver could be compared.

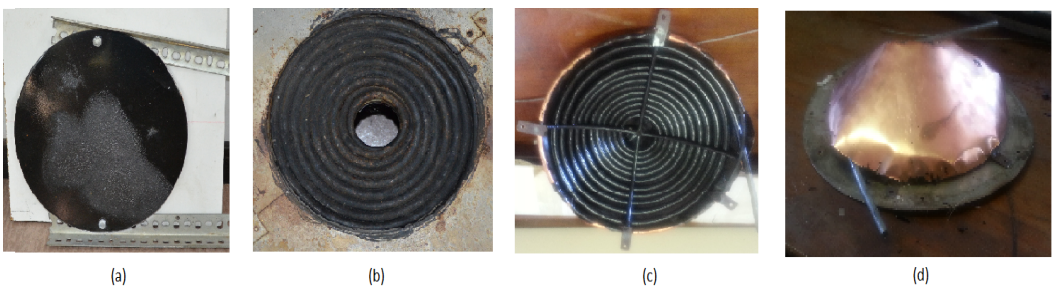

Figure 4.10: Photographs of the test plate and the receivers. (a) Test plate. (b) Flat coil receiver. (c) Cavity receiver from underneath. (d) Cavity receiver from above with copper covering.

The flat coil receiver consisted of a stainless steel pipe with dimensions 10 mm outer diameter and 8 mm inner diameter bent into a coil of diameter 250 mm. The pipe was stainless steel because stainless steel has a high melting point and has good resistance against corrosion. Copper is more maleable and therefore easier to bend into a coil and it is better at transferring heat than stainless steel, but it was feared that copper would react unfavourably with the oil that was used as the heat transfer fluid and so stainless steel was chosen as the better option. The flat coil was then encased in an insultating cylindrical stainless steel box with a 400 mm diameter and a height of 170 mm. This box was filled with a fibreglass insulation called Superwool. Since this receiver (used by Artur in her experiment [70]) was still in working order, it was decided to build a different type of receiver and compare the two. The differences between flat receivers and cavity receivers are discussed in Chapter 3. Figure 4.11 (a) is a photograph of the flat coiled receiver inside the insulating box before the insulation was installed, note the thermocouple probes at the entrance and exit of the coil. Figure 4.11 (b) is a photograph of the cavity receiver inside the insulating box, mounted onto the solar cooker system.

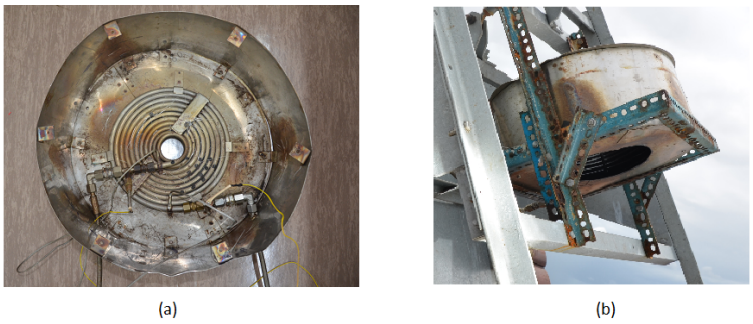

Figure 4.11: (a) Photograph of the flat coil receiver inside the insulating box. (b) Photograph of the cavity receiver inside the insulating box, mounted onto the solar cooker system.

The cavity receiver had the same pipe dimensions as the flat coil receiver. It was constructed by bending a pipe into a flat coil and then the cavity was formed by pushing the centre of the flat coil up to create a cup shape as seen in Figure 4.12. The cup shaped receiver was designed to have an aperture diameter of 250 mm and a depth of 125 mm however, difficulties in construction resulted in the receiver having an aperture diameter of 300 mm and a depth of 75 mm. This cup shaped spiral was then covered with a sheet of copper to stop solar radiation from passing through the gaps in the coil and to improve insulation. It improved insulation by limiting convection losses from the fibreglass insulation and also increased receiver efficiency by reflecting radiation onto the receiver coil. The same cylindrical insulating box was used for both receivers as the coils could be added or removed with relative ease.

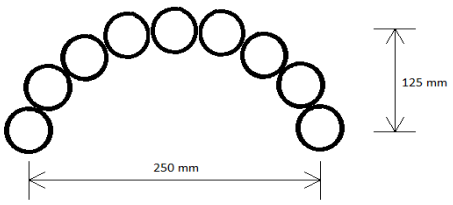

Figure 4.12: Cross section diagram of the cup shaped receiver.

4.3 Heat Transfer Fluid

The heat transfer fluid used in the old system was an oil called Calflo High Temperature Heat Transfer Fluid, manufactured by Petro-Canada. This oil is recommended for use in non pressurised, liquid phase, closed heat transfer systems. It is non toxic, not a respiratory or skin irritant and, unlike synthetic aromatic fluids, it is virtually odourless. These are important characteristics to take into account given that this system is used in the preparation of food. It has a maximum bulk operating temperature of 326 °C and a maximum tubeskin temperature of 343 °C and has strong thermal and oxidative stability, which means that it can be exposed to air without oxidising, though this is not recommended. The term 'tubeskin' refers to the layer of oil molecules in contact with the pipe surface and 'bulk temperature' refers to the average temperature of the entire volume of oil. Refer to Table B.1 in Appendix B for more Calfo HTF technical data. This oil was used by Artur [70] and since it performed well in her experiment and there was still plenty of it available, it was decided to use Calflo HTF as the heat transfer fluid in this experiment.

The oil was transferred through the system using flexible steel hoses of inner diameter 8 mm and outer diameter 10 mm. The oil was pumped through the system by a positive displacement gear pump taken from a motorbike, powered by a 24 V, 20 A DC electric motor that, at maximum power, could operate at a maximum speed of 4500 RPM and a maximum torque of 0.5 Nm. Figure 4.13 is a photograph of the pump, motor and hoses. The pump and

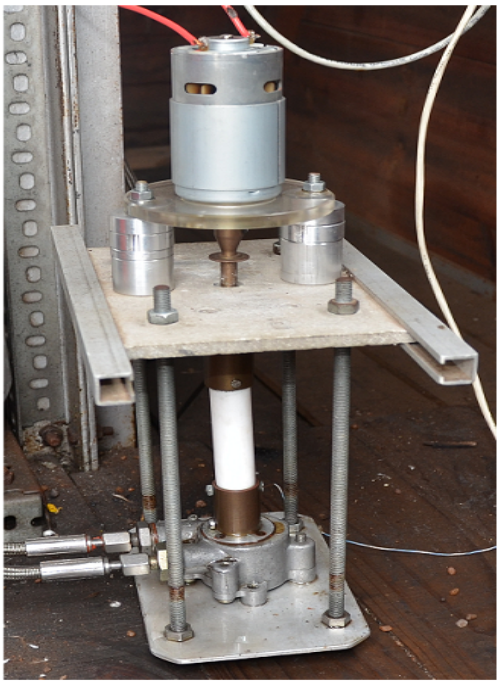

Figure 4.13: Photograph of the oil pumping mechanism.

the hoses were taken from the old system but the motor that powered the pump was new.

4.3.1 Laminar and Turbulent flow

There are three classifications of fluid flow, first distinguished by Osborne Reynolds in 1883, namely *laminar*, *transitional* and *turbulent* flow. In the extremely simplified case, laminar flow

consists of only one component of velocity, $\mathbf{V} = \mathbf{u}\hat{\imath}$, where $\hat{\imath}$ is the direction along the pipe and turbulent flow consists of $\mathbf{V} = \mathbf{u}\hat{\imath} + \mathbf{v}\hat{\jmath} + \mathbf{w}\hat{\mathbf{k}}$, with $u\hat{\imath}$ being the predominant value. In other words, during laminar flow, all the particles of the fluid move uniformly in the same direction at the same velocity. In the case of tubulent flow, while the overall movement of the fluid is in the direction of the pipe, the individual particles may move in any direction. Transitional flow exists when a flow is changing from laminar to turbulent or vice versa. During transitional flow, the fluid can be described as both laminar and turbulent as it has components of both.

The nature of the flow of a fluid moving through a pipe is governed by the Reynolds number, which is a dimensionless quantity defined as the ratio of the inertia to the viscous effects in the flow and is given by the following equation [92]

$$Re = \frac{\rho V D}{\mu} \tag{4.9}$$

where μ = fluid viscosity [N.s/m^2], ρ = fluid density [kg/m^3], V = mean fluid velocity [m/s] and D= pipe diameter [m].

The Reynolds number for laminar, transitional and turbulent flow is not precise because the flow also depends on other factors such as the roughness of the pipe and pipe vibrations. As a result, the Reynolds number in a round pipe is given as less than approximately 2100 for laminar flow and greater than approximately 4000 for turbulent flow. Anything between those two values is considered transitional flow.

In truth, laminar flow is not as uniform as the simplified case suggests. Any viscous fluid moving through a pipe, whether laminar, tubulent or transitional, has a velocity profile. This profile arises due to the fact that the fluid particles that are in contact with the surface of the pipe are stationary and those particles near the pipe surface move with a lower velocity than those in the centre of the pipe. In the case of this experiment, a laminar flow through the receiver would result in a steep temperature difference between the particles near the pipe surface and those in the centre of the pipe. This temperature difference would arise for two reasons: firstly, heat is transferred by conduction through the pipe walls of the receiver and thus the particles near the pipe surface receive this energy first and then pass it on towards the particles in the centre of the pipe and secondly, the particles near the pipe surface are moving more slowly than those near the centre, which means that they have more time to absorb more energy. Conversely, a turbulent flow would allow particles of oil to mix. Particles with a high temperature would come into contact with particles with a lower temperature, resulting in a more uniform distribution of thermal energy throughout the oil. A turbulent flow is considered preferable for this experiment because of the better energy distribution and because of the reduced risk of the oil particles in contact with the receiver surface reaching dangerous temperatures and charring.

4.3.2 Pipe Losses

Once the energy has been conducted from the oil to the outer surface of an uninsulated pipe, it is lost via radiation and convection. The higher the oil temperature and the longer the uninsulated pipe, the higher these losses can be expected to be. The pipes used in this experiment were not very long and the oil temperatures were not expected to be very high. This meant that the heat loss from the pipes was not expected to be particularly high and so the pipes were left uninsulated.

4.4 Storage

A new storage system was designed and constructed. This system consisted of a steel drum with a height of 400 mm and a diameter of 400 mm, which was filled with pebbles up to a height of 350 mm. The pebbles had a density of 2380 kg/m^3 and a specific heat of 1200 J/kg.K. The storage was wrapped in two layers of Superwool Plus thermal insulation which has a thermal conductivity of 0.025 W/m.K. Each layer of the insulation was 25 mm thick, resulting in a total insulation thickness of 50 mm. The heat transferred from the outer surface of the storage tank to the outer surface of the insulation would be transferred by conduction. Thus the power lost by the storage could be calculated using the Law of Thermal Conduction [94]. For example, if the temperature of the surface of the storage tank is 100 °C, or 373 K and the temperature of the surrounding air is 25 °C, or 298 K, the power loss due to thermal conduction would be

$$P = kA|\frac{dT}{dx}| = 0.025(\pi 0.4 \times 0.4)\frac{373 - 298}{0.05} = 18.85W. \tag{4.10}$$

where k is the thermal conductivity in W/m.°C and A is the cross-sectional area [94]. More layers of insulation would have reduced this power loss even more, but two layers were considered sufficient as a power loss of 18.85 W is not very much. The storage tank was fitted with an expansion tank, which connected through a flexible pipe to the bottom of the storage. This meant that when the oil heated up and began to expand, the cooler oil at the bottom of the storage was pushed into the expansion tank. When the system began to cool again, the oil contracted and re-entered the main storage vessel. The new system was designed in partnership with Mr Evans Zhandire at UKZN. Figure 4.14 (a) is a diagram of the storage. Figure 4.14 (b) is a photograph of the storage before it was filled with pebbles.

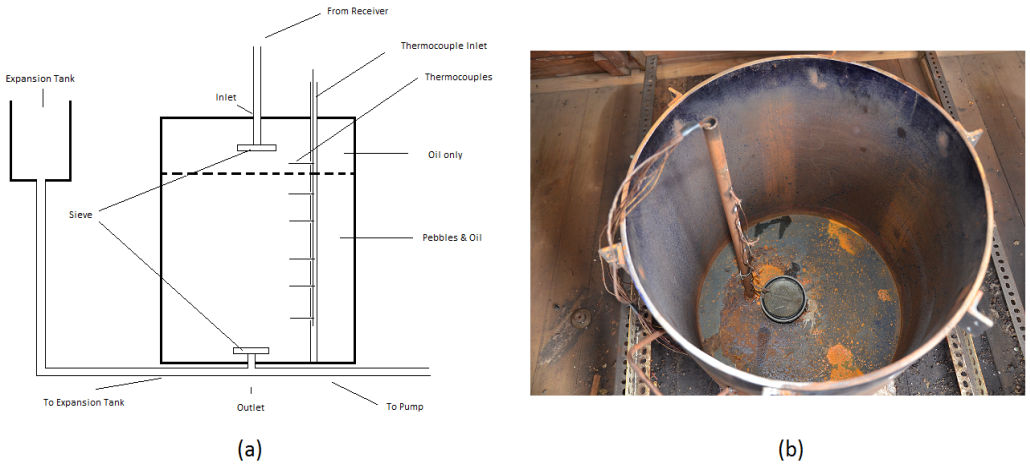

Figure 4.14: (a) Cross section diagram of the thermal energy storage. (b) Photograph of the storage before pebbles were added.

4.5 Solar Tracking

The solar tracking system was a two axis tracking system, as described in Chapter 3. The system had been designed by Van den Heetkamp as an integrated part of the overall system design and therefore could not be changed. However, the entire tracking system had to be

refurbished and the Matlab program that controlled the tracking was redesigned. The system consisted of a large movable structure, two DC motors (one to control the hour angle and one to control the declination) connected to a computer, running a Matlab program to control the motors. The following is a description of the new system.

4.5.1 Mechanical System

The mechanical tracking system was driven by two electric motors. The hour angle motor turned a sprocket which locked into a bicycle chain, which had been secured around the flat rotating disk on which the entire system rested. The disk was not perfectly symmetrical and as a result the motor had to be spring loaded so that the teeth of the sprocket were always at the correct depth within the chain. The spring loading also allowed the sprocket to be removed from the chain when the disk had to be turned by hand. Figure 4.15 is a photograph of the springloaded hour angle motor connected to the chain around the disk by means of a sprocket. The declination was controlled by a linear actuator, which adjusted the declination angle by extending or contracting the linear arm linkage. The motors controlled the mechanical tracking system, but they in turn were controlled by the electronic tracking system.

Figure 4.15: Photograph of the hour angle motor.

4.5.2 Electronic system

The electronic tracking system consisted of a computer, a K8055 USB experiment interface board, a K74V2 PC relay driver board, one single turn 1 kΩ high precision potentiometer, a voltage regulator and a number of DC power supplies. The system ran according to the flowchart in Figure 4.16, with the computer connected to the experiment interface board via a USB port and the interface board linked to the relay card via a parallel port. The entire system was controlled by a Matlab program, which was based on a program originally designed by Van den Heetkamp but modified significantly to suit the current system.

Once initiated, the program launched a Graphical User Inerface (GUI) as shown in Figure 4.17. The GUI was used to instruct the computer to connect to the experiment interface board, by clicking on the “Connect” button and then the user instructed the system to start, by clicking on “Start”. This instructed the program to begin calculating the solar time and the hour

and declination angles. It also instructed the experiment interface board to read the signal from the potentiometer. The program then converted the voltage from the potentiometer (using Equation 4.11 as discussed later in this chapter) to an angle and then compared the calculated and measured values. The program displayed all of these values on the GUI as shown in Figure 4.17. The user then had the option of tracking manually by clicking on "Manual" and then clicking on the "Left", "Right", "Up" or "Down". "J" was a toggle switch which allowed to the user to select whether they wanted the motor to operate continuously until another instruction was given or whether they wanted the motor to operate for a fraction of a second before stopping again, thus resulting in a fine adjustment of the collector position. The "Automatic" button allowed the user to let the system move the collector into position automatically. It did this by constantly comparing the calculated and measured position values until the difference was zero, at which point the motor stopped turning and held the collector in place. The user could then select the "Track" button and the system would constantly check the comparison and move whenever the difference between the measured and calculated value was not zero. Note that only the hour angle was measured. The declination changes very

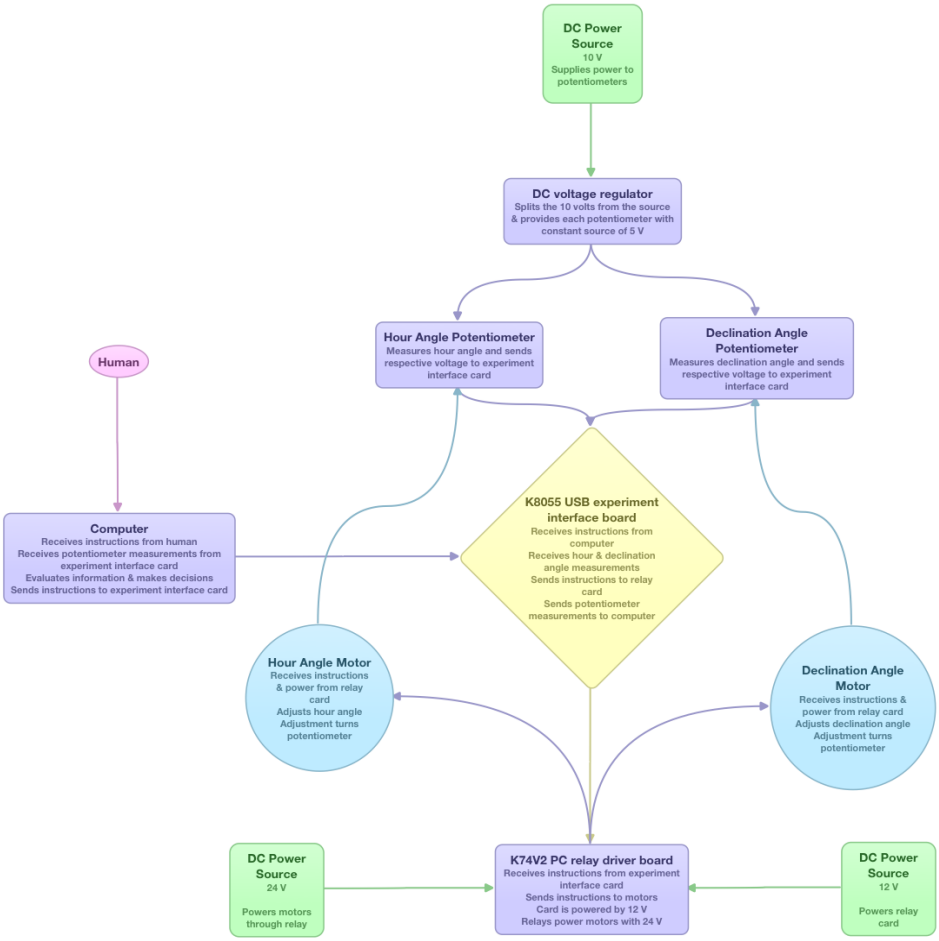

Figure 4.16: Flow diagram of the tracking program.

slowly over time and it was decided that the declination could be adjusted manually. The flow diagram in Figure 4.16 shows how the declination angle would be treated in the program, but this part of the program was omitted since the declination angle was determined manually.

Figure 4.18 is a circuit diagram showing how a pair of relays control the operation of a motor

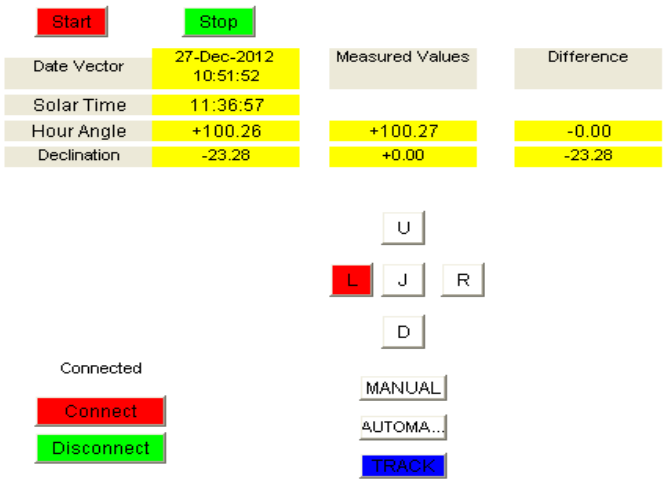

Figure 4.17: Screenshot of the tracking system's graphical user interface.

and Table 4.1 is a truth table describing how a pair of relays control the operation of a motor.

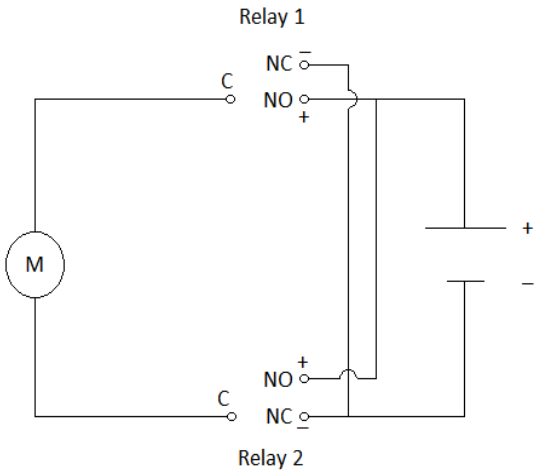

Figure 4.18: Circuit diagram of a pair of relays connected to a motor.

Table 4.1: Truth Table of Relay Operation

Relay 1	Relay 2	Motor Polarity	Motor Action
NO	NO	+ +	Brake
NO	NC	+ –	Clockwise
NC	NO	– +	Anticlockwise
NC	NC	– –	Brake

Tracking Program

The original program, designed by Van den Heetkamp, was able to calculate the solar time, the hour angle and the declination. It was also able to generate a graphical user interface and it enabled the user to track the sun manually. In addition, the new program was able to evaluate the difference between the calculated and the measured hour angle and make a decision about what it had to do to make those values the same. Thus the new program was able to move the system to where it was supposed to be and was able to track the sun continuously. The graphical user interface was also adjusted to accomodate these new features, to show the measured value and to show the difference between the measured and the calculated value.

4.5.3 Potentiometer Calibration

A potentiometer operates by changing its electrical resistance when it is turned. The resistance increases in one direction and decreases in another direction. This change in resistance is approximately linear and the better the quality of the potentiometer, the higher its precision and the more linear the relation between rotation angle and resistance. The potentiometer is powered by a 5 V DC power source, fed through a zener diode voltage regulator circuit to ensure that the potential difference provided to the potentiometer is always exact. The change in resistance of the potentiometer, results in a linear change in the potentiometer's output voltage. This output voltage is measured by the experiment interface board and this measurement is read in by the matlab program. The program then inserts this measurement into Equation 4.11 to find the accurate measure of the position of the dish.

The potentiometer was calibrated by moving the dish to several different hour angle positions and recording the voltage measurement as well as the angle indicated on the dial attached to the rotating disk to which the collector is attached. These values, shown in Table 4.2, were then plotted against one another and the equation of the resultant graph was used as the calibration equation.

Table 4.2: Potentiometer Calibration

Angle (degrees)	149	134	131	121	110	100.5	94.5	84	76	64
Voltagee (V)	131	124	118	111	102	95	90	82	76	67

The calibration equation is as follows:

$$TrueHourAngle = 1.28687 \times HourAngleMeasurement - 27.77206 \tag{4.11}$$

Figure 4.19 is a photograph of the hour angle potentoimeter as it was installed in the system, along with the angle measurement dial.

4.5.4 Tracking Difficulties

The tracking system was fairly accurate, but it was not perfect. One of the problems was that the parabolic dish petals were flexible. This meant that the petals would bend slightly early in the morning and late in the afternoon, when the dish was almost on its side, and this meant that the dish focus was not quite where it was supposed to be. Another problem was that even though the potentiometer was a high-precision device, its output voltage would still fluctuate quite rapidly. The new tracking program took this fluctuation into account and took several readings before determining an average. This resulted in a more stable reading from

Figure 4.19: Photograph of the hour angle potentiometer and the angle measurement dial.

the potentiomenter, which could then be used to perform the difference calculation and could be uploaded into the GUI. Some ideas for an improved tracking system are briefly discussed in the Discussion under the 'Further Work' section.

4.6 Data Aquisition

In order to ascertain the efficiency of the overall system, one must be able to determine how much energy is available to the system, how much energy is captured by the system and how much energy is stored by the system. This was done by measuring the total energy available from the sun, the surface temperature of the receiver, the temperature of the oil entering and exiting the receiver, the stratified temperature of the oil in the storage and the flow rate of the oil in the pipes. The flow rate of the oil was measured using a Hedland HLIT205-2G inline flowmeter. The ambient air temperature, average wind speed and wind direction measurements were taken using a Davis Vantage Pro2 weather station.

4.6.1 Temperature Measurement

The temperature of the oil was measured at the receiver and in the storage using a series of k-type thermocouple probes. At the receiver, thermocouple probes were placed in "T-joint" pipe connectors with the tip of the probe set to be in the centre of the flow through the pipe at the inlet and outlet of the receiver coil. Thermocouples were also placed on the surface of the pipe at the receiver entrance and exit to record receiver surface temperatures. A FLIR T335 infrared camera was used to measure the temperature distribution over the surface of the receiver, as well as the average receiver surface temperature. At the storage, a set of nine thermocouple probes were placed at set heights, 4 cm apart, in the centre of the storage to measure the stratified temperature of the storage. The thermocouples produced a DC voltage output which was related to the temperature at the tip of the probe. The voltage from the thermocouples was measured by one of two National Instruments NI9211 Data Acquisition (DAQ) units. These units have four thermocouple inputs. Thus, with two units, eight thermocouple measurements could be taken at one time. The DAQs were controlled by a Labview program that sampled the thermocouple readings once every 1000 seconds and recorded the values in a table that could be used to analyse the data later. The block diagram of the

Labview program is shown in Figure 4.20.

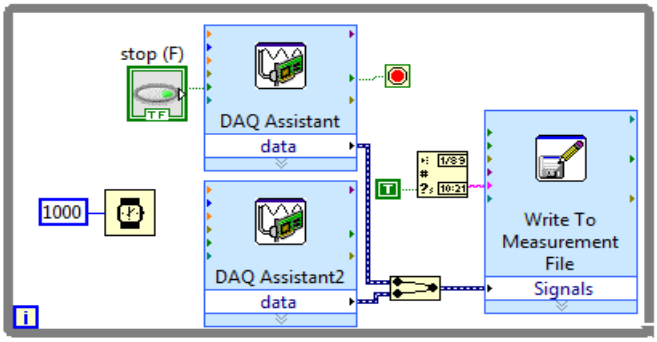

Figure 4.20: Labview data aquisition block diagram.

During the Receiver Test, the first DAQ measured the receiver inlet surface, receiver inlet oil, receiver outlet oil and receiver outlet surface temperatures, while the second DAQ measured the storage inlet, storage upper middle, storage lower middle and storage outlet temperatures.

4.6.2 Solar Radiation Measurement

The incident solar radiation was measured using the suite of radiometry equipment available at UKZN Westville Campus as described in Chapter 2. This measured the direct solar radiation as well as the global and diffuse solar radiation. Since the collector only concentrated direct solar radiation, only the direct solar radiation measurements were taken into consideration in determining the total amount of solar radiation available.

4.7 Analysis of the Overall System

Before discussing the thermodynamics of the system, some important definitions must be made clear. An adiabatic wall is a perfect insulator that does not allow energy to pass through it in the form of heat [93]. An adiabatic process is thus a process that occurs while enclosed by an adiabatic wall. An isothermal process is a process that has a constant temperature. An isobaric process is one that occurs at constant pressure and an isovolumetric process is one that occurs at constant volume.

The system under investigation is the heat transfer oil and the pebbles in the storage, with boundary layers wherever the oil comes into contact with any other substance other than the pebbles. That is, the pipe walls, the surfaces of the pump gears, the surfaces of the thermocouple probes, the storage walls and the surface of the air. The storage system is not completely closed off to the environment, which means that it is subject to fluctuations in atmospheric pressure, as well as changes in pressure due to the velocity of the fluid and the height of the point of interest. The storage system also contains air, which can be compressed and pushed out of the system when the oil expands due to an increase in thermal energy. Thus this system is not isobaric or isovolumetric. Given that there are diffferences in oil temperature throughout the system, it is certainly not isothermal and since the entire purpose of the experiment is to determine how effectively thermal energy can be transferred into and out of the oil in the form of heat passing through the boundary layer at the receiver and in the storage, it is also

not adiabatic.

Heat is defined as the transfer of energy across the boundary of a system due to a temperature difference between the system and its surroundings. Heat was originally measured in calories, the amount of energy required to raise the temperature of 1 g of water from 14.5 °C to 15.5 °C, but is now more commonly measured in Joules, with 1 cal = 4.186 J. Heat capacity is the amount of energy required to raise the temperature of a susbtance by 1 $°C$ and specific heat capacity is the heat capacity per unit mass of the substance given by

$$c = \frac{Q}{m\Delta T} \tag{4.12}$$

in units of J/kg.°C.

4.7.1 Energy Transfer Mechanisms Applied to the System

Figure 4.21 illustrates how energy, or in this case power as the rate of energy transfer, is transferred through the system. The figure shows power being provided to the collector, which consists of the concentrator and the receiver, and shows how this power is transferred through the collector to the storage. The arrows labelled *L1* to *L6* indicate power that has been lost from the system. The power entering the collector comes from the incident solar radiation. The power lost, *L1*, is due to atmospheric absorption and other such losses as discussed in Chapter 2. The power transferred to the receiver from the concentrator, the 'Power Available', is less than the power received by the concentrator. This is a consequence of power losses *L2* and *L3*, where *L2* is concerned with gathering the available power and *L3* is concerned with delivering it to the receiver. The losses at *L2* are due to absorption of energy by the reflective tiles and due to the gaps between the tiles, which result in less than the entire concentrator surface being reflective. The losses at *L3* are due to poor solar tracking and inaccurate focusing of the incident solar radiation onto the receiver and would thus be deemed 'optical losses'.

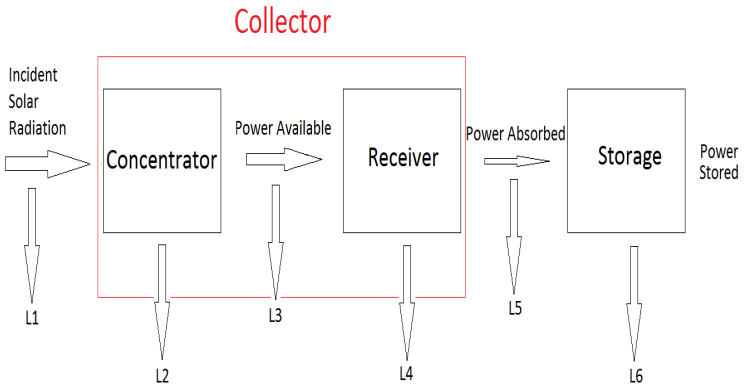

Figure 4.21: Block diagram of the power transfer through the system.

Power is transferred to the receiver the following manner: the surface of the receiver is heated up by concentrated incident solar radiation from the concentrator. This power is transferred throughout the receiver by conduction. Oil is pumped through the receiver, resulting in power transfer from the receiver to the oil via conduction and both forced and natural convection. This is the 'Power Absorbed'. Power is lost at the receiver, indicated by *L4* in Figure 4.21, by radiation and convection. The power radiated away is a result of the receiver absorbing energy

and increasing its temperature above that of its surroundings. The power lost to convection is as a result of air coming into contact with the receiver, absorbing energy and then moving away with it. In both cases, power is conducted throughout the surface of the receiver before it is lost by one of the other two mechanisms.

The oil in the receiver is pumped to the storage, where the absorbed power is transferred from the moving oil into the stationary oil in the storage as well as to the pebbles and to the storage walls. During this transportation, a small amount of power is lost through the pipes by radiation and convection, similar to the losses at the receiver. This power loss is indicated by *L5* in Figure 4.21. Finally, power is lost from the storage, indicated by *L6*, by means of radiation and convection after being conducted through the walls of the storage tank and the power remaining in the tank is the 'Power Stored'. Thus, 'Power Available' is the power provided to the receiver from the concentrator, having experienced losses *L1* to *L3*, 'Power Absorbed' is the 'Power Available' after having experienced losses *L4* and the 'Power Stored' is the 'Power Absorbed' after having experienced losses *L5* and *L6*.

Receiver

The power available to the receiver is given by

$$P_{Available} = A_{Aperture} I_{Direct} - (L2 + L3) \tag{4.13}$$

where $A_{Aperture}$ is the aperture area of the concentrator, I_{Direct} is the intensity of the incident direct solar radiation and *L2* and *L3* are the losses as defined in Figure 4.21. The power absorbed by the receiver is the power that is transferred from the receiver surface to the oil that passes through the receiver coil. This power is less than the power available because some of the available power is lost, as discussed previously. The total amount of power transferred to the oil from the receiver is

$$P_{Absorbed} = P_{Conducted} = P_{Available} - P_{Radiated} - P_{Convected}. \tag{4.14}$$

where $P_{Conducted}$ is the power conducted from the receiver surface to the oil that passes through the receiver coil, $P_{Radiated}$ is the net radiated power loss and $P_{Convected}$ is the power lost to the air around the receiver by means of convection. At temperatures below which radiated power loss may be neglected, the performance of the receiver may be expressed as

$$P_{Absorbed} \simeq P_{Available} - P_{Convected} = \eta_0 A_{Aperture} I_{Direct} - U A_{Receiver}(T_{Receiver} - T_{Ambient}) \tag{4.15}$$

where η_0 is the optical efficiency and U is the overall heat loss factor. Essentially, this model determines the amount of power absorbed by calculating the amount of power lost and subtracting that from the amount of power available. Measuring the amount of power lost would be very difficult to achieve experimentally, as the overall heat loss factor is unknown. Thus a different approach is required.

It is possible to determine the amount of power absorbed by the receiver, simply by measuring the temperature of the oil at the inlet and outlet of the receiver, as well as the mass flow rate of the oil, and then applying an equation derived from the conservation of energy and Bernoulli's equation. Several assumptions are required. First of all, the fluid moving through the receiver is assumed to be incompressible. Since the fluid is not subject to large or rapid changes in pressure, temperature or density, this assumption can be considered valid. It is also assumed that no work is done by the fluid on the pump and no work is lost by the fluid in overcoming friction. The pipes are narrow, relative to other dimensions in the system, and so the height z

is considered constant across the cross section of the pipe. Figure 4.22 is a diagram of a fluid moving through a pipe from height z_1 to z_2. A mass m enters the control volume at point 1 and an equal mass exits the control volume at point 2. The mass at point 1 is defined by $m = \rho A_1 u_1 \Delta t$ and the mass at point 2 is defined by $m = \rho A_2 u_2 \Delta t$, where A is the cross-sectional area of the pipe and u is the speed of the fluid. The balance of energy of the fluid within the control volume can be given by [34]

$$mg(z_1 - z_2) + [(p_1 A_1)(u_1 \Delta t) - (p_2 A_2)(u_2 \Delta t)] = \frac{1}{2} m(u_2^2 - u_1^2), \tag{4.16}$$

where p is pressure. This equation reduces to

$$\frac{p_1}{\rho} + g z_1 + \frac{1}{2} u_1^2 = \frac{p_2}{\rho} + g z_2 + \frac{1}{2} u_2^2, \tag{4.17}$$

which is known as Bernoulli's equation [34].

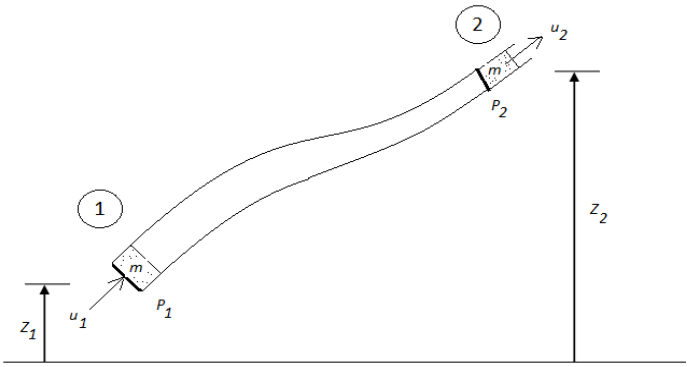

Figure 4.22: Diagram of fluid mass moving through a pipe from height z_1 to z_2.

Now, in the solar cooker system, the fluid will be passing through the receiver, and power $P_{absorbed}$ will be added to the fluid. This situation is described by Figure 4.23. Thus heat, in the form $E = P_{absorbed} \Delta t$, must be added to the energy inputs on the left hand side of Equation 4.16. The mass m entering the control volume at 1 has a temperature T_1 and contains mcT_1 J of thermal energy, where c is the specific heat capacity of the fluid. Mass exiting the control volume at 2 has temperature T_2 and contains mcT_2 J of thermal energy. The net heat carried out of the control volume in time Δt, given by $mc(T_2 - T_1)$, is added to the right hand side of Equation 4.16 and the resulting equation, corresponding to Equation 4.17 is given by

$$\frac{p_1}{\rho} + g z_1 + \frac{1}{2} u_1^2 + c T_1 + \frac{P_{absorbed}}{\rho A_1 u_1} = \frac{p_2}{\rho} + g z_2 + \frac{1}{2} u_2^2 + c T_2. \tag{4.18}$$

While Equation 4.18 treats the general case, the receivers used in this project did not have significant changes in z, u, A or p between the inlet and the outlet of the receiver. As such, Equation 4.18 can be reduced to

$$P_{absorbed} = \rho c A u (T_2 - T_1) \tag{4.19}$$

and this can further be reduced to

$$P_{absorbed} = \dot{m} c \Delta T. \tag{4.20}$$

We now have a model to calculate the absorbed power from a few simple measurements, rather than a number of complicated ones.

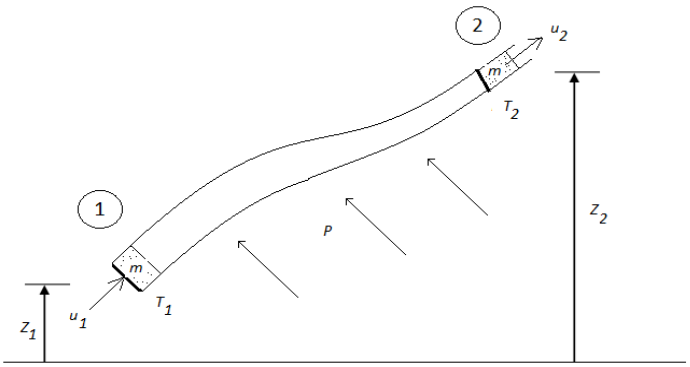

Figure 4.23: Diagram of fluid mass moving through a pipe from height z_1 to z_2.

4.8 Experimental Method

4.8.1 Receiver Test

Every receiver test consisted of the following sequence. First the thermocouple measurement system was run to ensure that it was working. Then the pump was switched on and set to the correct velocity. Once the oil was flowing, it was safe to focus the dish and begin tracking. The thermocouple measurements were taken automatically and the tracking was automatic. The incident solar radiation and ambient weather conditions were also automatically recorded as described earlier and a thermal image of the receiver was taken every fifteen minutes to record average receiver surface temperatures. The flowmeter had to be read manually and the gauge had very large graduations, so it was decided to keep the flow rate constant at 0.75 litres/min. This meant that the flow meter had to be monitored constantly and the current to the DC motor turning the pump had to be adjusted to adjust the speed of the motor. The flowmeter also had a temperature limit of 115 °C, so the storage outlet temperature had to be monitored and the system was shut down when the outlet temperature reached 100 °C for safety. Unfortunately, the flow rate of 0.75 litres/min was unable to induce turbulent flow in the pipes (see Table C.1), but the oil was too viscous at low temperatures for the pump to be able to operate any faster, so this had to suffice. Once the test was complete, the collector was moved out of focus and the receiver was allowed to cool. Once the receiver surface temperature was below 100 °C, the pump motor was turned off and everything could be shut down and stored away.

4.8.2 Storage Test

After a receiver test had been performed, the thermocouples from the receiver were disconnected from the DAQ and replaced with more thermocouples from the storage. The temperatures at different levels within the storage were then measured overnight to determine the rate of heat loss of the storage.

4.8.3 Analysis

The data that was measured in this experiment was the incident solar radiation or insolation, the ambient air temperature, the average wind speed and direction, the surface temperature of the receiver, the inlet and outlet oil temperatures of the receiver, the inlet and outlet temperatures of the thermal storage, and the temperatures of the upper middle and lower

middle levels of the storage. The following is a description of the analysis that was performed on the measured data. The power available at the receiver was calculated using the area of the concentrator aperture and the incident direct solar radiation as follows [34]:

$$P_{available} = r\varepsilon A_{aperture} I_{direct}, \tag{4.21}$$

where r is the reflectivity of the glass mirror, taken to be 0.92 and ε is the emissivity of the receiver surface, equal to the absorptivity α, taken to be 0.92. Note that this available power calculation did not take gaps between the mirror tiles on the concentrator into account. In otherwords, it was assumed that the concentrator surface was completely covered with reflective material. This assumption was made because the same concentrator was used in all tests, and therefore would not affect the comparison between the two receivers.

The power absorbed at the receiver was calculated using the mass flow rate ($\dot{m}$ in kg/s) of the oil, which was kept constant at 0.75 litres per minute (or 0.01 kg/s), the specific heat (c in J/kg. K) of the oil, which depended on the temperature of the oil in the receiver (values given in Table B.1) and the difference in oil temperature between the inlet and the outlet of the receiver. The oil temperature in determining the specific heat was taken to be the average between the inlet and outlet receiver oil temperatures. The power absorbed was calculated using Equation 4.20 as follows:

$$P_{absorbed} = \dot{m}c(T_{outlet} - T_{inlet}). \tag{4.22}$$

The receiver efficiency was then determined using

$$\eta = \frac{P_{absorbed}}{P_{available}}, \tag{4.23}$$

expressed as a percentage.

The power lost by the storage was calculated by measuring the change in temperature of the oil in the storage while it was not being charged or discharged. The oil temperature was measured at different levels within the storage and then averaged to provide a mean storage temperature. The storage was made up of oil and pebbles. The total storage volume is given by

$$V_{Total} = \pi r^2 h \tag{4.24}$$

the volume of a cylinder. The storage was not completely filled with pebbles (see Figure 4.14), so the total volume can be split into

$$V_{Total} = V_{PebblesandOil} + V_{OilOnly}, \tag{4.25}$$

where $V_{PebblesandOil}$ is the volume of the storage up to the top of the pebbles and oil mixture and $V_{OilOnly}$ is the volume of the storage from the top of the pebbles to the top of the storage. These can be calculated using the equation for the volume of a cylinder. The volume of the stones is then given by

$$V_{Pebbles} = (1 - \epsilon)V_{PebblesandOil} \tag{4.26}$$

where ϵ is the void fraction of the pebbles, experminetally determined to be 0.44 and the volume of the oil can be calculated by

$$V_{Oil} = V_{OilOnly} + V_{PebblesandOil} - V_{Pebbles}. \tag{4.27}$$

The mass of the oil in the storage was determined by multiplying the volume of the oil with its density and similarly for the mass of pebbles. The energy lost by the storage was then calculated using

$$E_{Lost} = m_{Pebbles}c_{Pebbles}(T_1 - T_2) + m_{Oil}(c_{Oil1}T_1 - c_{Oil2}T_2) \tag{4.28}$$

where the subscript *1* indicates conditions at the beginning of the test and the subscript *2* indicates the conditions at the end of the test. The values of ρ_{Oil} and c_{Oil} depend on temperature, which is why the two terms for oil energy in Equation 4.28 cannot be grouped as one term. The power lost was calculated using

$$P_{Lost} = \frac{E_{Lost}}{t} \tag{4.29}$$

where t was the length of time that the test ran for, in seconds. The efficiency of the storage was calculated by

$$\eta = \frac{FinalEnergy}{InitialEnergy} \tag{4.30}$$

expressed as a percentage.

Chapter 5

Results and Discussion

The small scale concentrating solar cooker was tested on the roof of the Physics Building during the months of December 2012 and January 2013. December and January are summer months in South Africa and, in Durban, the summer weather tends to be hot and humid. This results in a large number of overcast days during summer, which are unsuitable for testing due to the low intensity of direct solar radiation. The graphs in Figure 5.1 show the average direct solar radiadion that accumulated between the hours of 09:00 and 15:00 per day in December 2012 and January 2013. For example, if the direct solar radiation incident upon an area of 1 m^2, averaged over an hour, was exactly 833 Wh, every hour for the six hours between 09:00 and 15:00, then the accumulated average direct solar radiation for that time period would be 4998 Wh. These graphs show that there were very few days during December 2012 and January 2013 with an accumulated average direct solar radiation above 5000 Wh.

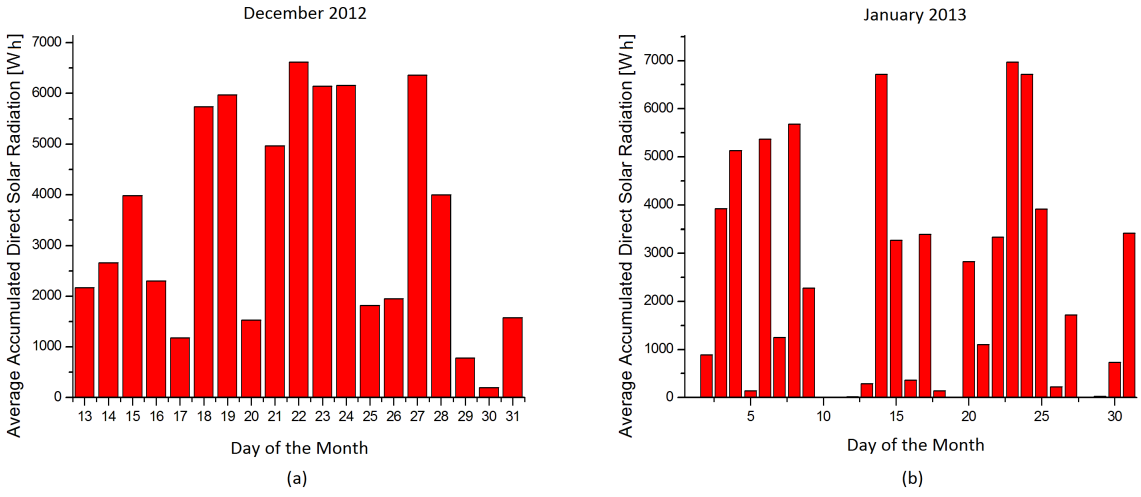

Figure 5.1: Graphs of average direct solar radiation accumulated per day between 09:00 and 15:00 during December 2012 and January 2013.

Tests were conducted on 24 and 27 December 2012 with the flat coil receiver and on 08 and 14 January 2013 with the cavity receiver. An extra test was conducted on 24 January with the cavity receiver, just out of curiosity, with regards to possibilities for further testing. In December 2012, the days before the 24th were spent setting up the system. The days immediately following 27 December 2012 had poor conditions for testing and it was decided

to change receivers after only two tests because of time constraints. The days leading up to the test with the new receiver on 08 January 2013 were spent changing the receiver. Following the test on 08 January 2013, conditions were extremely poor until the test on 14 January 2013, which was then followed by several days of poor conditions. The scarcity of days with good test conditions, combined with time constraints, meant that fewer tests could be conducted than one would like and certain data is included in this dissertation, that would otherwise have been abandoned for more complete data from another test, had the conditions allowed further testing. For example, there was a disruption to the electricity supply on 08 January 2013 that lasted for about half an hour between 12:30 and 13:00, which interrupted a test with the cavity receiver on a day with ideal conditions. During this time, the system had to be defocused and the receiver allowed to cool, otherwise the oil would have begun to burn in the receiver as there was no electricity to operate the pump. This disruption obviously had an effect on the results, but it was decided to include these results for the aforementioned reasons. Similarly, during the test on 24 December, the thermocouple that measured the receiver outlet oil temperature had a loose connection that was only noticed once the test had begun. The loose connection was repaired and the test continued, but about an hour of data was lost. The results from this test were also included for the aforementioned reasons.

5.1 Receiver Test

Two solar radiation receivers and one test plate were tested under similar conditions during December 2012 and January 2013. The test plate was used to determine the correct focal length for the concentrator. This was done by placing the plate at various distances from the concentrator and measuring the stagnation temperature of the plate using a thermal imaging camera. A focal length of 0.840 m had been determined using raytracing, as discussed in Chapter 4 (see Figure 4.9), and this was confirmed when the test plate achieved a peak stagnation temperature of 677 °C at that focal length. Figure 5.2 is a thermal image of the test plate at stagnation temperature, with the scale on the right hand side indicating temperature. The flat coil receiver was tested on the 24 and 27 December 2012 and the cavity receiver was

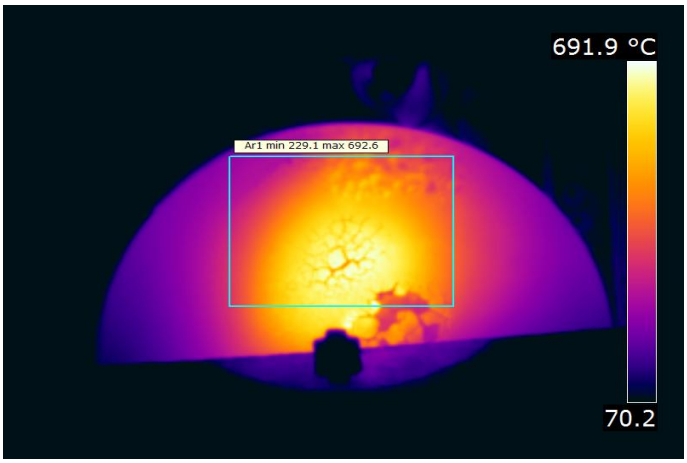

Figure 5.2: Infrared image of the test plate at stagnation temperature at a focal length of 0.84 m.

tested on the 08 and 14 January 2013. Figure 5.3 is an infrared image and a photograph of the flat coil receiver operating under concentrated direct solar insolation during testing on 27 December 2012. This image is shown as a sample of many photographs and thermal images that were taken every fifteen minutes during the tests to determine the average surface

temperature of the receiver. The thermal images were analysed using software called FLIR (Forward-Looking InfraRed imaging systems) Quick Report 1.2, which was provided with the thermal imaging camera. Figure 5.4 is a thermal image and a photograph of the cavity receiver operating under concentrated direct solar insolation during testing on 14 January 2013 and is another example of many such readings that were taken during these tests. Some shading can be seen on the coil because the cavity opening is smaller than the coil aperture. Table 5.1 is a summary of the results, averaged over the entire day, obtained from those tests.

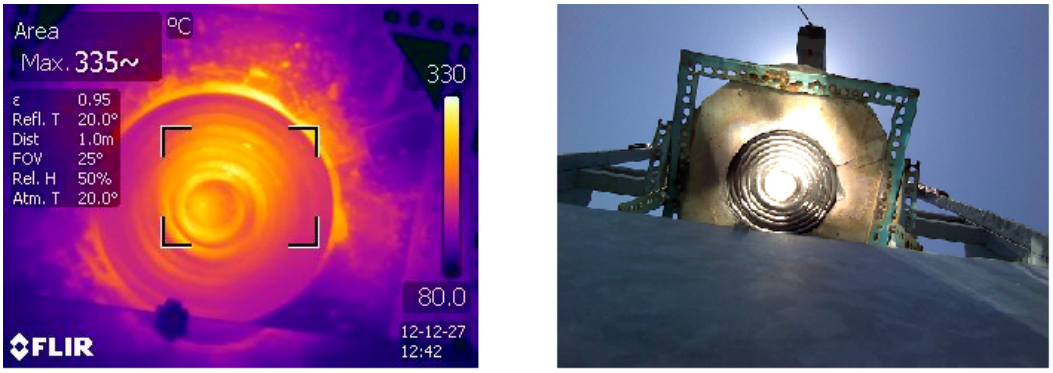

Figure 5.3: (a) Infrared image of the flat coil receiver taken at 12:42 pm on 27 December 2012. (b) Photograph of the flat coil receiver taken at 12:42 pm on 27 December 2012.

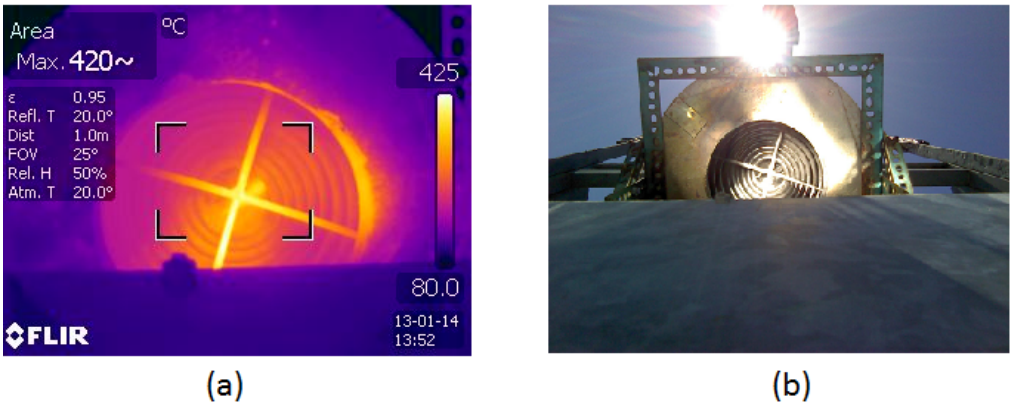

Figure 5.4: (a) Infrared image of the cavity receiver taken at 13:52 on 14 January 2013. (b) Photograph of the cavity receiver taken at 13:52 on 14 January 2013.

Table 5.1: Summary of Receiver Test Results

Date	Receiver	Insolation	Power Available	Power Absorbed	Efficiency	Wind Speed
		(W/m^2)	(W)	(W)	(%)	(m/s)
24 Dec	Flat Coil	915 ± 10	1751 ± 21	695 ± 180	40 ± 11	3 ± 1
27 Dec	Flat Coil	955 ± 11	1827 ± 22	728 ± 185	40 ± 11	4 ± 1
8 Jan	Cavity	885 ± 10	1693 ± 20	625 ± 168	38 ± 11	5 ± 1
14 Jan	Cavity	958 ± 11	1866 ± 22	869 ± 208	47 ± 12	2 ± 1

5.1.1 Insolation

Figures 5.5 and 5.6 are graphs of the direct solar insolation recorded over time on the respective test dates. The direct insolation, averaged over a minute, was recorded by the pyrheliometer discussed in Chapter 2. The average solar insolation for each day of testing is recorded in Table 5.1 The graphs in Figures 5.5 and 5.6 show that the amount of insolation available on

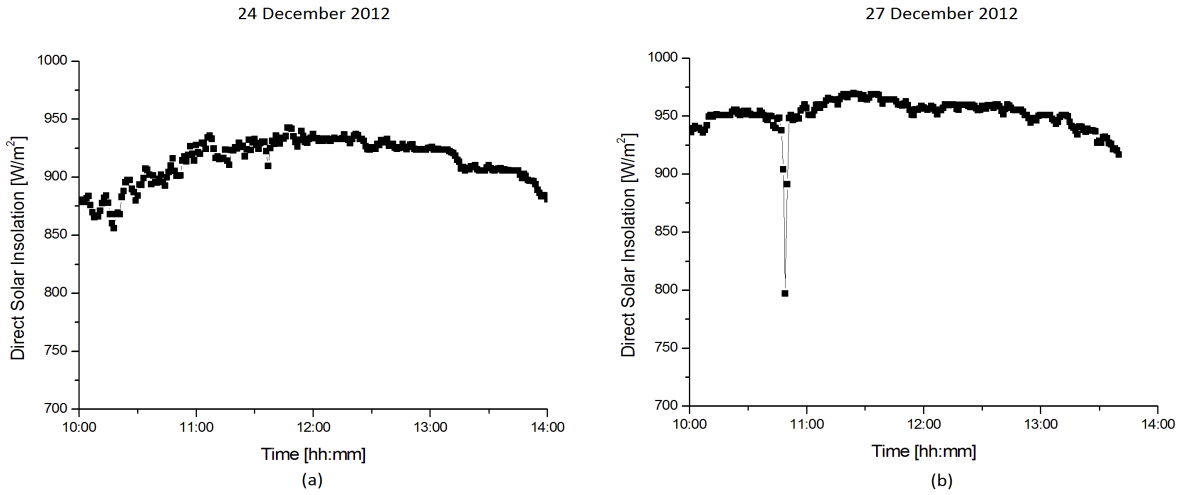

Figure 5.5: Graph of the direct solar insolation measured over time on 24 and 27 December 2012.

test dates was fairly consistent as, in general, the insolation for all four days does not exceed 990 W/m^2 and does not drop below 820 W/m^2, except for a few brief exceptions. The sharp drop to 797 W/m^2 at 10:49 am in Figure 5.5 (b) was probably due to brief obstruction of the sun by a cloud. The test on 08 January 2013 was interrupted by an electricity failure between 12:30 and 13:00, which explains the gap in readings in Figure 5.6 (a). All four graphs display a tendency of the direct solar radiation intensity to increase from morning to midday and then to decrease again after midday towards evening. This is due to the fact that during the period of time around solar noon, the sun is directly overhead and therefore the solar radiation has the least volume of air to travel through, meaning that less radiation is scattered, reflected or absorbed.

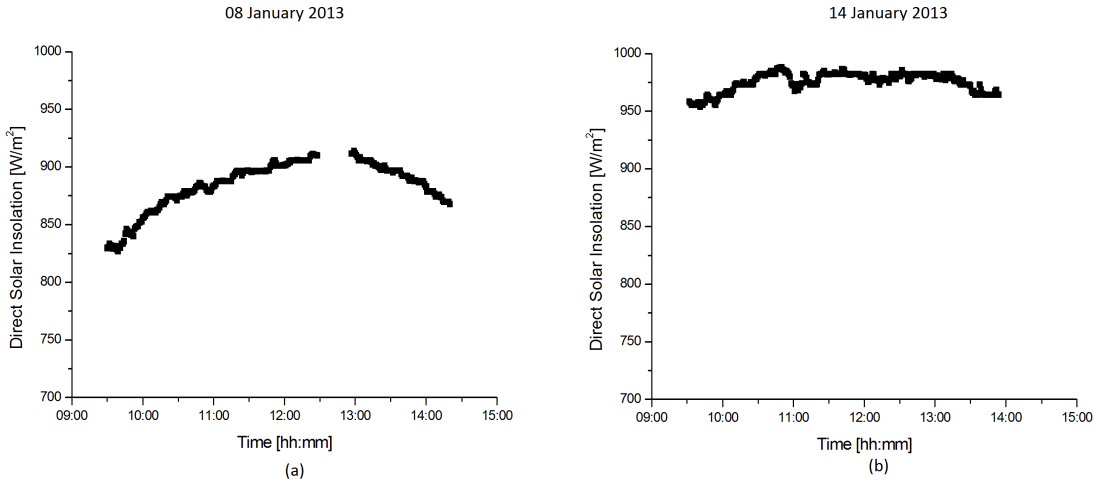

Figure 5.6: Graph of the direct solar insolation measured over time on 08 and 14 January 2013.

5.1.2 Power

Figures 5.7 and 5.8 are graphs of the power that was available to the receiver and the power that was absorbed by the receiver, measured over time on the respective test dates. The power available was determined using Equation 4.21 and the power absorbed was determined using Equation 4.22. The consistency of the direct solar radiation available on the respective test

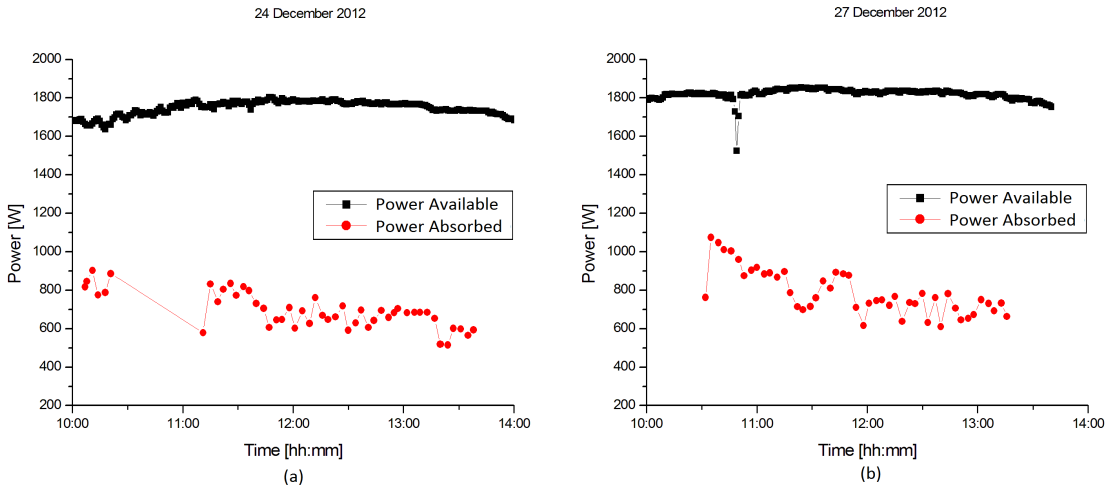

Figure 5.7: Graph of the power available to the flat coil receiver and the power absorbed by the flat coil receiver, measured over time on 24 and 27 December 2012.

dates, as shown in Figures 5.5 and 5.6, resulted in a very consistent available power. The available power is a measure of the amount of energy per unit time that was concentrated onto the receiver. The power absorbed is a measure of how much of that energy per unit time was absorbed by the receiver and transferred to the oil that was passing through the receiver. While the power available was very consistent, never venturing much above 2000 W

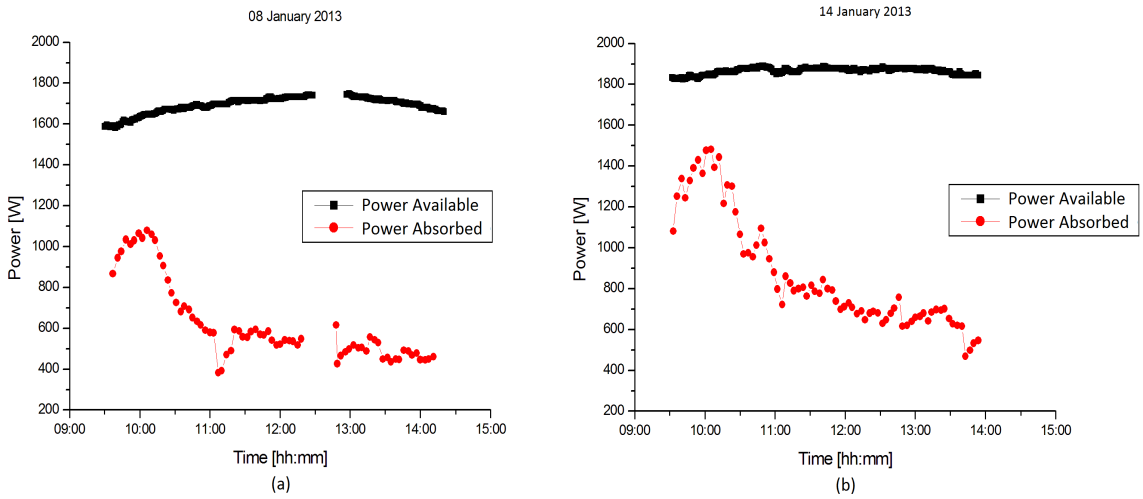

Figure 5.8: Graph of the power available to the cavity receiver and the power absorbed by the cavity receiver, measured over time on 08 and 14 January 2013.

or much below 1800 W, the power absorbed showed a rather different characteristic. The power absorbed was very high in the first hour of the test, usually around 1000 W and, in the final test with the cavity receiver on 14 January 2013, up to over 1500 W. This was due to the large difference in temperature between the oil entering the receiver and the oil exiting the receiver. Later in the test, as the receiver inlet oil temperature increased, the outlet temperature could not increase by as much due to various losses to be discussed later, and thus the temperature difference was not as great as before and thus the power absorbed decreased. The gap in readings in Figure 5.7 (a) was due to a loose connection in the thermocouple. The gap in readings in Figure 5.8 (a) was due to the electricity failure and the slight drop in absorbed power between when the testing stopped and when it started again was due to the fact that the receiver surface and the oil had lost some thermal energy during the stoppage.

5.1.3 Efficiency

Figures 5.9 and 5.10 are graphs of the receiver efficiency, measured over time on the respective test dates. The efficiency was calculated using Equation 4.23. The efficiency of the receiver followed a similar trend to that of the power absorbed in each test. The efficiency peaked in the first hour of the test, and then gradually levelled out around 30 %. The similarity between the efficiency curve and the power absorbed curve is due to the fact that the power available was so consistent. The test on 27 December 2012 was slightly shorter than the other tests and so the final efficiency has not yet dropped to the level of the other three tests, but is consistent with the level of the other three tests after three hours. The test on 27 December 2012 had to be stopped eary because some air was stuck in the storage tank and had begun to expand excessively, resulting in a large amount of oil being pushed into the expansion tank. The reason the air could not escape was because the hole where the thermocouples entered the storage tank had been sealed after the test on 24 December 2012. This problem was corrected after the test on 27 December 2012 and the remaining tests did not experience similar problems.

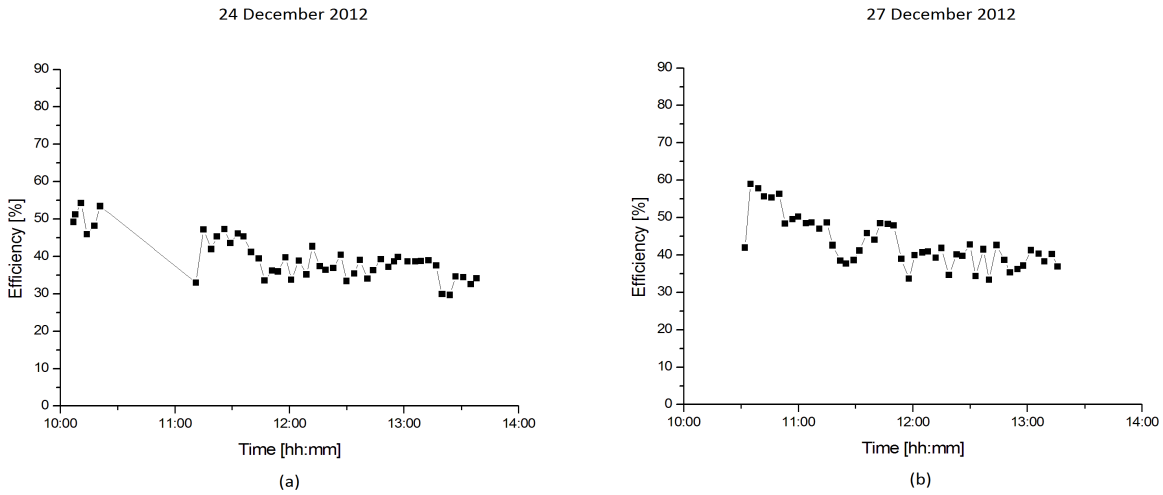

Figure 5.9: Graph of the efficiency of the flat coil receiver, measured over time on 24 and 27 December 2012.

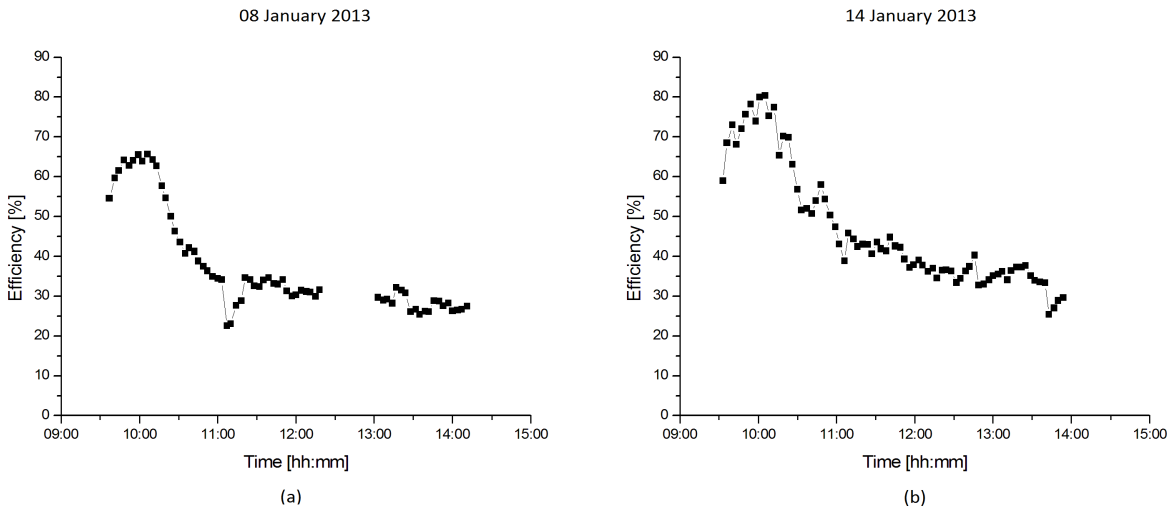

Figure 5.10: Graph of the efficiency of the cavity receiver, measured over time on 08 and 14 January 2013.

5.1.4 Receiver Temperatures

Figures 5.11 and 5.12 are graphs of the receiver temperatures, measured over time on the respective test dates. Figure 5.11 shows the receiver outlet and average surface temperatures,

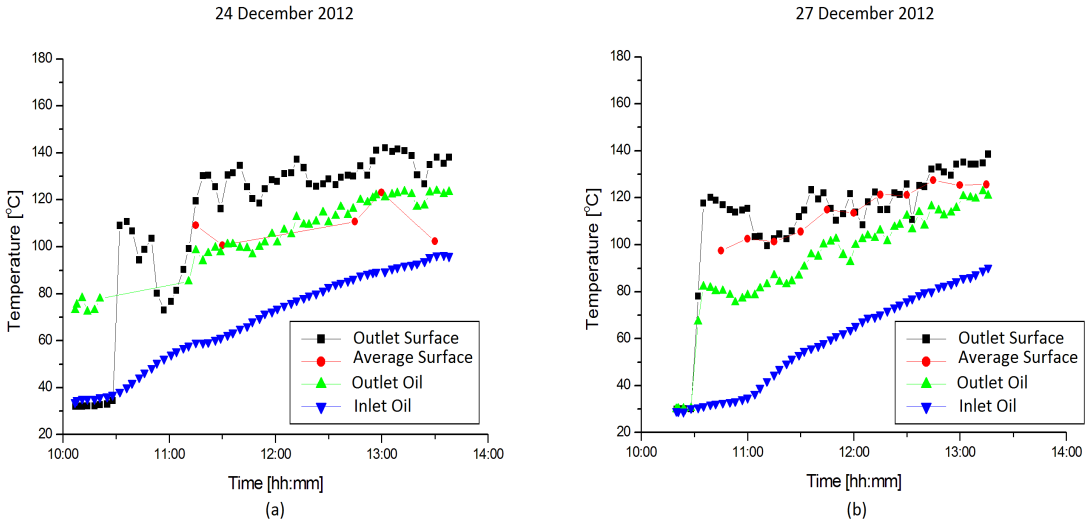

Figure 5.11: Graph of the receiver temperatures, measured over time on 24 and 27 December 2012 for the flat coil receiver.

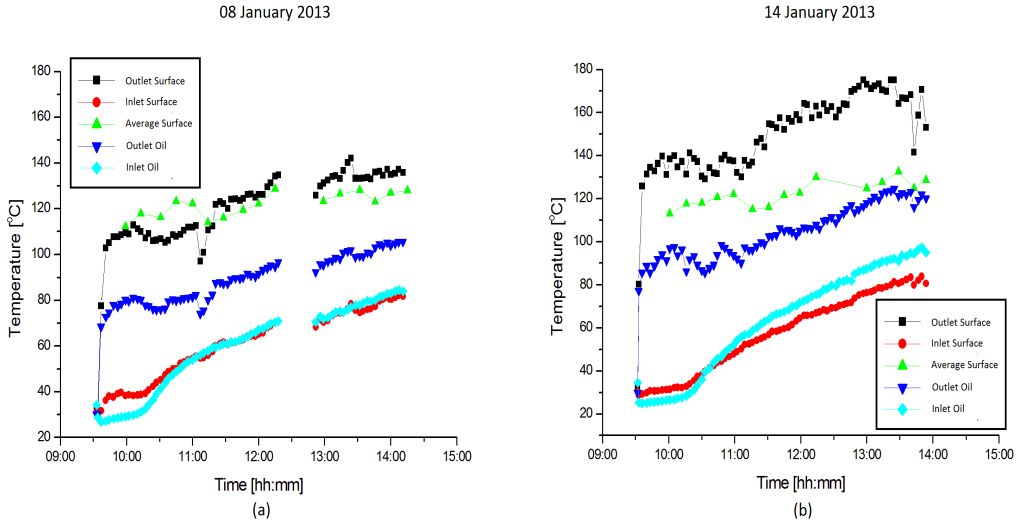

Figure 5.12: Graph of the receiver temperatures, measured over time on 08 and 14 January 2013 for the cavity receiver.

as well as the receiver inlet and outlet oil temperatures for the flat coil receiver. Figure 5.12 shows the receiver inlet, outlet and average surface temperatures as well as the receiver inlet and outlet oil temperatures. Note that the colours and symbols of the data points in Figure 5.11 represent different measurements to those in Figure 5.12. It is interesting to note that all the measurements followed a similar trend with a fairly linear increase after an initial heating up period which took place during the first hour of the test. The gap in outlet oil temperature

readings in Figure 5.11 (a) is due to the faulty thermocouple connection described earlier and the gap in all readings in Figure 5.12 (a) is due to the power failure described earlier.

When the receivers were exchanged on 08 January 2013, the cavity receiver was placed at the same focal length as the flat coil receiver had been. It was clear, once the concentrator was focused onto the receiver, that the correct focal length for the flat coil recevier was not the correct focal length for the cavity receiver as the reflection from the individual petals of the concentrator could be seen on the surface of the cavity receiver, along with gaps inbetween each reflected petal where no radiation was reflected. It was decided to test the cavity at this focal height anyway and then to repeat the test another day with the correct focal length. This was determined by reducing the focal length by half of the depth of the cavity receiver, which meant that the focal area was now in the centre of the cavity. This was done on 14 January 2013. Figure 5.12 (b) shows that the cavity receiver at the correct focal length, as it was during the test on 14 January 2013, achieved much higher temperatures than either receiver achieved during the other tests.

5.1.5 Efficiency vs Receiver Outlet Oil Temperature

Figures 5.13 and 5.14 are graphs of the receiver efficiency as a function of receiver outlet oil temperature for the respective test dates. Figure 5.13 shows that the efficiency of the flat

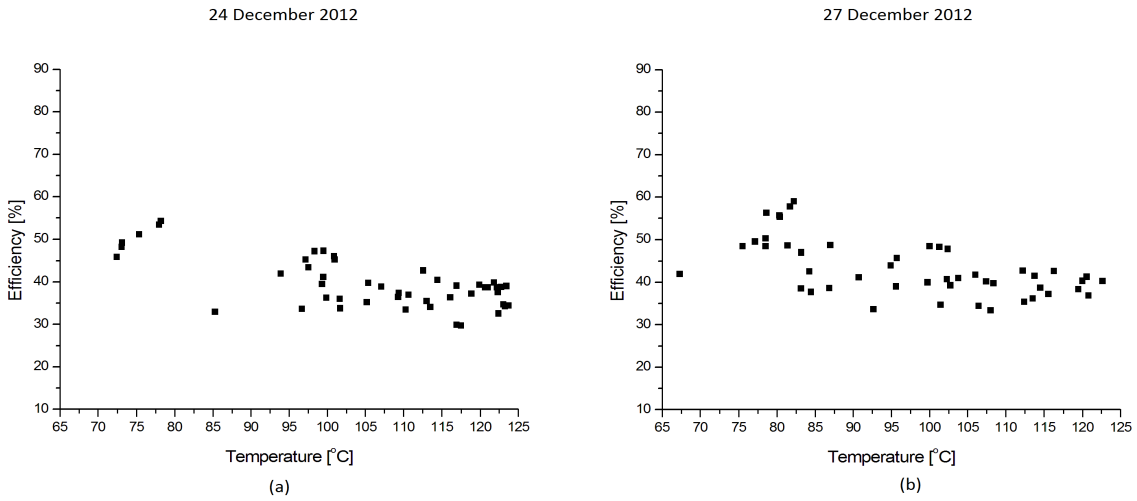

Figure 5.13: Graph of the receiver efficiency as a function of receiver outlet oil temperature on 24 and 27 December 2012 for the flat coil receiver.

coil receiver had a fairly linear relationship with temperature. Figure 5.14 shows that the efficiency of the cavity receiver had a fairly linear relationship with temperature at higher temperatures, but at low temperatures the efficiency increased dramatically. The efficiency does not depend solely on temperature, which is why there are sometimes several efficiency values for one temperature, for example Figure 5.14 (a) has about six values for the efficiency at a temperature of 80 °C. These different values of efficiency for the same temperature measurement are a result of different conditions present at the time that the measurement was made. Under strict laboratory conditions, if variables such as power available, wind speed and direction, oil flow rate and tracking errors could be kept constant, then a proper relationship between receiver efficiency and receiver temperature could be established.

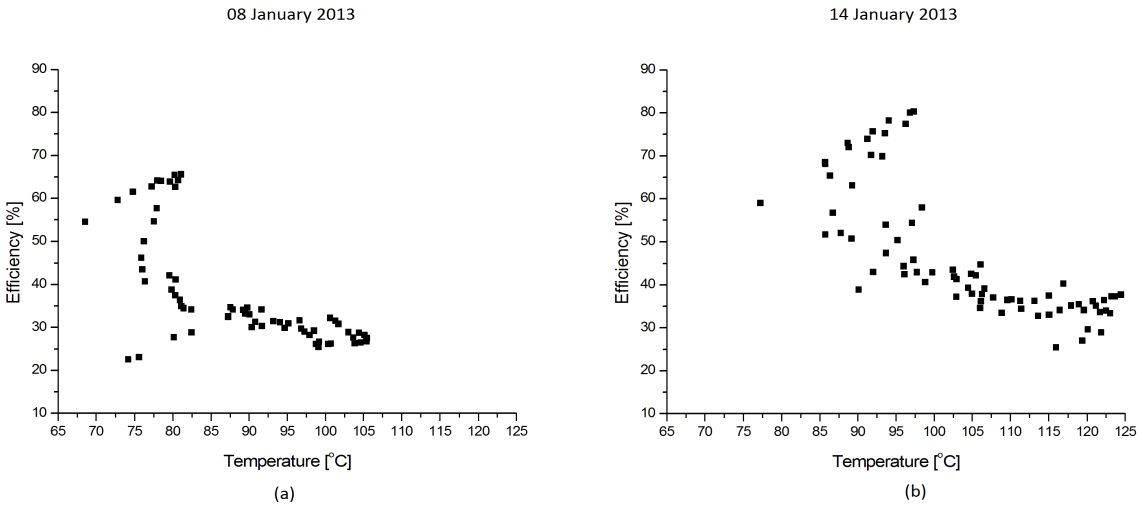

Figure 5.14: Graph of the receiver efficiency as a function of receiver outlet oil temperature on 08 and 14 January 2013 for the cavity receiver.

5.1.6 Wind Effects

Figures 5.15 and 5.16 are graphs of the average receiver temperatures and average wind speeds and wind directions, measured over time on the respective test dates. As shown in the graphs

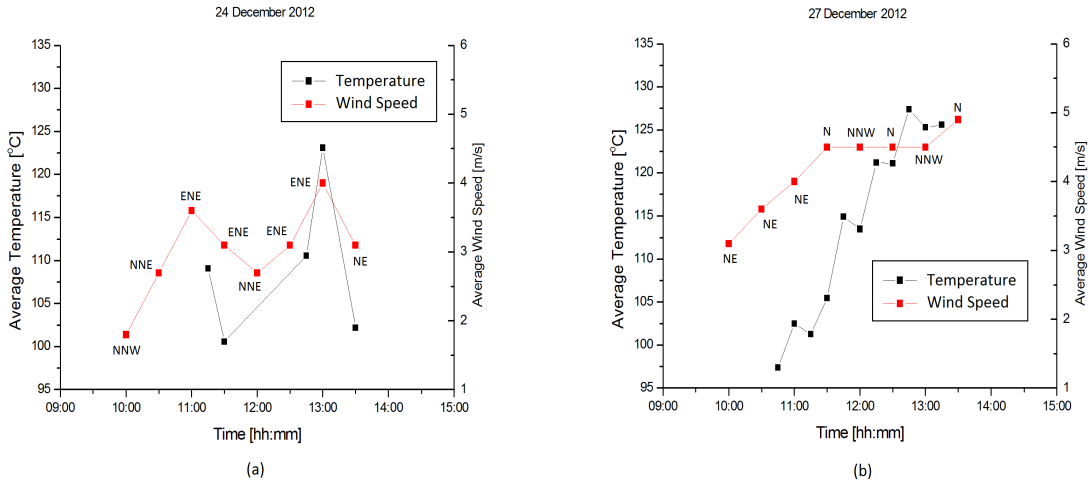

Figure 5.15: Graph of the average receiver temperatures and average wind speeds, measured over time on 24 and 27 December 2012 for the flat coil receiver.

of Figures 5.15 and 5.16, all four test dates were affected by strong winds. There are some correlations where a high wind speed in a certain direction resulted in a drop in average receiver surface temperature and vice versa. For example, Figure 5.16 (b) shows an east-north-easterly wind moving at over 3 m/s corresponding to an average receiver temperature drop of about 10 °C at 11:30 and shows a north-north-westerly wind of under 2 m/s corresponding to a rise in average surface temperature of about 10 °C at 13:30. However, there is also evidence

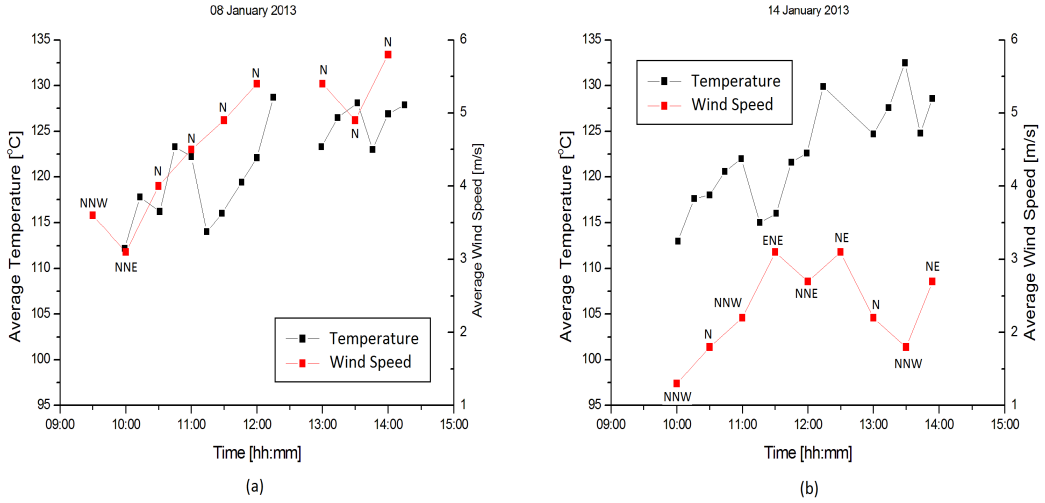

Figure 5.16: Graph of the average receiver temperatures and average wind speeds, measured over time on 08 and 14 January 2013 for the cavity receiver.

of wind speed and direction having no effect on average receiver surface temperature. For example, Figure 5.15 (b) shows a north-north-westerly wind moving at over 4 m/s during the peak average surface temperature of the test. The results could not be compared to results from a day with no wind as such conditions were not prevalent during the test time period. Another reason that these results are inconclusive is because the wind data was only recorded every fifteen minutes, which does not provide a good enough resolution for a conclusive test.

5.2 Storage Test

Figures 5.17 and 5.18 are graphs of the storage temperatures, measured at different levels within the storage vessel over time on the respective test dates. Temperature measurements were taken from thermocouples placed at four different heights along the central vertical axis of the storage tank. All of these thermocouples were placed beneath the surface level of the pebbles, with the thermocouples at the inlet and the oultet of the storage placed at the surface of the sieve (see Figure 4.14). The storage temperature at the oil inlet rose the quickest and remained the hottest for the entire test. This meant that the upper half of the storage contained the most thermal energy per unit volume. This was to be expected as it was closest to the receiver and hot fluids are less dense than cool fluids and therefore rise to the top of any container. As the test proceeded, the thermal energy spread downwards from the top of the storage tank and so the temperature of the upper middle level of the storage rose until it reached approximately the same temperature as the top of the storage tank. This trend continued all the way down the storage tank, with the difference in temperature between the inlet and outlet of the storage steadily decreasing. The test on 27 December, shown in Figure 5.17 (b) shows the inlet of the storage having a lower temperature than the two levels below it. The reason for this was briefly explained in the Efficiency section of the results and is explained in more detail in the following paragraph.

After the test on 24 December 2012, it was noticed that a small amount of oil was leaking from the pipe where the thermocouples exited the storage. This occured because the pipe was not long enough to be above the level of the top of the expansion tank. When the expansion tank

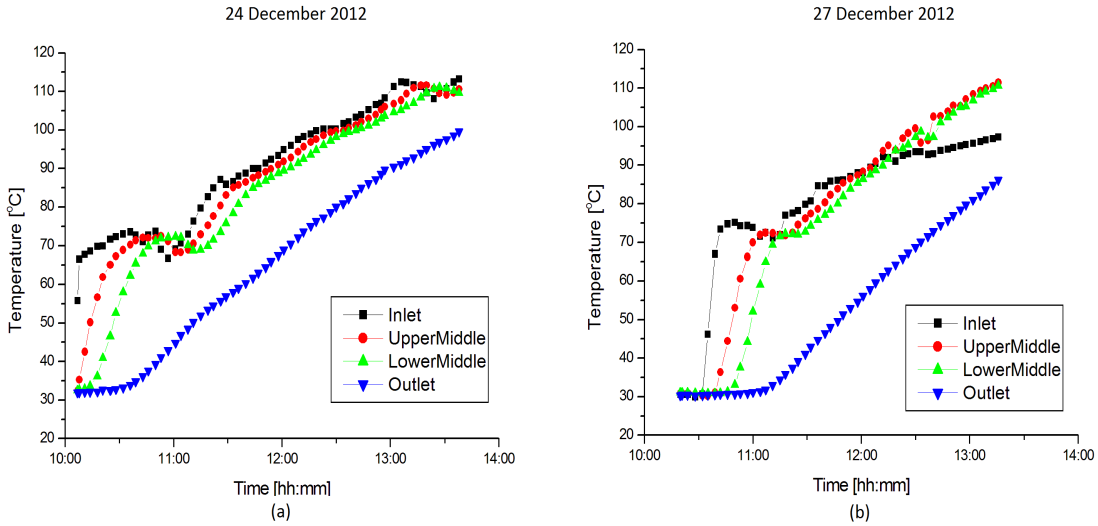

Figure 5.17: Graph of the storage temperatures, measured over time on 24 and 27 December 2012.

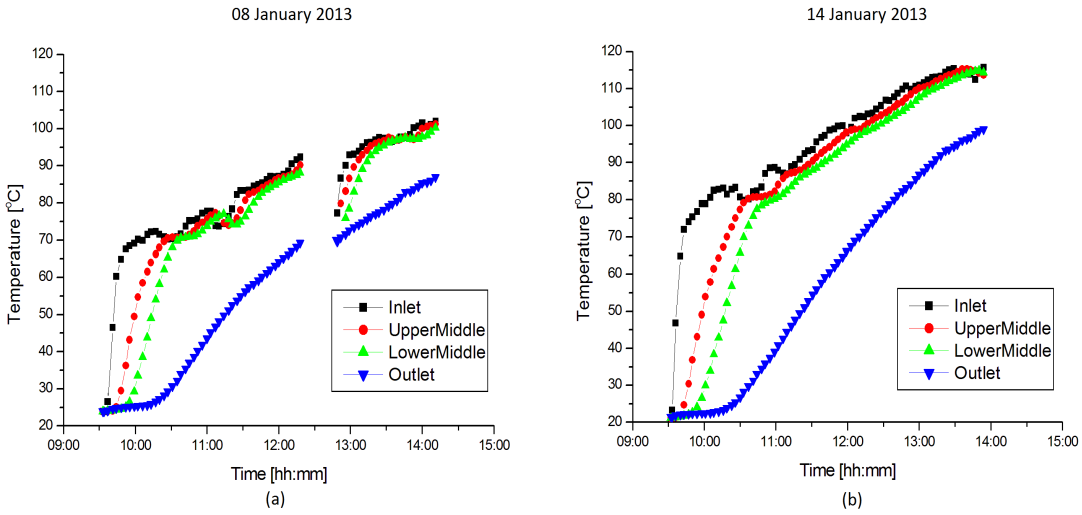

Figure 5.18: Graph of the storage temperatures, measured over time on 08 and 14 January 2013.

began to fill, the oil level in the expansion tank moved above the height of the thermocouple exit pipe and so oil began to exit through the tiny hole in the poorly sealed thermocouple exit pipe. This hole was filled the following morning with silicone. Unfortunately, there was some air trapped in the storage and it could not escape, now that the hole had been plugged. Thus, during the test on 27 December 2012, the trapped air expanded considerably and soon the expansion tank was overflowing. As a result of the expanding air, the oil was pushed out of the storage tank and the top of the pebbles was exposed. This is why the temperature at the inlet of the storage dropped below the temperature of the middle of the storage, as seen in Figure 5.18 (b). The same figure shows that the temperature of the oil at the outlet of the storage was unaffected and thus the receiver test was not compromised by the situation. It was feared that the system was losing too much oil and thus the test was stopped after only three hours. It was decided to still use the data from this test as the receiver test still performed as expected and that was the main focus of this project. The problem was solved by inserting a long 'breather pipe' into the thermocouple exit pipe to allow trapped air to escape the system without allowing oil to escape. Obviously, the 'breather pipe' extended well above the level of the expansion tank.

5.2.1 Cooling

Temperature measurements were taken on two separate occasions from thermocouples placed at eight different heights along the central vertical axis of the storage tank. On each occasion, the storage had been charged and temperature measurements were taken overnight to determine how much heat was lost, thus determining the efficiency of the storage. Table 5.2 is a summary of the results determined from measurements taken during the cooling tests. Figure 5.19 shows a pair of graphs depicting these measurements. In both cases the rate of change

Table 5.2: Summary of Cooling Test Results

Date	Initial Temp	Final Temp	Heat Lost	Time	Power Lost	Efficiency
	(K)	(K)	(kJ)	(hh:mm)	(W)	(%)
8 Jan	370 ± 1.5	330 ± 1.5	5446 ± 478	18:58 ± 1 min	80 ± 7	87 ± 3
14 Jan	382 ± 1.5	328 ± 1.5	7569 ± 435	18:44 ± 1 min	112 ± 6	83 ± 3

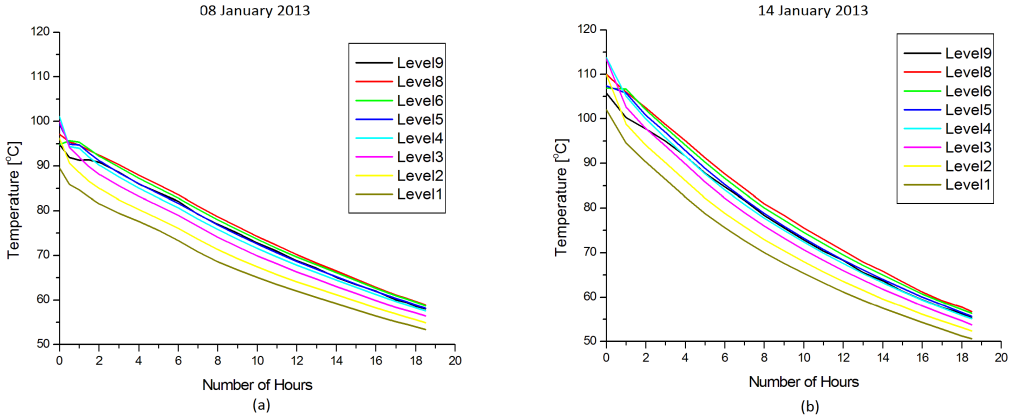

Figure 5.19: Graph of the storage temperatures, measured over time on 08 and 14 January 2013.

of temperature was very consistent between each level in the storage. This was expected since the storage was evenly insulated. The readings labelled Level 1 were the readings from the thermocouple at the storage outlet. Those labelled Level 8 were the readings from the thermocouple at the storage inlet. The readings labelled Level 9 were readings from a thermocouple that was in the oil only section of the storage (see Figure 4.14). It is interesting to note that the temperatures of the oil only section of the storage were lower than those of the oil and pebble mixed section. This implies that the pebbles were able to retain thermal energy better than the oil.

5.3 Error Calculations

The error in the mass flow rate was half the smallest graduation on the scale. Thus, a flow rate of 0.75 litres/min had an absolute error of ± 0.125 litres/min and a relative error of ± 17 %. K-type thermocouples have an absolute error of 1.5 °C. Thus the dT term in Equation 4.22 carries an absolute error of 3 °C. The error for the power absorbed is calculated by adding the relative error of the mass flow rate and the relative error of the thermocouple measurements. This error is very high because the scale on the flow meter was not very precise.

The relative error of the pyrheliometer, as stated in Chapter 2, was 1.1 %. The absolute error for the tile dimensions is 1 mm. Thus the error of the power available is determined by adding the relative error of the pyrheliometer readings to the relative error of the aperture area. Thus the relative error for the power available is 1.2 %. A problem with the calculated available power is that the equation used, Equation 4.1 does not take the fact that the reflective surface is an approximated surface into account. That is, it does not consider the fact that there are gaps between the mirror tiles, and that the mirror tiles were hand crafted and therefore not perfectly cut to size. The surface area of the dish, calcuated using Equations 4.7 and 4.8 is 2.49 m^2. The surface area of the mirror tiles, calculated by determining the area of each trapezoidal tile (tile dimensions are given in Table A.1 in Appendix A) and adding them together is 2.19 m^2. This means that only about 88 % of the parabolic surface is actually covered by the reflective surface and thus the power available could be reduced to 88 % of the calculated value shown in table 5.1. This would result in a corresponding increase in receiver efficiency of around 5 %. The error of the efficiency is determined by adding the relative error of the power available and the power absorbed.

In Table 5.2, the temperature error was the absolute error of the thermocouples and the heat loss error was determined by adding the relative error of the volume and the relative error of the temperature, since both the density and specific heat were given quantities (see Table B.1 in Appendix B). An absolute error of one minute was considered sufficient for the time and thus the error of the power lost was calculated by adding the relative error of the heat lost and the time. The error of the efficiency was calculated by adding the relative error of the initial energy and the relative error of the final energy of the storage system.

5.4 Extra Test

A brief test was conducted on 24 January 2013 to investigate the effect of heat transfer fluid flow rate on receiver and storage temperatures and receiver efficiency. For this test, the cavity receiver was used and the oil flow rate was set to 0.25 litres/min and the test ran for two hours. Figures 5.20 and 5.21 are graphs of the results for this test. The receiver inlet oil and surface temperatures were much higher than in all previous tests at comparable levels of

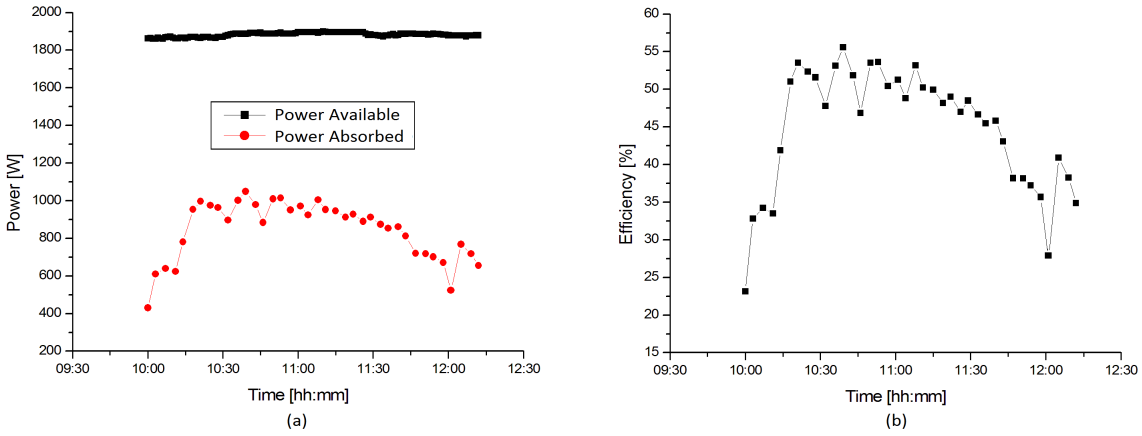

Figure 5.20: (a) Graph of power available and power absorbed vs time. (b) Graph of efficiency vs time.

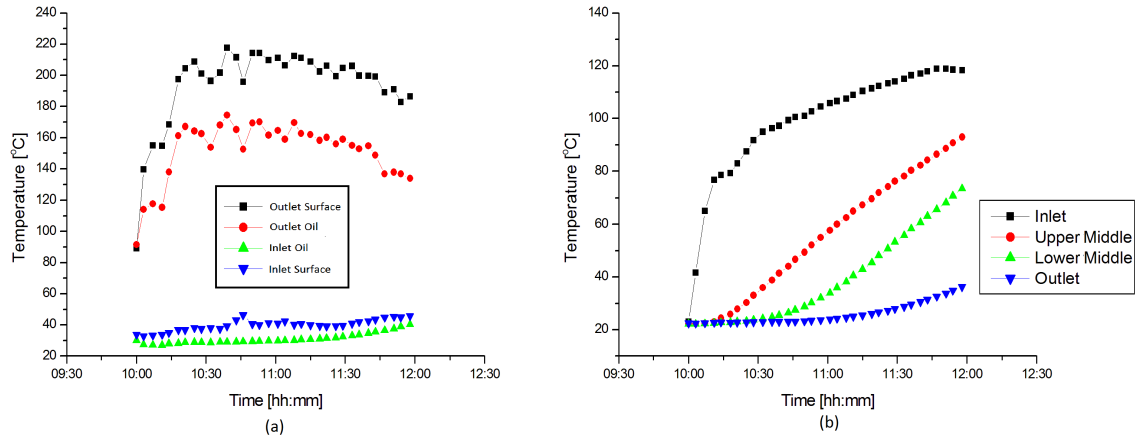

Figure 5.21: (a) Graph of receiver temperatures vs time. (b) Graph of storage temperatures vs time.

available power. This was because the oil moved more slowly and therefore did not transport the energy away from the surface of the receiver as quickly as in previous tests and this allowed the surface temperature to increase far beyond that of the previous tests. The slower flow rate of the oil also meant that the oil was in the receiver for a longer time, allowing it to absorb more energy and reach a higher outlet temperature than in previous tests. These increased temperatures resulted in increased heat losses, evidenced by the fact that the receiver efficiency was lower in these tests than it was all the other tests. The flow rate of the oil and the temperature difference between the inlet and the outlet of the receiver affect the efficiency of the receiver. Clearly, for such a slow flow rate, a higher temperature difference would be expected if the receiver were to achieve an efficiency similar to that achieved in previous tests.

The storage temperatures also present an interesting situation. Figure 5.21 (b) shows that the temperature of the oil at the inlet of the storage reached 100 °C well within the first hour of the test, something that took well over two hours to achieve in all the previous tests. However, a much larger stratification in storage temperatures is seen at the slow flow rate. This test was conducted purely out of curiosity and certainly yielded some interesting results. It could be possible that different flow rates are required at different temperatures to produce maximum efficiency. It must be stressed that a much more accurate flow rate meter, able to withstand high temperatures, would be required to make this kind of investigation.

5.5 Discussion

Figure 5.1 showed that there were so few days with the required weather conditions during December 2012 and January 2013 that it was difficult to perform more than a few tests. It was also not possible to test for several consecutive days, which would have been very interesting as the efficiencies on all test days dropped as the receiver inlet oil temperature increased. This was due to the fact that as the receiver increased in temperature, its losses also began to increase. High receiver temperatures would have resulted in large radiation losses because radiated power is proportional to T^4. The increased heat loss meant that the receiver outlet oil temperature was not able to increase as rapidly as the receiver inlet oil temperature (which depended on the storage outlet oil temperature), resulting in reduced efficiency. Testing on consecutive days would have meant that the oil in the storage would have had a much higher initial temperature, resulting in higher initial receiver inlet oil temperatures and consequently, higher temperatures all round.

The aims of this project were to refurbish the small scale solar cooker on the roof of the Physics building at UKZN, Westville campus, to automate the solar tracking system, to design and construct a new receiver, to test both the receiver from the original system and the new receiver and to comare their efficiencies, and to determine the efficiency of the thermal energy storage. All of these aims were achieved. The cooker was refurbished, the solar tracking system was automated, a new receiver was designed and constructed, both receivers were tested and so was the thermal storage. The results of these tests have been stated and the receivers will now be compared.

The flat coil receiver was tested on 24 and 27 December 2012 under similar conditions of direct solar insolation, wind speed and ambient air temperature. The receiver performed similarly in both tests, achieving an average efficiency of 40 ± 11 %. The cavity receiver was tested on 8 and 14 January 2012 under similar conditions to those of previous tests. The test on 8 January 2012 had the highest average wind speed and was at the incorrect focal length. The combination of these two factors lead to the worst receiver performance in these tests, with

an average efficiency of 38 ± 11 %. The test on 14 January 2012, at the correct focal length and with the lowest average wind speed had the highest average receiver efficiency of 47 ± 12 %.

All four tests were conducted under similar conditions of incident solar radiation, which means that the amount of power available to the receiver was similar in each test. The efficiency of the flat coil receiver declined in a generally linear fashion as the temperature of the oil and the temperature of the receiver surface increased. By contrast, the efficiency of the cavity receiver rose to greater heights than that of the flat coil receiver, before dropping away quite rapidly and then levelling out to around 30 %, a similar value to that of the flat coil receiver. With such few tests, and no consecutive tests, it is difficult to conclude which receiver has the better efficiency, but the evidence tends to indicate that the efficiency of the cavity receiver is greater than that of the flat coil receiver.

The cavity receiver was tested at the correct focal length on 14 January 2013. During this test, the receiver outlet surface temperature was higher than it was in all other tests. Similarly, the receiver outlet oil temperature reached a higher temperature than in all other tests, and far more quickly than in other tests. For example, the graph in Figure 5.12 (b) shows that the receiver outlet oil temperature was nearing 100 °C within the first half hour of the test, something that took the other tests over an hour to achieve. Figure 5.12 also shows the receiver inlet surface temperature, a measurement that was not included in the flat coil receiver test. This measurement showed that the oil temperature at the inlet of the receiver soon exceeded that of the receiver inlet surface. This means that the oil was losing power at the receiver inlet, rather than gaining it.

The effect of wind speed and direction on the average receiver surface temperature for both receivers was also investigated. While it is clear that the wind certainly had an effect on the performance of the receivers, this data did not provide a clear indication of what that effect was. There are several reasons for this lack of clarity in the data. One problem was that the wind speed and direction was only measured every half an hour. There were very many changes in wind speed and direction in between measurements that went undetected, yet had an effect on the receiver performance. An improved frequency of measurements is required to accurately determine the effect of the wind on receiver performance. Another problem was that the wind was very inconsistent from day to day, meaning that no two tests had the same wind conditions. This problem would be eliminated if the test of wind effects on receiver performance were performed in a laboratory. A final problem was the angle of the receiver relative to the wind. At different times of day, the receiver is at a different angle because the cooker has to track the sun. Once again, laboratory conditions would make the test easier. There have been many investigations of wind effects on receiver performance and since such an investigation was not a major aim of this experiment, no more will be said on the matter other than to conclude that wind did have an effect on both receivers and that a receiver that is unaffected by wind conditions would be more efficient than one that is affected by the wind.

The storage temperatures were recorded while the receivers were being tested. The storage behaved similarly in all four tests, though the test on 27 December 2012 was slightly different because of the air that was trapped in the storage tank, as discussed in the Storage section of the Results. The large difference in temperatures between the upper half of the storage and the lower half indicates that perhaps a smaller storage tank was required. In a smaller tank, the thermal energy would have been distributed throughout the tank more quickly because it would contain less mass to be heated up, resulting in higher temperatures at the storage outlet. Higher storage outlet temperatures would result in higher receiver inlet temperatures,

which would result in higher temperatures throughout the system. However, a smaller storage tank would saturate more quickly, meaning that it would not be able to absorb as much thermal energy as a large tank. A smaller tank, containing less thermal energy than a large tank, would not be able to provide thermal energy for as long as the large tank. So perhaps two storage tanks are required, a small one for short term storage (to last a few hours) and a large one for long term storage.

The storage test was conducted over night on 08 and 14 January 2013. In both tests, the storage behaved similarly with a linear decline in temperatures at all levels, although a slight decline in the rate of cooling was noticed towards the end of the test as the surrounding air temperature and the storage temperatures approach similar values. Some strange behaviour occured during the first few hours of each test. The temperature measurements of level 6, 5 and 4 increased before settling into a linear decline, while level 9 (at the top of the storage tank) did not have the highest temperature and its temperature measurements fluctuated while following a general trend of decline after an initail rise.

The reason for the behaviour of level 9's measurements is that level 9 contained only oil, while the rest of the storage tank contained a mixture of oil and pebbles. The pebbles have a lower specific heat than the oil, which means that for the same amount of heat added, the pebbles will reach a higher temperture than the oil. Thus, the temperature of the oil at level 9 was lower than the temperature of the pebble and oil mixture beneath it. In such a situation, where a cooler fluid is placed on top of a hotter fluid, natural convection occurs as the hotter fluid moves upwards and the cooler fluid moves downwards. This movement of fluid is accompanied by a movement of thermal energy and hence the fluctuation in temperature of level 9.

The reason for the initial increase in temperature of levels 4 to 6 is that the oil was no longer being pumped around the system and the oil and pebbles in level 8 were hotter than in the levels below. Thus, thermal energy from level 8 was transferred to the levels below, resulting in their increased temperature. Once a quasi-equilibrium had been reached, the entire system began to lose energy to its surroundings at a consistent rate. Both tests ran for similar lengths of time and had similar initial and final temperatures. The test with the slightly higher initial temperature fo 382 $\pm$ 1.5 K on 14 January 2013 had a slightly lower efficiency of 83 $\pm$ 3 %, when compared to that of the previous test, which had an efficiency of 87 $\pm$ 3 %. This reduced efficiency was due to the fact that a higher initial temperature meant that there was a larger temperature difference between the storage tank and its surroundings, resulting in a higher loss of power.

5.5.1 Losses

The system lost energy through the energy transfer mechanisms discussed in Chapter 4. The storage lost energy by conducting heat through its walls and into the insulation. This energy was then either radiated away or lost by convection into the surrounding air. The pipes, which connected the receiver to the storage, lost energy by conducting heat through their walls and then radiating and convecting it away into the surrounding air. The energy losses at the receiver were more complicated. Apart from the heat that was radiated and convected away into the surrounding air, the receiver also suffered optical losses. Any solar radiation that the concentrator did not focus onto the absorbing surface of the receiver is considered an optical loss. Many photographs and infrared images of the receiver, such as those shown in Figures 5.3 and 5.4, were taken during the tests. The bright reflection of concentrated solar radiation around the coil, shown in these photographs, is an indication of energy that is not

being absorbed due to optical losses.

The infrared images of the receiver showed that optical losses were not the only concern. They showed that the area outside of the receiver absorbing surface, that was irradiated with concentrated solar radiation, was at a much lower temperature than that of the absorbing surface. This implies that the radiation that was missing the receiver absorbing surface did not have a high intensity when compared to the radiation on the receiver absorbing surface. The infrared images showed that only a small area on the receiver coil, about nine centimetres in diameter, achieved high surface temperatures above 300 °C, while the rest of the receiver surface only achieved temperatures of around 100 °C. This means that the main focal area of the concentrator is actually much smaller than the area of the coil, which means that a large part of the coil is not absorbing energy, but losing energy. This could severely affect performance at higher temperatures, especially in terms of radiative heat losses. Clearly, if higher temperatures are to be achieved, a much smaller receiver will be required as a smaller receiver would result in smaller thermal losses.

Two unavoidable sources of energy loss, in this project, were inaccurate tracking and oil leakage. Since the receivers were larger than the focal area of the concentrator, imperfect tracking resulted in the focal area moving around on the surface of the receiver. This resulted in conduction losses as a new part of the receiver had to be heated up, and convection losses as the section of the receiver that had been receiving the most energy cooled down. Perfect tracking would have reduced these losses.

Although every pipe connection in the system was covered in high-temperature resistant silicone and every connection was made as tight as humanly possible, some oil still managed to leak out of the system. The leaking was worse when the oil was hot because at high temperature, the oil was less viscous and therefore more easily able to slip through the miniscule gaps in the pipe connections.

Chapter 6

Concluding Remarks and Future Perspectives

A small scale solar concentrating cooker was developed and partially reconstructed from a previous system on the roof of the Physics building at UKZN, Westville campus in Durban, South Africa. The system included automated solar tracking and a new cavity receiver, which was compared to the original flat coil receiver. Both receivers were tested under similar conditions of solar insolation, wind speed and ambient air temperature during the months of December 2012 and January 2013. The flat coiled receiver achieved a peak efficiency of 59 % and an average efficiency of 40 ± 11 %. The cavity receiver achieved a miximum efficiency of 80 % and an average efficiency of 47 ± 12 %. These errors in the efficiency calculation were mainly due to uncertainties in the flow rate measurement device.

The best average efficiency achieved by the storage was 87 ± 3 %. In the case of both the receiver and the storage tests, the efficiencies were rather high due to the low temperatures achieved. These temperatures were limited by the fact that the flow meter could only withstand temperatures up to 115 °C and the fact that tests could not be run on consecutive days due to poor weather conditions. More tests and a better flow meter are required to prove conclusively which receiver is more efficient, however the results from this experiment indicate that the cavity receiver was able to lose less heat due to convection and thus was able to achieve higher temperatures than the flat coil receiver. This meant that the cavity receiver was able to absorb more of the available power than the flat coil receiver and thus was more efficient than the flat coil receiver.

6.1 Further Work

A brief test was conducted on 24 January 2013 to investigate the effect of a slower flow rate on the temperatures and efficiency of the system. It was found that a slower flow rate resulted in higher temperatures at the receiver outlet and a larger stratification of oil temperatures in the storage tank, but it also resulted in a lower heat absorption and therefore a lower efficiency because the mass flow rate was so low. What this brief experiment showed was that the flow rate of the heat transfer fluid had a large effect on the performance of the system. Thus, a theoretical model could be developed to determine the optimum flow rate of the heat transfer fluid at different oil temperatures. This model could then be tested experimentally.

The solar tracking is a part of the system that requires further work. The tracking program

should be programmed onto a microcontroller to reduce the amount of human input required and remove the need for a computer in operating the tracker. A camera or a set of photodiodes could be added to the tracking program to improve accuracy. The camera could be placed onto the structure in such a way that it faces the sun directly when the system is properly aligned. A program could be developed to read in the data from the camera and determine what changes need to be made to hour and declination angles in order to correct the alignment. The photodiodes could be placed on either side of some kind of sheet. If the sheet casts a shadow onto one of the diodes, it would give a different reading to the other one. A program could be designed to read this data and decide which direction to turn the system. Two sets of diodes would be required, one for the hour angle and one for the declination.

Experiments could also be performed to optimise the receiver. These optimisations could include a wind shield such as a glass cover over the receiver aperture to limit convection losses and the design and construction of a smaller receiver to reduce radiation losses at high temperatures. Different concentrators, such as a Fresnel lens or a double reflector could also be tested, as well as different reflective materials such as perspex mirrors, polished aluminium and aluminium foil.

Finally, a different heat transfer fluid such as water could be tested, the entire system could be redesigned to be lighter and smaller and a photovoltaic power system could be used to power the solar tracking system and the pumping system, thereby eliminating the need for electricity from the grid. It must also be noted that the system, as it was operated during this project, was not actually a solar cooker, as it had no way of using the energy that it had stored. It was more of a solar energy harvester, with thermal energy storage. Thus, a cooking system needs to be designed, constructed, added to the system and tested. This could either be done by placing a cooking surface on the top of the storage, or by adding another pipe network with a new pump that could transport the hot oil from the storage to the cooking surface and back again. If a suitable cooking system were implemented, the system would certainly be able to heat water and, if operated for a longer period of time than it was in these tests, should attain high enough temperatures to cook food and should be able to store enough energy to cook food after the sun has set.

Bibliography

[1] Kharseh M, Altorkmany L, Nordell B. Global warming's impact on the performance of GSHP. Renewable Energy 2011;36:1485-1491.

[2] Naidu CV, Satyanarayana GCh, Durgalakshmi K, Malleswara Rao L, Jeevana Mounika G, Dharma Raju A. Changes in the frequencies of northeast monsoon rainy days in the global warming. Global and Planetary Change 2012;92-93:40-47.

[3] Nordell B. Thermal Pollution causes global warming. Global and Planetary Change 2003;38:305-312.

[4] Lean J, Rind D. Earth's response to a variable sun. Science 2001;292:234-236.

[5] Mende W, Stellmacher R. Solar variability and the search for corresponding climate signals. Space Science Reviews 2000;295-306.

[6] Kharseh M, Altorkmany L. How global warming and building envelope will change buildings energy use in central Europe. Applied Energy 2012;97:999-1004.

[7] Volker Quaschning, Understanding Renewable Energy Systems, 1st Edition, Earthscan, 2005.

[8] http://history-world.org/Industrial%20Intro.htm [retrieve on 22.10.12].

[9] http://www.indexmundi.com/south_africa/electricity_consumption.html [retrieve on 22.10.12].

[10] http://mdgs.un.org/unsd/mdg/SeriesDetail.aspx?srid=749&crid= [retrieve on 22.10.12].

[11] http://www.eskom.co.za/c/article/584/key-facts/ [retrieve on 22.10.12].

[12] Mohamad MA, El-Ghetany HH, Abdel Dayem AM. Design, construction and field test of hot-box solar cookers for African Sahel region. Renewable Energy 1998;14:49-54.

[13] Pohekar SD, Kumar D, Ramachandran M. Dissemination of cooking energy alternatives in India - a review. Renewable and Sustainable Energy Reviews 2005;9:379-93.

[14] Wentzel M, Pouris A. The development impact of solar cookers: a review of solar cooking impact research in South Africa. Energy Policy 2007;35:1909-19.

[15] Biermann E, Grupp M, Palmer R. Solar cooker acceptance in South Africa: results of a comparative field test. Solar Energy 1999;66(6):401-7.

[16] Archimedes of Syracuse (287 212 B.C.). http://natureofmathematics.wordpress.com/lecture-notes/archimedes/ [retrieve on 23.07.12].

[17] http://web.mit.edu/2.009/www/experiments/deathray/10_ArchimedesResult.html 1 [retrieve on 10.07.12].

[18] Panwar NL, Kaushik SC, Surendra Kothari. State of the art solar cooking: An overview. Renewable and Sustainable Energy Reviews 2012;16:3776-3785.

[19] Leonardo Da Vinci. http://www.crystalinks.com/davinci.html [retrieve on 23.07.12].

[20] Solar Energy In the Seventeenth Century. http://www.solarfasttrack.com/English/chap3/chap3a.htm [retrieve on 23.07.12].

[21] http://www.eee.hku.hk/∼ccst9004/Database_food_prepare_solar_cooker.html [retrieve on 10.07.12].

[22] Horace de Saussure and his Hot Boxes of the 1700's. http://solarcooking.org/saussure.htm [retrieve on 23.07.12].

[23] Nothing new under the sun part ii. http://csirosolarblog.com/tag/lavoisier/ [retrieve on 23.07.12].

[24] Solar Energy In the Nineteenth Century. http://www.solarfasttrack.com/English/chap3/chap3b.htm [retrieve on 23.07.12].

[25] History of Solar Cooking. http://www.solarcooker-at-cantinawest.com/solarcooking-history.html [retrieve on 23.07.12].

[26] http://siarchives.si.edu/collections/siris_sic_8184 [retrieve on 10.07.12].

[27] History of Solar power. http://www.saint-gobain-solar-power.com/saint-gobain-solar-power/thermosolar-such-story-4 [retrieve on 23.07.12].

[28] http://www.thesolarguide.com/solar-thermal/history.aspx [retrieve on 23.07.12].

[29] http://web.mit.edu/invent/iow/telkes.html [retrieve on 23.07.12].

[30] Muthusivagami RM, Velraj R, Sethumadhavan R. Solar cookers with and without thermal storage - A review. Renewable and Sustainable Energy Reviews 2010;14:691-701.

[31] Duffy & Beckman, Solar Engineering of Thermal Processes, 2nd Edition, John Wiley & Sons, INC, 1991.

[32] Bent Sorensen, Renewable Energy, 3rd Edition, Elsevier Academic Press, 2004.

[33] Mukherjee & Chakrabarti, Fundementals of Renewable Energy Systems, 1st Edition, New Age International (P) Ltd., Publishers, 2004.

[34] Twidel & Weir, Renewable Energy Resources, 2nd Edition, Taylor & Francis Group, 2006.

[35] Claud C, Cagnazzo C, Keckhut P. The effect of the 11-year solar cycle on the temperature in the lower stratosphere. Journal of Atmospheric and Solar-Terrestrial Physics 2008;70:2031-2040.

[36] N Robinson, Solar Radiation, 1st Edition, Elsevier Publishing Company, 1966.

[37] Kinsell L Coulson, Solar & Terrestrial Radiation, 1st Edition, Academic Press, 1975.

[38] http://www.powerfromthesun.net/Book/chapter02/chapter02.html [retrieve on 20.02.13].

[39] http://meteonorm.com/download/maps/ [retrieve on 30.10.12].

[40] http://geomodelsolar.eu/_pics/SolarGIS-solar-map-South-Africa-Direct-Normal-Irradiation-DNI.jpg [retrieve on 07.03.13]

[41] http://www.physicalgeography.net/fundamentals/6h.html [retrieve on 30.10.12].

[42] Qiblawey HM, Banat F. Solar thermal desalination technologies. Desalination 2008;220:633-644.

[43] Viebahn P, Lechon Y, Trieb F. The potential of concentrated solar power (CSP) in Africa and Europe - A dynamic assessment of technology development, cost development and life cycle inventories until 2050. Energy Policy 2011;39:4420-4430.

[44] Larraín T, Escobar R. Net energy analysis for concentrated solar power plants in northern Chile. Renewable Energy 2012;41:123-133.

[45] http://zeroemissionproject.com/blog/article/40/do-photovoltaic-solar-panels-need-more-energy-to-be-manufactured-than-what-they-generate [retrieve on 06.12.12].

[46] http://www.solarthermalmagazine.com/2010/11/17/trading-up-from-water-heaters-to-solar-water-heaters/ [retrieve on 06.12.12].

[47] http://www.lifeskillsinternational.com/Survival/energy/02solar-ovens/box/05collapsable-oven.html [retrieve on 06.12.12].

[48] Tang R, Yang Y, Gao W. Comparitive studies on thermal performance of water-in-glass evacuated tube solar water heaters with different collector tilt angles. Solar Energy 2011;85:1381-1389.

[49] Soo Too YC, Morrison GL, Behnia M. Performance of solar water heaters with narrow mantle heat exchangers. Solar Energy 2009;83:350-362.

[50] Redpath D. Thermosyphon heat-pipe evacuated tube solar water heaters for nothern maritime climates. Solar Energy 2012;86:705-715.

[51] Bourke G, Bansal P. New test method for gas boosters with domestic solar water heaters. Solar Energy 2012;86:78-86.

[52] Ekechukwu OV, Ugwuoke NT. Design and measured performance of a plane reflector augmented box-type solar-energy cooker. Renewable Energy 2003;28:1935-1952.

[53] Kumar S. Estimation of design parameters for thermal performance evaluation of box-type solar cooker. Renewable Energy 2005;30:1117-1126.

[54] Harmim A, Merzouk M, Boukar M, Amar M. Mathematical modeling of a box-type solar cooker employing an asymmetric compound parabolic concentrator. Solar Energy 2012;86:1673-1682.

[55] Negi BS, Purohit I. Experimental investigation of a box type solar cooker employing a non-tracking concentrator. Energy Conversion and Management 2005;46:577-604.

[56] Kaushik SC, Gupta MK. Energy and exergy efficiency comparison of community-size and domestic-size paraboloidal solar cooker performance. Energy for Sustainable Development 2008;12:60-64.

[57] Ouyang J, Xia Y. High-performance polymer photovoltaic cells with thick P3HT:PCBM films prepared by a quick drying process. Solar Energy Materials & Solar Cells 2009;93:1592-1597.

[58] Lee E, Kim J, Kim C. Polymer tandem photovoltaic cells with molecularly intimate interfaces achieved by a thin-film transfer technique. Solar Energy Materials & Solar Cells 2012;105:1-5.

[59] Zhu XZ, Gao CH, Xu MF, Gu W, Shi XB, Lei YL, Wang ZK, Liao LS. Enhancement of device efficiency in CuPc/C_{60} based organic photovoltaic cells by inserting an $InCl_3$ layer. Synthetic Metals 2012;162:2212-2215.

[60] Barlev D, Vidu R, Stroeve P. Innovation in concentrated solar power. Solar Energy Materials & Solar Cells 2011;95:2703-2725.

[61] Tao T, Hongfei Z, Kaiyan H, Mayere A. A new trough solar concentrator and its performance analysis. Solar Energy 2011;85:198-207.

[62] Öztürk HH. Experimental determination of energy and exergy efficiency of the solar-parabolic cooker. Solar Energy 2004;77:67-71.

[63] Mills D, Morrison G. Compact linear Fresnel reflector solar thermal powerplants. Solar Energy 1999;68:263-283.

[64] Sonune AV, Philip SK. Development of a domestic concentrating cooker. Renewable Energy 2003;28:1225-1234.

[65] Franco J, Saravia L, Javi V, Caso R, Fernandez C. Pasteurization of goat milk using a low cost solar concentrator. Solar Energy 2008;82:1088-1094.

[66] Chern Sing Lim, Li Li. Flux distribution of solar furnace using non-imaging focusing heliostat. Solar Energy 2009;83:1200-1210.

[67] http://www.nrel.gov/data/pix/searchpix.php?getrec=00036&display_type=verbose [retrieve on 06.12.12].

[68] http://xaharts.org/Whirlwheel_dir/reflecting_disks/reflecting_disks.html [retrieve on 06.12.12].

[69] http://techbells.blogspot.com/2012/07/working-of-csp-parabolic-trough.html [retrieve on 06.12.12].

[70] Artur CD. Assessment of the efficiency of solar radiation concentrating system. Masters thesis, 2010.

[71] Shuai Y, Wang F, Xia X, Tan H, Liang Y. Radiative properties of a solar cavity receiver/reactor with quartz window. International Journal of Hydrogen Energy 2011;36:12148-12158.

[72] Habeebullah MB, Khalifa AM, Olwi I. The oven receiver: an approach toward the revival of concentrating solar cookers. Solar Energy 1995;54:227-237.

[73] Hernández N, Riveros-Rosas D, Venegas E, Dorantes RJ, Rojas-Morín A, Jaramillo OA, Arancibia-Bulnes CA, Estrada CA. Conical receiver for a paraboloidal concentrator with large rim angle. Solar Energy 2012;86:1053-1062.

[74] Franco J, Cadena C, Saravia L. Multiple use communal cookers. Solar Energy 2004;77:217-23.

[75] Reddy KS, Sendhil Kumar N. Combined laminar natural convection and surface radiation heat transfer in a modified cavity receiver of solar parabolic dish. International Journal of Thermal Sciences 2008;47:1647-1657.

[76] http://www.infrared-thermography.com/material-1.htm [retrieve on 30.11.12].

[77] Prakash M, Kadare SB, Nayak JK. Investigations on heat losses from a solar cavity receiver. Solar Energy 2009;83:157-170.

[78] Nuwayhid RY, Mrad F, Abu-Said R. The realization of a simple solar tracking concentrator for university research applications. Renewable Energy 2001;24:207-222.

[79] Chong KK, Wong CW. General formula for on-axis sun-tracking system and its application in improving tracking accuracy of solar collector. Solar Energy 2009;83:298-305.

[80] Sharan AM, Prateek M. Automation of minimum torque-based accurate solar tracking systems using microprocessors. Journal of Indian Institute of Science 2006;86:415-437.

[81] Poulek V, Libra M. New solar tracker. Solar Energy Materials & Solar Cells 1998;51:113-120.

[82] Poulek V, Libra M. A new low-cost tracking ridge concentrator. Solar Energy Materials & Solar Cells 2000;61:199-202.

[83] Mawire A, McPherson M. A feedforward IMC structure for controlling the charging temperature of a TES system of a solar cooker. Energy Conversion and Management 2008;49:3143-3154.

[84] Schwarzer K, Vieira da Silva ME. Solar cooking system with or without heat storage for families and intitutions. Solar Energy 2003;75:35-41.

[85] Schwarzer K, Vieira da Silva ME. Characterization and design methods of solar cookers. Solar Energy 2008;82:157-63.

[86] Pohekar SD, Ramachandran M. Multi-criteria evaluation of cooking devices with special reference to utility of parabolic solar cooker (PSC) in India. Energy 2006;31:1215-27.

[87] Pohekar SD, Ramachandran M. Utility assessment of parabolic solar cooker as a domestic cooking device in India. Renewable Energy 2005;31:1827-1838.

[88] Hosny Z, Abou-Ziyan. Experimental investigation of tracking paraboloid and box solar cookers under Eqyptian environment. Applied Thermal Engineering 1998;18:1375-94.

[89] Patel NV, Philip SK. Performance evaluation of three solar concentrating cookers. Renewable Energy 2000;20:347-355.

[90] http://www.montgomerycollege.edu/.../es100c/.../parabolic%20antennas.pd...[retrieve on 01.11.12].

[91] Mlatho JSP, McPherson M, Mawire A, Van den Heetkamp RJJ. Determination of the spatial extent of the focal point of a parabolic dish reflector using a red laser diode. Renewable Energy 2012;35:1982-1990.

[92] Bruce R Munsen, Donald F Young, Theodore H Okiishi, Fundamentals of Fluid Mechanics, 4th Edition, John Wiley & Sons, INC, 2002.

[93] Micheal J Moran, Howard N Shapiro, Fundamentals of Engineering Thermodynamics: SI Version, 3rd Edition, John Wiley & Sons Ltd, 1998.

[94] Young HD, Freedman RA. Sears and Zemansky's University Physics with Modern Physics, 13th Edition, Addison-Wesley, 2010.

Appendix A

Mirror Tiles

Table A.1: Summary of Mirror Tile Dimensions per Petal

Ring no	No of tiles required	Tile height	Upper side	Lower side
		(mm)	(mm)	(mm)
1	3	75 ± 1	72.0 ± 1	46.0 ± 1
2	4	75 ± 1	74.5 ± 1	55.0 ± 1
3	5	75 ± 1	75.6 ± 1	60.0 ± 1
4	6	75 ± 1	76.0 ± 1	63.0 ± 1
5	7	75 ± 1	76.5 ± 1	65.5 ± 1
6	8	75 ± 1	76.5 ± 1	67.0 ± 1
7	9	75 ± 1	76.5 ± 1	68.0 ± 1
8	10	75 ± 1	76.0 ± 1	69.0 ± 1
9	11	75 ± 1	76.0 ± 1	69.5 ± 1
10	12	75 ± 1	76.0 ± 1	70.0 ± 1
11	13	75 ± 1	75.5 ± 1	70.0 ± 1
12	14	75 ± 1	75.0 ± 1	70.0 ± 1
13	15	75 ± 1	75.0 ± 1	70.0 ± 1
14	15	90 ± 1	80.0 ± 1	75.0 ± 1

Appendix B

Heat Transfer Fluid

Table B.1: Calflo Technical Data

Temperature	Density	Kinematic Viscosity	Specific Heat Cap	Thermal Conductivity
(°C)	(kg/m^3)	(m^2/s) $\times$ 10^{-5}	(J/kg.K)	(W/m.K)
20	851.9	8.8783	1910	0.142
30	845.1	5.0518	1940	0.142
40	838.4	3.119	1970	0.141
50	831.7	2.1244	2000	0.141
60	824.9	1.5174	2040	0.14
70	818	1.1276	2070	0.14
80	811.5	0.8663	2100	0.139
90	804.7	0.6845	2140	0.138
100	798	0.5539	2170	0.138
110	791.2	0.4576	2200	0.137
120	784.5	0.3847	2230	0.137
130	777.8	0.3284	2270	0.136
140	771	0.2841	2300	0.136
150	764.3	0.2488	2330	0.135

Appendix C

Reynold's Number

Table C.1: Table of calculated Reynold's Number for different temperatures at constant flow rate.

Temperature	Density	Kin. Viscosity	Pipe Diameter	Fluid Velocity	Re
(°C)	(Kg/m3)	(m^2/s) $\times 10^{-5}$	(m)	(m/s)	
20	851.9	8.8783	0.008	0.25	22.41
30	845.1	5.0518	0.008	0.25	39.38
40	838.4	3.1190	0.008	0.25	63.78
50	831.7	2.1244	0.008	0.25	93.65
60	824.9	1.5174	0.008	0.25	131.11
70	818	1.1276	0.008	0.25	176.43
80	811.5	0.8663	0.008	0.25	229.65
90	804.7	0.6845	0.008	0.25	290.64
100	798	0.5539	0.008	0.25	359.17
110	791.2	0.4576	0.008	0.25	434.75
120	784.5	0.3847	0.008	0.25	517.14
130	777.8	0.3284	0.008	0.25	605.80